Tropical Pacific signals of suborbital-scale climate variability during the mid-Pleistocene climate transition

LAUREN FRANCES CRAVEN-NIEMCZYK

Lauren Craven-Niemczyk

Tropical Pacific signals of suborbital-scale climate variability during the mid-Pleistocene climate transition

Material Abstract

The mid-Pleistocene climate transition (MPT) marks the shift in dominance from 41- to 100-kyr high latitude climate cyclicity between the early and late Quaternary. The fundamental mechanisms responsible for the MPT, and consequent 100-kyr cycle dominance is much debated, suffering from a paucity of data particularly from the low-mid latitudes. A large proportion of studies have focused on northern hemisphere ice sheet growth associated with the MPT. However, this thesis seeks to explore the hypothesis that not only do the tropical latitudes hold valuable information pertaining to the cause/s and development of the transition, but also the possibility that they play a key role in the initiation of the MPT itself, through powerful feedbacks holding the potential to alter global climate. In this study, both the physical (SST, thermocline depth) and biological (primary productivity) properties of the east Pacific are examined across the MPT.

This study finds that prior to and including MIS 22, the glacial-stage tropical Pacific operates under a La Niña-like state, suggested here to be caused by strengthened meridional temperature gradients which alter the tropical ocean-atmosphere system. MIS 22 culminated in an intense upwelling event, indicating a threshold has been crossed, agreeing with “900-ka event” theories of an extreme glaciation. This research does not find evidence for a pervasive cooling prior to the onset of the MPT in the tropical Pacific, negating the notion of strengthened Walker circulation as a driver for the MPT. Instead, an enhanced glacial biological carbon pump is presented as a more plausible explanation.

Tropical Pacific signals of suborbital-scale climate variability during the mid-Pleistocene climate transition

Lauren Craven-Niemczyk

Masters by Research

Department of Geography

Durham University

2015

Table of Contents

List of Illustrations

List of Abbreviations

Declaration

I hereby certify that the work described in this thesis is my own, except where otherwise acknowledged, and has not been submitted previously for a degree at this or any other University.

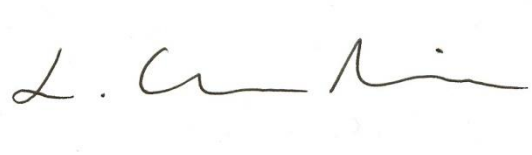

Acknowledgements

Firstly I wish to thank Dr Erin McClymont and Dr Jerry Lloyd for their unfailing academic support and helpful advice throughout this process.

Secondly, thanks goes to the laboratory staff at Durham University for being a friendly teaching resource and good company; particularly Martin, Amanda, Kathryn, Alison, Eleanor and Jess.

I am hugely grateful to Durham University for the MRes bursary which enabled me to undertake this research, and also to the Ocean Drilling Program for supplying additional samples during the course of the project.

Finally, I couldn't have completed this without the encouragement and enthusiasm of my close friends and family; particularly my parents and step-parents, Laurie, and Sophie. Thank you for helping me finally get here!

Chapter 1: Introduction

1.1 Quaternary climate change

The Quaternary climate (2.58 million years ago to the present day) is punctuated by glacial-interglacial cycles (figure 1.1). Milankovitch theory argues for astronomical obliquity (~41 thousand year (kyr) cycle), eccentricity (~100 kyr) and precession (~23/~19 kyr) as a regulator of Quaternary climate (Milankovitch, 1930). These orbital cycles determine the distribution and quantity of solar radiation which reaches the Earth's surface, with the Milankovitch theory identifying 65°N as the key latitude for ice-sheet response to orbital forcing, since here the balance between winter snow accumulation and summer ablation is considered to be critical to large continental ice sheet build-up (Milankovitch, 1941). The Milankovitch theory is a widely accepted explanation for the frequency with which glacial-interglacial cycles alternate, referred to as 'orbital forcing' (Milankovitch, 1941; Paillard, 2001). However, the periodicity and amplitude of these glacial cycles shows some variability that it still not fully understood.

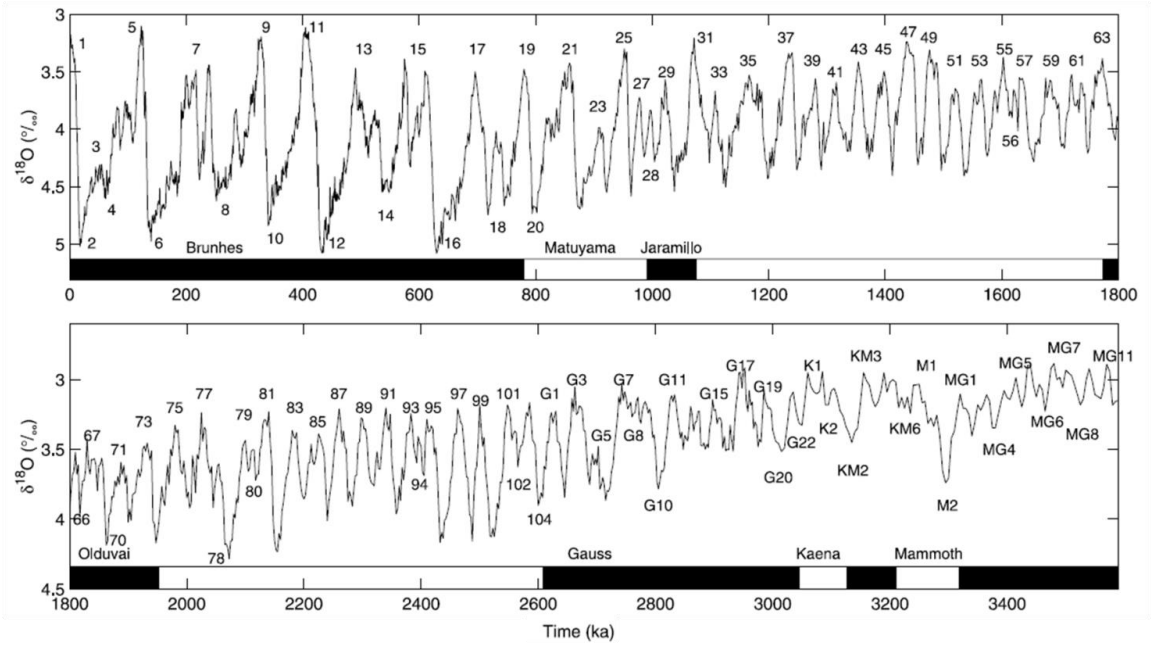

Figure 1.1: LR04 benthic δ¹⁸O stack created from 57 globally distributed benthic δ¹⁸O records between ~3600 ka and the present day. The stack is plotted using the LR04 age model described in Lisiecki and Raymo (2005). Note the marine isotope stages, magnetic field reversals, and vertical axis scale changes. Source: Lisiecki and Raymo (2005).

Prior to 2.8 million years ago (Ma), no unequivocal and prominent precessional or obliquity frequency cycles have been identified in the records of past global ice volume. From around 2.75 Ma onwards, an increase in global ice volume occurred, referred to as the intensification of northern hemisphere glaciations, after which a prominent 41 kyr cyclicity began (Shackleton et al, 1990; Ruddiman et al, 1989; Raymo et al, 1992). This 41 kyr frequency was the primary modulator of ice volume and high latitude sea surface temperature (SST) until the mid-Pleistocene Transition (MPT) around 1 Ma. The MPT marks the change in dominance from the 41 kyr to the 100 kyr high latitude climate cyclicity between the early and late Quaternary (Prell, 1982; Raymo et al, 1997; Schmieder et al, 2000; Wang et al, 2001; Imbrie et al, 1992; Jouzel et al, 2007). The amplitude of glacial-interglacial climate change increased across the transition from 41 to 100 kyr cycles (as

visible in figure 1.1), reflecting more severe glaciations after the MPT (Pisias and Moore, 1981; Clark and Pollard, 1998; Berger and Loutre, 1999, Clark et al, 2006).

The underlying mechanisms driving the MPT, and subsequent 100 kyr cycle dominance, is one of the big puzzles in Quaternary climate research; due somewhat to the scarcity of data beyond the benthic (deep-dwelling) $\delta^{18}O$ time series which originally identified the MPT (Pisias and Moore, 1981; Prell, 1982; Start and Prell, 1984; Ruddiman et al, 1986; 1989; DeBlonde and Peltier, 1991; Berger et al, 1993a; Shackleton, 2000). It is impossible to explain the MPT using only Milankovitch theory; any changes in total solar radiation receipt driven by eccentricity cycles alone cannot explain the increased amplitude of glacial-interglacial cycles seen across the MPT (Jin and Jian, 2013), and there was no observed change in the magnitude of eccentricity forcing across the MPT (Imbrie et al, 1993). Therefore, the two main speculated theories are that the 100 kyr cycles are caused by either an amplification of a perturbation in insolation forcing, or a self-sustained variability internal to the climate system, acting in a non-linear fashion (Ashkenazy-Tziperman, 2004). The MPT is then paced by the weak Milankovitch forcing, thus 'phase locking' the climate system to 100 kyr terminations (Ashkenazy-Tziperman-2004).

The dominant interpretation of the increased global ice volume during the MPT has called for more expansive northern hemisphere ice-sheets, across modern day Canada and Scandinavia, therefore many studies have focused on the effects of the MPT in the northern hemisphere. This is compounded by the identification of the latitude at 65°N being key to orbital forcing and thus any significant ice sheet changes (Milankovitch, 1941). More recently however, studies in the tropics have demonstrated vital climate changes during the MPT, with the potential to create feedback loops with high-latitude climate (Liu and Herbert, 2004; Garidel-Thoron et al, 2005; McClymont and Rosell-Melé, 2005). These developments and the links between high and low latitudes cannot be fully explained at the moment; and this is something this thesis seeks to explore.

1.2 Aims and objectives

The aim of this thesis is to assess the response of the tropical Pacific to the MPT. Examining records of changing circulation in the east tropical Pacific, a region which we know is an important part of the modern climate system, will allow us to better understand the oceanic and climatic responses beyond the ice sheets. This aim will be addressed through 3 objectives:

1. Reconstruct a sub-orbital scale resolution record of sea surface temperatures across the MPT (1.15 to 0.6 Ma) using alkenone biomarkers
2. Reconstruct a sub-orbital scale resolution record of primary productivity using chlorin and alkenone biomarkers
3. Reconstruct a sub-orbital scale resolution record of water column structure using stable isotope analyses of two species of surface-dwelling foraminifera

This study will add to, and in most cases significantly increase the temporal resolution of existing SST records from the east tropical Pacific through the MPT (e.g. McClymont, 2004; Lawrence et al, 2006; Wara et al, 2005; Dekens et al, 2007). A multi-proxy approach will also be developed here in

order to explore more than just SST, but also detailed information on the nature of the ocean circulation changes. The approach of this thesis is to draw on both organic biomarker proxies, which are molecular fossils, and the chemical analysis of foraminiferal carbonate shells to reconstruct past east equatorial Pacific (EEP) changes. These proxies will identify evidence for SST, productivity, upwelling versus stratification, and links to atmospheric circulation changes. The site of interest, ODP (Ocean Drilling Program) site 849, lies within the heart of the east Pacific cold tongue, an upwelling region whose intensity in the modern climate is sensitive to tropical Pacific circulation changes.

The average resolution between SST samples is 3.65 kyr, extending a previous study (McClymont and Rosell-Melé, 2005). The sub-orbital-scale analyses target evidence for climate variability superimposed upon the glacial-interglacial cycles; such patterns have been detected in the high-latitudes across the MPT (e.g. Hernandez-Almeida et al, 2012) but have not yet been investigated in detail in the tropical Pacific. This high resolution sampling will enable investigation of the hypothesis that tropical forcing plays a vital role in the regulation of mid-Pleistocene climate.

1.3 Regional climate and oceanographic setting

This study has used deep-ocean sediment cores from ODP site 849, extracted in 1995 during ODP Leg 138. ODP site 849 is located in the EEP (figure 1.2). The core is situated on the western slope of the East Pacific Rise mid-oceanic ridge, with a water depth of 3851m (0°11’ N, 110°31’ W) (Mix et al, 1995), and is located within the equatorial divergence region, in the present day EEP cold tongue. At the cold tongue, the eastern boundary Peru Current mixes with the Southern Equatorial Current (SEC). This area is characterised by high productivity levels (from high nutrient concentrations in the euphotic zone) and cool SSTs (due to a shoaling subsurface equatorial undercurrent [EUC; figure 1.2] and contributions from the cold Peru Current) (Liu and Herbert, 2004). The core site has not moved in latitude since ca.7 Ma, making it an ideal site location to monitor past ocean circulation and climatic changes (Mayer et al, 1992).

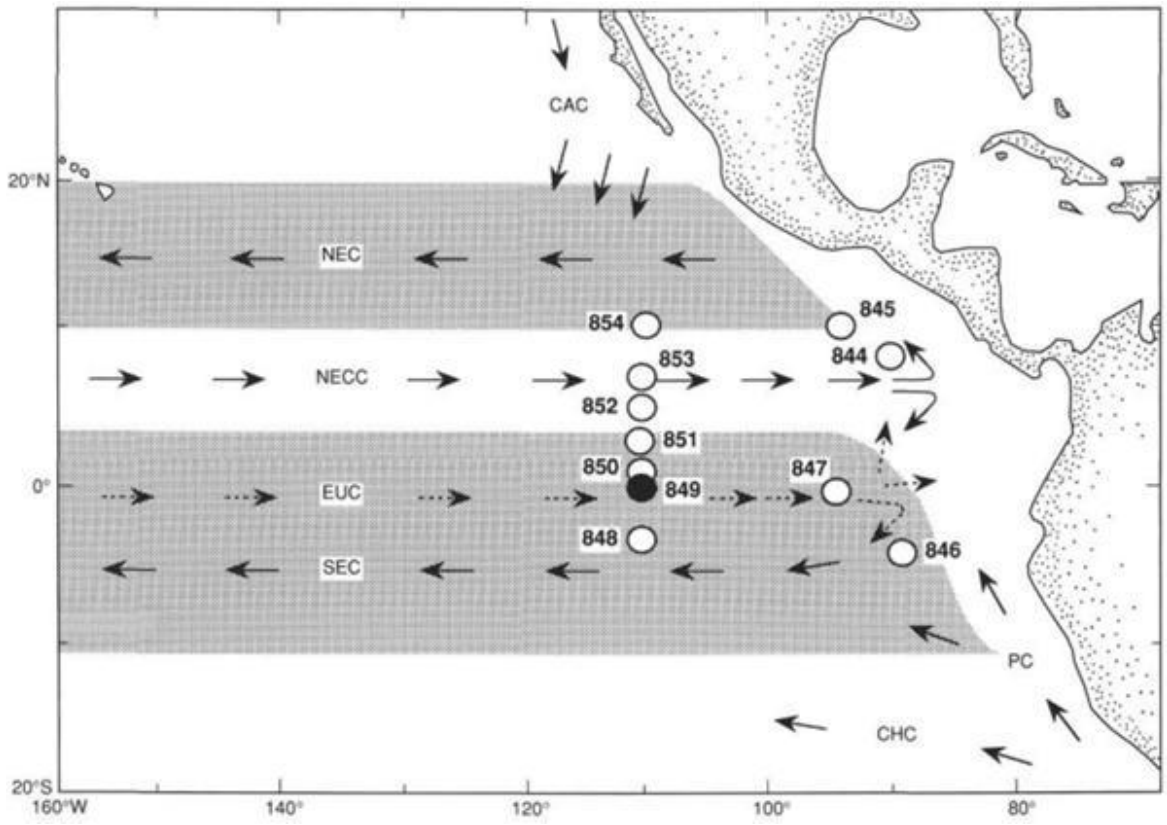

Figure 1.2: Site location of ODP site 849 and surrounding ODP Leg 138 sites. Solid arrows indicate surface currents; dashed arrows indicate subsurface currents. CAC = California Current; NEC = North Equatorial Current; NECC = North Equatorial Countercurrent; EUC = Equatorial Undercurrent; SEC = South Equatorial Current; PC = Peru Current; CHC = Chile Current. Shaded area illustrates general latitudinal extent of the SEC and NEC. Source: Mayer et al (1992).

1.4 Thesis structure

Firstly the MPT, tropical Pacific and relevant paleoceanographic proxies will be assessed with reference to the literature, followed by an examination of the site location and previous studies carried out in the EEP. The methodology will then be outlined, followed by the results and key observations of the data. Finally, the discussion will critically evaluate the events and key trends within the data, with comparison from supporting datasets from the tropical Pacific.

In summary:

- Literature Review
- Methodology (lab work plus age model generation)
- Results
- Discussion and Wider Implications
- Conclusions and Future Work

Chapter 2: Literature Review

2.1 The mid-Pleistocene climate transition

The MPT was initially identified in marine sediments in the $\delta^{18}O$ of planktonic (surface dwelling) foraminiferal calcite, then later in benthic foraminiferal $\delta^{18}O$; a record which reflects a strong signal of global ice volume (Shackleton and Opdyke, 1973; 1976; Prell, 1982; Pisias and Moore, 1981; Clark and Pollard, 1998; Ruddiman and McIntyre, 1981). Subsequently, the MPT was identified in loess-paleosol layers, which began to mimic ice volume fluctuations around 1.5 Ma (Rutherford and D'Hondt, 2000). Since then, the MPT has been identified in numerous proxy records globally (e.g. Raymo et al, 1997; Schmieder et al, 2000; Wang et al, 2001; 2004; Jian et al, 2000; Zheng et al, 2005; Wang and Abelmann, 2002; Sun et al, 2003; Tian et al, 2002; Clark et al, 2006; McClymont et al, 2013). The onset of the MPT was marked not only by significant ice sheet growth and a drop in mean global temperature (Ruddiman et al, 1989; Berger et al, 1993; Shackleton, 2000), but also an increase in the equatorial Pacific zonal SST gradient and large fluctuations in thermocline depth, largely reflected in SST variations in the east Pacific cold tongue (Garidel-Thoron et al, 2005; Zheng et al, 2005; Li et al, 2008; McClymont and Rosell-Melé, 2005; McClymont et al, 2013).

Mudelsee and Schulz (1997) define the MPT as occurring between marine isotope stage (MIS) 16 and 22; from 920-640 ka. This is based on time and frequency domain analysis on multiple high resolution $\delta^{18}O$ time series records and a simple ice bedrock model. Although the exact date of the onset of the MPT varies between sites and how the MPT is defined, the onset is generally attributed to ca.900 ka, at the boundary between MIS 22 and 23, at the onset of the first intense glaciation (figure 1.1), and ending at ca.700 ka, when the first recognisable 100 kyr cycle is identified in the $\delta^{18}O$ record (Pisias and Moore, 1981; Clark and Pollard, 1998; Berger and Loutre, 1999; Prell, 1982; Berger et al, 1993). Whether the transition to 100 kyr cycles was gradual or abrupt is still contested (Ruddiman et al, 1989; Berger and Jansen, 1994).

Some authors argue that an increase in ice mass leads to climate feedbacks which control the 100 kyr cycles (Clark and Pollard, 1998; Ashkenazy and Tziperman, 2004; Huybers and Wunsch, 2005). Mudelsee and Schulz (1997) identified an abrupt increase in ice mass (from $\delta^{18}O$ records) between 942 and 902 ka, approximately 280 kyr prior to the unequivocal regulation of 100 kyr cycles. Elderfield et al (2012) used a new technique to extract deep water temperature from the benthic $\delta^{18}O$ signal, and as a result they identified an abrupt increase in $\delta^{18}O$ which was attributed to an increased ice volume (rather than deep water temperature change) between 950 and 870 kyr. Since the water masses which are recorded at Elderfield et al's (2012) site (ODP site 1123, Southwest Pacific) are sourced in the Antarctic, this sudden increase in ice volume has been attributed to a more extensive Antarctic ice sheet.

However, evidence exists to suggest that the climate system may have been evolving into a 100 kyr world prior to any change in ice sheet volume ca.900 ka. For example, studies on the periodicity of the global $\delta^{18}O$ record have determined that the advent of the 100 kyr cyclicity may have been as early as 1.5 Myr (Park and Maasch, 1993; Hagelberg et al, 1991). Chen et al (1995) found high amplitude 100-kyr cycles from 1.2 Ma in benthic $\delta^{18}O$ in the Indian Ocean 1.2 Ma. Clark et al (2006) based their conclusion for a gradual transition, and an increase in the northern hemisphere long-term ice volume beginning at 1250 ka, on the LR04 benthic stack of $\delta^{18}O$ records

(figure 1.1). Clark et al. (2006) state that the advantage of using this globally-derived stacked record is to filter out regional 'noise'. However, Elderfield et al (2012) argue that the stack is biased towards Atlantic and EEP sites, and may not represent the global benthic $\delta^{18}O$ signal. The first incident of drastically reduced North Atlantic Deep Water (NADW) during a glacial was recorded at 1.6 Ma by benthic $\delta^{13}C$ and dissolution of $CaCO_3$ in the low-latitude Atlantic (Raymo, et al, 1990; Bickert et al, 1997). Finally, McClymont et al (2013) showed that globally, SSTs began to cool at ~1.2 Ma. There are many more examples of early Pleistocene climatic shifts (Clemens et al, 1996; Bloemendal et al, 1995; deMenocal, 1995).

The timings of the symptoms of the MPT are critical in determining whether the transition was caused by ice sheet evolution, or the advent of a climate supportive of larger (thicker) ice sheets.

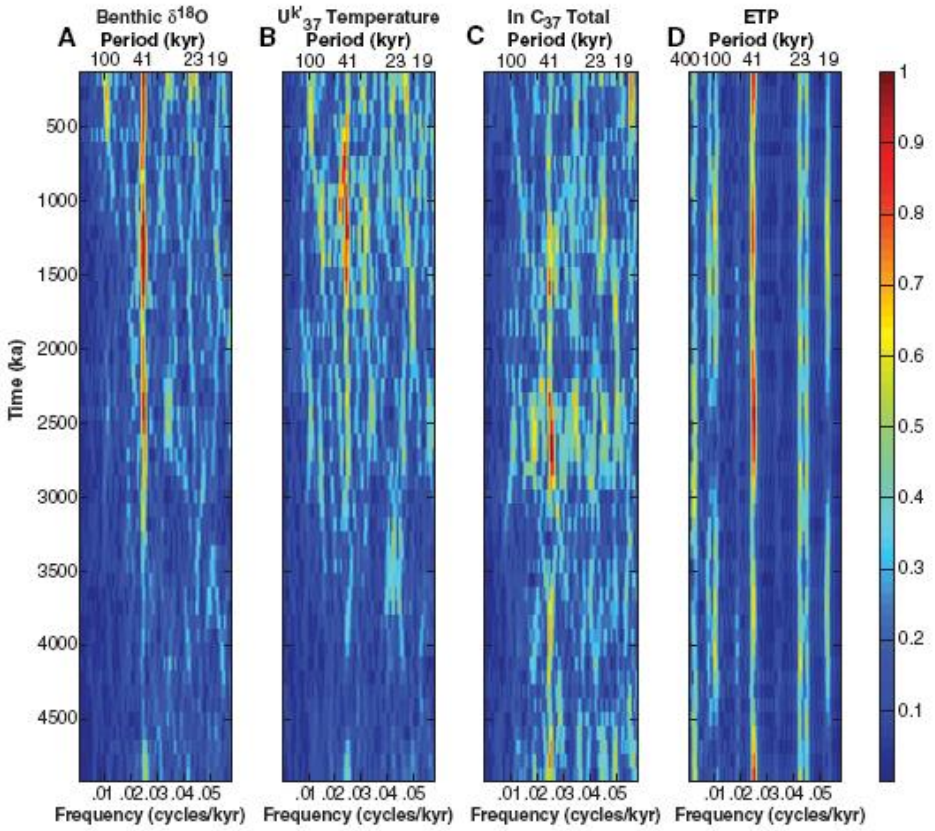

Figure 2.1: The MPT as reflected in records of global ice volume, SST and insolation (Eccentricity, obliquity (tilt) and precession- 'ETP'). Core ODP 846 (A) Benthic $\delta^{18}O$, showing that since the MPT, the strength of the 41 kyr obliquity cycle in ice volume has not abated, but that the 100 kyr cycles emerge from 1000 ka at this site. Source: Lawrence et al (2006)

The MPT was not accompanied by any significant change to orbital forcing (figure 2.1), and so the advent of a powerful 100 kyr climate cycle has led to a "100 kyr problem", whereby the strength of the eccentricity variations are not sufficient to sustain the 100 kyr cycles that emerge post-MPT; in addition to this, the 100 kyr forcing is somewhat out of phase with the climate response (Imbrie et al., 1992; 1993). The presence of 41 kyr obliquity forcing has remained throughout the Pleistocene (figure 2.1) (Liu and Herbert, 2004; Lawrence et al, 2006; Huybers and Wunsch, 2005). Compared to obliquity and precessional insolation forcing, eccentricity has weak power and therefore a small

effect on global insolation. This points to either an internal amplification mechanism of a non-linear climate response, or a cause internal to the climate system to explain the MPT.

However, despite the research focus on perturbations to eccentricity and precessional orbital frequencies to explain the MPT and the 100 kyr cycles, the obliquity frequency has been proven statistically to play a large part in the timing of terminations, as Huybers and Wunsch (2005) point out in their assessment of numerous 'orbital forcing hypothesis' models. Huybers and Wunsch (2005) explain the 41 kyr forcing pacing of 100 kyr glacial-interglacial changes, through the climate system skipping multiple obliquity 'beats' before deglaciating at either 80 or 120 kyr periods. For example, as obliquity increases and high-latitude solar insolation peaks, if the ice sheet is thin and basal melting is not significant, deglaciation will not occur – resulting in a 'missed beat'. As the glacial progresses and the ice sheet thickens and basal pressure is high, obliquity heating has a larger effect and can trigger deglaciation through enhanced lubrication at the ice-rock interface. The pre-MPT climate supports this hypothesis whereby a warmer overall climate enables obliquity-related insolation heating and therefore terminations at the first 'beat'.

The pattern of glacial-interglacial cycles also shifts across the MPT. The 100 kyr oscillations are distinguished by characteristically severe and asymmetric glaciations; long intervals of cooling and glacial growth are followed by a relatively short period of warming and deglaciation, enabling large continental ice sheets to develop (Pisias and Moore, 1981; Clark and Pollard, 1998; Ashkenazy and Tziperman, 2004). This contrasts with the 41 kyr cycles of the early and mid-Quaternary (figure 1.1), with smaller ice sheet build-up (a quarter to a third of the size of last glacial maximum [LGM] ice sheets) and more symmetrical glacial-interglacial cycles (Raymo and Nisancioglu, 2003). The form and amplitude of the 41 kyr cycles suggest these are a linear response to obliquity insolation forcing. However, some studies have suggested that pre-MPT glacial-interglacial cycles are actually considerably asymmetric, giving rise to the theory that glacial oscillations both before and after the MPT could be self-sustained (Zhonghui and Herbert, 2004; Ashkenazy-Tziperman, 2004).

Dansgaard–Oeschger (D-O) cycles are millennial-scale oscillations in climate that occurred during the last glacial; the cycles are characterised by saw-tooth glacial oscillations and abrupt warming at terminations (Bond et al, 1993). D-O cycles were first identified in oxygen isotope data from Greenland ice cores, then SST records from North Atlantic Ocean sediments (Dansgaard et al, 1993; Bond et al, 1993). D-O events depict large variations in air temperature and atmospheric circulation over Greenland (Broecker, 1991). Greenland air temperature is regulated in part by the surface heat emitted from the North Atlantic Ocean (Bond et al, 1993). NADW formation drives the Atlantic Meridional Overturning Circulation (AMOC), which in turn transmits heat to the North Atlantic surface water via the Thermohaline Circulation (THC); therefore D-O events have been accredited to perturbations in the THC (Broecker et al, 1989; Broecker, 1991). D-O cycles draw parallels with asymmetric 100 kyr cycles (rapid warming, slow cooling), and being that the cause of the millennial-scale D-O fluctuations may be related to reorganisations in the ocean-atmosphere system, this highlights the role it may play in the MPT (Bond et al. 1993; Denton et al, 2010 Blunier et al, 1998). Heinrich events are another example of abrupt climate fluctuations, and further highlight the instability of the North Atlantic (Dansgaard et al, 1993). Heinrich events are short-lived extreme cold periods, first documented from anomalous purge events of ice-rafted lithic debris in

the North Atlantic (Heinrich, 1988). They are considered to have been associated with abrupt changes in the AMOC; the large input of fresh water from a Heinrich event causes NADW formation to be greatly reduced or terminated, as shown in sediment records from the North Atlantic (Rahmstorf, 2002; Kienast et al, 2006). Relatively recent evidence suggests that abrupt climate changes related to Heinrich events are also present in the tropical latitudes, and are argued to reflect a low-latitude response to the high-latitude forcing through changes to atmospheric circulation (Hendy and Kennett, 2000; Peterson et al, 2000; Leduc et al, 2007; 2009; Wang et al, 2001; Stott et al, 2002; Ivanochko et al, 2005; Weldeab et al, 2007). A compelling hypothesis thus now exists linking the tropics and their potential contribution to these abrupt climate changes, but the hypothesis focuses on there being a predominantly northern hemisphere, high latitude forcing.

Therefore as with D-O events, Heinrich events and the last glacial termination, interactions between the ocean and atmosphere have the power to set up global feedbacks and accelerate climate change (Bond et al, 1993, Denton et al, 2010; Blunier et al, 1998). In summary, much is still unknown relating to the speed of the climate transition marked by the MPT, including whether the ice sheet expansion or the 100 kyr cyclicity truly came first, and the extent of the role the ocean-atmosphere system plays in the transition. This thesis seeks to address these questions.

2.2 The 900-ka event

The period of intense cooling that preceded the beginning of the MPT ended in a particularly cool glaciation; at ca.900 ka BP (MIS 22-24). In paleoclimate records across the globe, MIS 22-24 stands out as a turning point in the MPT (figure 2.3).

The global LR04 benthic $\delta^{18}O$ stack depicts emergence of a longer ~80 kyr signal starting at 900 ka (Lisiecki and Raymo, 2004). Elderfield et al's (2012) $\delta^{18}O$ of seawater reflected an abrupt increase in Antarctic ice ca.900 ka. Zheng et al (2005) found planktonic foraminiferal species abundance changes in the South China Sea (SCS) were most variable at ca.900 ka, as well as rapid decreases in winter SST (28 to 17.5ºC, as derived from planktonic foraminiferal $\delta^{18}O$) and shallowing of the thermocline (Jian et al, 2000; Zheng et al, 2005). In some sites in the North Atlantic, SSTs reached their coolest values at 900 ka (Ruddiman et al, 1989). Similarly, Schefuβ et al's (2004) alkenone-derived SST record in the eastern tropical Atlantic displays a severe and lengthy cooling event at 900 ka, at the same time that SSTs in the Southern Ocean became more variable, with warmer interglacial values indicating reduced polar sea ice (Becquey and Gersonde, 2002). In the EEP, SST records from Liu and Herbert (2004) and McClymont and Rosell-Melé (2005) display a progressive cooling of 1.5ºC from the start of the MPT until 900 ka, after which average SSTs stabilised. In the review paper by McClymont et al (2013), a marked cooling is noticeable in the majority of sites, even those which displayed minor SST changes throughout the MPT, for example in the tropics (figure 2.4a). However, in the west Pacific, Mg/Ca-derived SSTs predicted a stable 26.8ºC during this same period (MIS 22-23) suggesting local factors such as the East Asian Winter Monsoon may be playing a role (Garidel-Thoron et al, 2005).

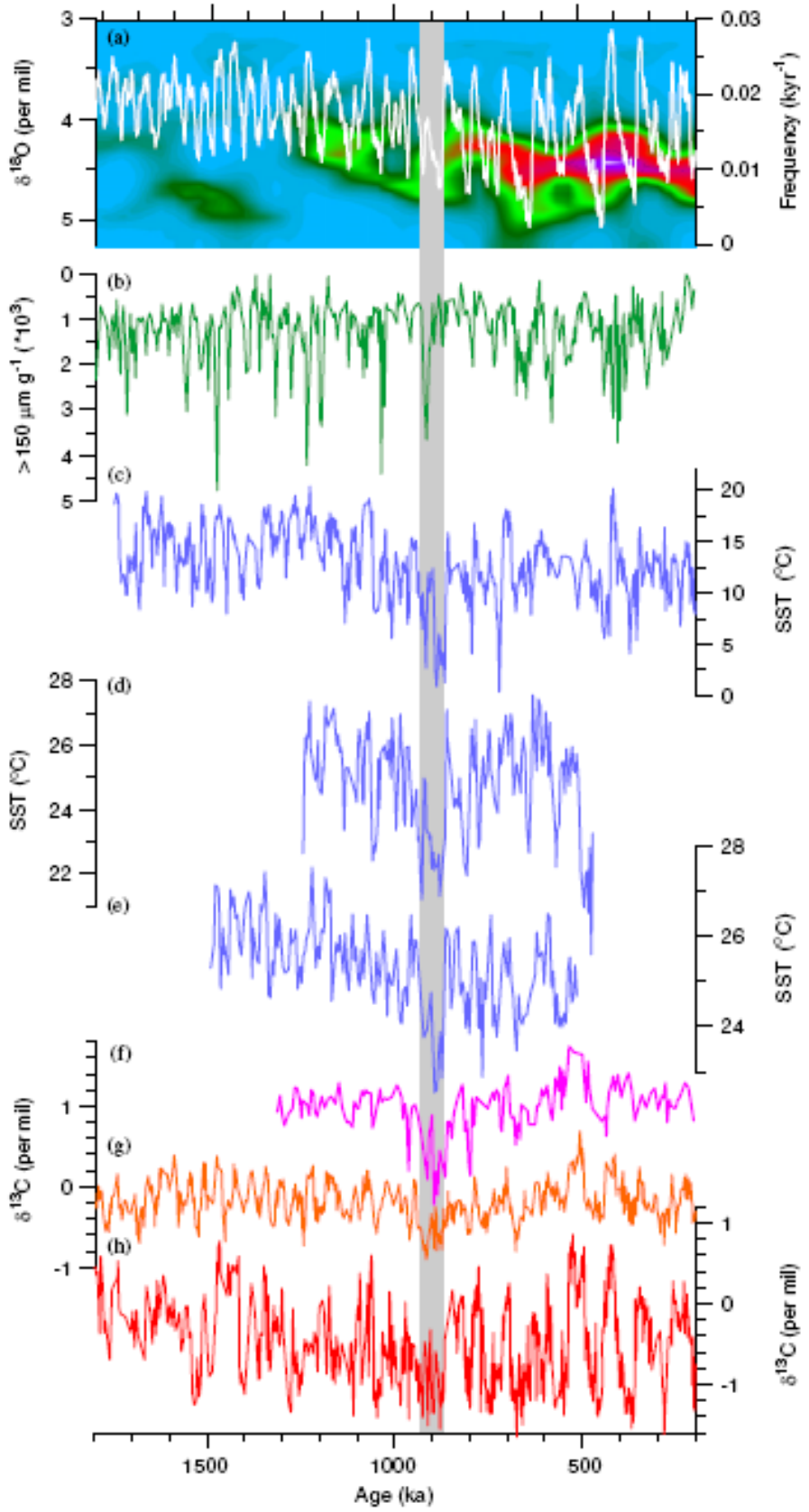
(a)
δ18O (per mil)
Frequency (kyr-1)
(b)
>150 μm g-1 (*10³)
(c)
SST (°C)
(d)
SST (°C)
(e)
SST (°C)
(f)
(g)
(h)
δ13C (per mil)
δ13C (per mil)
Age (ka)

Figure 2.3 (overleaf): Paleoclimate records demonstrating changes during the 900 ka event. (a) Time-frequency spectrogram (moving window Fourier transform) showing the distribution of low-frequency power in the 100-kyr filtered LR04 benthic $\delta^{18}O$ stack (cycles/kyr); superimposed on spectrogram is LR04 benthic $\delta^{18}O$ stack (Lisiecki and Raymo, 2005), (b) Ice rafted debris in the Norwegian Sea (Jansen et al, 2000), (c) North Atlantic SSTs from census counts of foraminifera (Ruddiman et al, 1989), (d) Eastern tropical Atlantic Alkenone-derived SSTs off the west coast of Africa (Schefuß et al, 2004), (e) EEP Alkenone-derived SSTs (ODP site 849) (McClymont and Rosell-Melé, 2005), (f) $\delta^{13}C$ record from Cibicidoides wuellerstorfi in North Atlantic (Raymo et al, 1990), (g) $\delta^{13}C$ record from EEP (ODP site 849) (Mix et al, 1995a,b), (h) $\delta^{13}C$ record from the South Atlantic/Southern Ocean (Hodell et al, 2003). Source: Clark et al (2006)

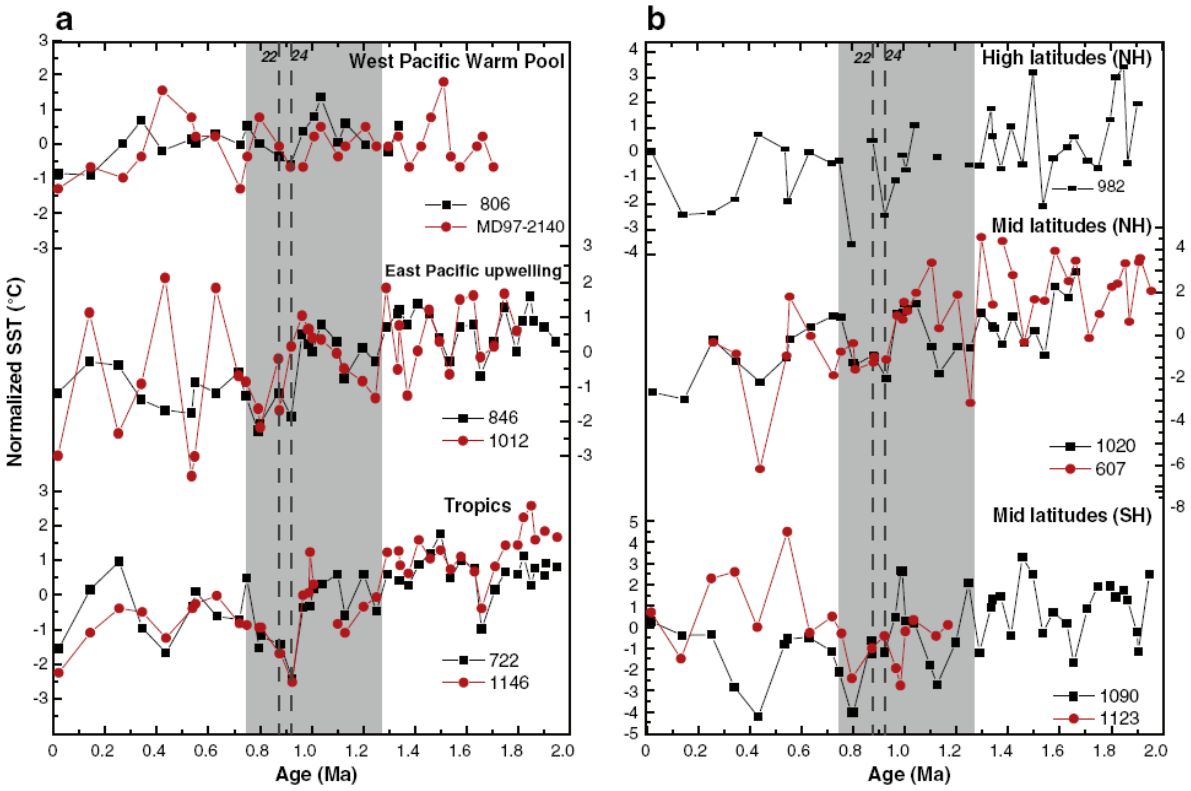

Figure 2.4: Glacial normalized SST trends from (a) tropical latitudes, (b) high northern and southern latitudes. Source: McClymont et al (2013)

Records of the Asian monsoon during the 900 ka event also pointed to an increase in wind intensity and aridity (increase in mean grain size and flux of terrigenous sediments) (Clark et al, 2006). More C4 vegetation was found in the Congo basin, suggesting more arid conditions (Schefuß et al, 2003). Deep ocean sites in the North Atlantic and Southern Ocean revealed low $\delta^{13}C$ values at ca.900 ka, and $\delta^{13}C$ values in both the central Atlantic and the Pacific (ODP core 849) were the most depleted at MIS 22 in the full 5 Ma record (Raymo et al, 1997; Hodell et al, 2003; Hoogakker et al, 2006). Elderfield et al (2012) argues the $\delta^{13}C$ excursion reflects an abrupt, rather than long-term, reorganisation of climate. Raymo et al (1997) suggest the cause for this was a contribution of terrestrial ^{12}C-enriched carbon into the oceans indicating arid terrestrial conditions and a reduced biosphere. However, this would potentially accompany an increase in atmospheric CO_2 (Broecker, 1982), which seems unlikely during the pronounced cooling as observed in SSTs

(McClymont et al, 2013). Another critique of this hypothesis is that during similar increases in aridity, low benthic $\delta^{13}C$ values were not recorded (Clark et al, 2006). Elderfield et al (2012) found a close relationship between seawater $\delta^{18}O$ and benthic $\delta^{13}C$ values from the west Pacific, and in fact $\delta^{13}C$ led $\delta^{18}O$ very slightly, suggesting that the low sea level and the resultant erosion of slope deposits may not be able to explain the $\delta^{13}C$ excursion over 100-ka timescales. Elderfield et al (2012) show a good relationship between a hydrographic tracer and their $\delta^{13}C$ values indicating the cause for $\delta^{13}C$ changes at their ODP site 1123 was partly deep ocean circulation, but also partly carbon reservoir.

The number of climate shifts across the globe at ca.900 ka suggests that an important threshold was crossed within the MPT. This thesis aims to reconstruct a sub-orbital-scale paleoclimate record during this time interval in the early Pleistocene. Very few studies have focused on this period in high resolution; in particular within the tropics and sub-tropics as high sedimentation rates prevent continuous, well-preserved sediment sequences (Zheng et al, 2005).

2.3 Proposed causes of the MPT

2.3.1 High latitude ice sheet dynamics

The majority of 'internal climate system' hypotheses put forward to explain the MPT and subsequent dominance of 100 kyr glacial interglacial cycles centre around high latitude northern hemisphere dynamics, such as sea-ice or ice sheet changes (Clark and Pollard, 1998; Ashkenazy and Tziperman, 2004; Huybers and Wunsch, 2005). This is partly an effect of the vast field of research dedicated to northern hemisphere climate and the large ice sheets that reside there. It has been argued that once the northern hemisphere ice volume exceeded a certain threshold value, the climate was tipped into a new phase of glacial cycles (Berger and Jansen, 1994; Clark and Pollard, 1998; Ashkenazy and Tziperman, 2004; Huybers and Wunsch, 2005). The cause for the increased ice-sheet size may be varied; from topography changes (e.g. tectonic uplift or regolith erosion), or a change in sensitivity to albedo and atmospheric CO_2 (Bergen and Jansen, 1994; Clark et al, 2006). Clark and Pollard (1998) have suggested that the cause for the change from high frequency, low amplitude glacial cycles (41 kyr) to low frequency, high amplitude cycles (100 kyr) is due to progressive sub-glacial erosion altering the soft-bedded Laurentide Ice Sheet to one of mainly hard bedrock. Their one dimensional ice sheet and bedrock model displayed linear deglaciation responses to orbital changes under "pre-MPT" deformable bed conditions, creating a thin ice sheet. With the "post-MPT" bedrock-sediment layer, the ice sheets were thicker and more likely to respond in a nonlinear fashion, and importantly would have sufficient inertia to escape deglaciation during increases in insolation (as discussed by Huybers and Wunsch, 2005). However, Elderfield et al (2012) suggest that anomalously low summer insolation in the southern hemisphere during MIS 23 suppressed melting of the ice sheet growth of MIS 22, and therefore the source of the MPT lies in the Antarctic. McClymont et al (2005) reconstructed a pronounced cooling of SSTs in the south east Atlantic ~230 kyr prior to the MPT, at around 1150 ka (MIS 32). Evidence exists to support the northwards migration of the Antarctic Circumpolar Current atmospheric fronts (Becquey and Gersonde, 2002; Diekmann and Kuhn, 2002) and the resultant reduction of warm

Agulhas waters into the study site, causing the SST drop. These cases give credence to the role the southern hemisphere may play in the development of the MPT.

However, on orbital timescales, Medina-Elizalde and Lea (2005) state that SST changes from three records within the EEP and WEP (west equatorial Pacific) lead foraminiferal $\delta^{18}O$ by 3 to 7 kyr at the 41 kyr period. This finding demonstrates that tropical SSTs lead continental ice volume, and argues against tropical climate variability being controlled by high latitude northern hemisphere ice dynamics (Medina-Elizalde and Lea, 2005). Rutherford and D'Hondt (2000) point out that pre-Pleistocene records which show 100 kyr climate oscillations were present when large ice sheets were not, and therefore the hypothesis whereby ice sheet growth is paced by Milankovitch forcing at eccentricity periods reveals inconsistencies (Herbert and Fischer, 1986; D'Hondt et al, 1996; Beaufort and Aubry, 1990; Crowley et al, 1992; Beaufort, 1994).

2.3.2 Greenhouse gas composition

Atmospheric greenhouse gas concentration changes have the capability to change climate on a global scale. Broccoli (2000) considers atmospheric CO_2 to be the primary source of radiative forcing during the LGM in the tropical ocean regions. The capacity for the atmosphere to absorb radiation is increased as greenhouse gas concentration increases (such as CO_2, CH_4, water vapour and nitrous oxides). Changes in concentration of these gases can occur due to a number of reasons; an increase in biological carbon pump strength, weathering and tectonic uplift, more tropical soils (as sources of CH_4 and N_2O) or more sea ice (reducing atmospheric partial pressure of CO_2 [pCO_2] from upwelling in the Southern Ocean) (Raymo, 1994; Flückiger et al, 1999; Stott et al, 2002; Stephens and Keeling, 2000; Sarnthein et al, 1988; Berger et al, 1999; Shackleton, 2000; Wang et al, 2003; in Zheng et al, 2005; Hönisch et al, 2009; Clark et al, 2006). Variations in greenhouse gas concentrations may explain the synchronicity of hemispheric glacial-interglacial cycles; orbital fluctuations are opposed between the northern and southern hemispheres but ice sheet development at orbital timescales throughout the majority of glacial-interglacial cycles is simultaneous between the polar regions, which suggests a process is in place to modulate insolation and create equivalent climatic responses at a global scale (Rays et al, 1976; Broecker and Denton, 1990).

Reconstruction of atmospheric gas content is notoriously difficult. Ice core records have captured direct atmospheric pCO_2 values back to 800 ka; between 450-800 ka, pCO_2 values were between 172 and 260 parts per million by volume (ppmv), compared to between 180 and 300 ppmv between 420 ka and the present (Petit et al, 1999; Siegenthaler et al, 2005; Lüthi et al, 2008). Prior to 800 ka (i.e. including the MPT), proxy records are employed to determine greenhouse gas levels.

Mudelsee and Schulz (1997) argue that a lower atmospheric CO_2 content would support an abrupt change in ice mass during the MPT (which would support their abrupt increase in benthic $\delta^{18}O$ values between ~942-902 kyr) as it would permit a higher rate of ice accumulation under cooler climate conditions. Carbon cycling modelling by Clark et al (2006) supports the hypothesis for thicker post-MPT ice sheets by Clark and Pollard (1998) by demonstrating that the weathering of marine shelf sediments during glacial lowstands would also reduce atmospheric pCO_2. Further

evidence for the atmospheric CO_2 driver lies in the late Pleistocene benthic foraminiferal record, where $\delta^{18}O$ has been shown to lag atmospheric CO_2 changes by a few thousand years, whereas atmospheric CO_2 is in phase with Antarctic air temperatures (Petit et al, 1999; EPICA community members, 2004), tropical SSTs (Lea, 2004) and bottom water temperatures (Shackleton, 2000).

If long-term atmospheric CO_2 changes were responsible for driving the MPT, a global cooling before and during the MPT would be expected. Medina-Elizalde and Lea (2005) found some observed variability in SST in the WEP, which it is argued could not be caused by varying thermocline depth as in the WEP it is deep and relatively impervious to changes in temperature. They found that lower SSTs in the west Pacific warm pool (WPWP) preceded changes in global ice volume (Medina-Elizalde and Lea, 2005). The equatorial Pacific is distant from the radiative effect of large continental ice sheets and therefore most easily influenced by radiative forcing from elsewhere, such as atmospheric greenhouse gas composition (Broccoli, 2000; Lea, 2004; Garidel-Thoron et al, 2005). Similarly, reductions in SSTs across the MPT have been observed in the North Atlantic (Ruddiman et al, 1989), tropical Atlantic (Schefuβ et al, 2004), and in the equatorial Pacific (Liu and Herbert, 2004; McClymont and Rosell-Melé, 2005); however not all studies agree. Schefuβ et al (2004) find that SSTs in the tropical Atlantic remained relatively stable before the ice volume increase. In the WEP, Garidel-Thoron et al (2005) found that temperatures were reasonably stable throughout the transition. McClymont et al (2013) found that SST records from a selection of sites globally did not show any cooling during interglacials prior to the ice expansion at 900 ka. Therefore in the absence of consistent global cooling beginning before the ice volume increase at ca.900 ka, Medina-Elizalde and Lea (2005) conclude that there is no evidence for long-term reduction in atmospheric CO_2, but suggest that changes in pCO_2 are important on orbital timescales, with the global carbon cycle being paced by obliquity in the early Pleistocene to precession after the MPT.

Hönisch et al (2009) use a multi-proxy approach in the equatorial Atlantic to build a low-resolution picture of the pCO_2 from 2.1 Ma to the present. Importantly, they determine pre-MPT pCO_2 levels were relatively stable. Glacial pCO_2 was slightly higher before the MPT (~1 Ma), which is explained somewhat by the characteristic smaller ice volume during 41 kyr glacials, and supported by higher pre-MPT SSTs, but importantly, interglacial pCO_2 was comparable to the late Pleistocene (Hönisch et al, 2009; Medina-Elizalde and Lea, 2005). Therefore they find little evidence that falling atmospheric CO_2 was a major driver for the MPT as there is no statistically significant shift on long timescales. Similarly, Hoogakker et al (2006) studied stacked benthic foraminifera $\delta^{13}C$ records from global oceans from 0-1.2 Ma and found a significant decrease in $\delta^{13}C$ from 1-0.9 Ma, followed by an increase from 0.9-0.5 Ma. A carbon cycle box model was used to infer the cause for these fluctuations, and the largest shift in atmospheric pCO_2 during the MPT was ~20 ppmv (parts per million by volume), which suggests the MPT was not driven by changes in atmospheric CO_2 concentrations (Hoogakker et al, 2006).

2.3.3 Tropical heat transfer

In addition to their potential effect on atmospheric greenhouse gas composition discussed above, the tropics provide heat and moisture to higher latitudes via ocean and atmospheric pathways.

Rutherford and D'Hondt (2000) found semi-precessional cycles (~11.5 kyr) present in within $CaCO_3$ and aeolian dust accumulation records in the tropical and sub tropical Atlantic from 1.5 Ma. Semi-precessional cycles are caused by insolation forcing from the bi-annual passage of the sun across the equator as part of each precessional cycle (Short et al, 1991) which in turn enhances meridional temperature gradients, and strengthens heat and moisture transport via ocean or atmospheric circulation to the poles from the low latitudes (Hernandez-Almeida et al, 2012). Therefore Rutherford and D'Hondt (2000) hypothesise increased oceanic or atmospheric heat transfer from the tropics to high latitudes since 1.5 Ma strengthened the semi-precessional cycle in the northern hemisphere, triggering the sustained glacial cycles on a 100 kyr timescale. Complementing this, numerical model research has suggested that cycles with a duration of 10 kyr are able to propagate higher amplitude 100 kyr cycles (LeTreut and Ghil, 1983).

Between 1350 and 900 ka, the EEP upwelling zones underwent long term surface cooling (Liu and Herbert, 2004), despite the WEP and northern hemisphere overall maintaining a relatively stable climate (in their review paper, McClymont et al (2013) determined there to be no statistically significant trend in WEP SSTs over the past 2 Ma). McClymont and Rosell-Melé (2005) suggest that the subsequent increased temperature difference between the east and west Pacific strengthened the Walker circulation. This may then have had the capability to reduce meridional heat transport, and increase moisture transport to the Laurentide ice sheet and higher latitudes via ocean and atmospheric processes, enabling ice sheet growth (McClymont and Rosell-Melé , 2005; Garidel-Thoron et al, 2005). The potential causes for cooling in upwelling zones are varied. Lyle et al (1992) found that SSTs in the equatorial Pacific are primarily influenced by southern hemisphere wind patterns over the past 250 kyr. This suggests the 10-15 kyr lead that central equatorial Pacific SSTs have over global ice volume may be due to a southern hemisphere influence, reflecting the slight asynchrony of insolation forcing between hemispheres (Lyle et al, 1992). Martinez-Garcia et al (2010) discover pronounced subpolar SST cooling between 1.8 and 1.2 Ma in both hemispheres, suggesting subpolar conditions expanded equatorward and caused contraction of tropical oceans. This cooling coincides with the marked increase in SST gradient between the WEP and EEP, and therefore the subpolar cooling is hypothesised to have caused thermocline shoaling in the EEP, driving the development of the EEP cold tongue and more intense atmospheric circulation (Martinez-Garcia et al, 2010; McClymont and Rosell-Melé, 2005; Bush and Philander, 1998). Another theory is that EEP SST changes may be related to discrete density variations in the deep ocean, due to the proximity of the eastern boundary currents to deep water-forming areas. This is indicated by similar $\delta^{13}C$ records in the North Atlantic and Pacific, which points to a reorganisation of deep ocean circulation (Mix et al, 1995). These density variations are capable of influencing water column stratification and shallowing thermocline depth, thus affecting surface ocean temperature (Philander and Federov, 2003; McClymont and Rosell-Melé, 2005; Garidel-Thoron et al, 2005; Medina-Elizalde and Lea, 2005). Similarly, cooling of deep waters during the Pliocene and Pleistocene (e.g. Lear et al, 2000; Tian et al, 2002) and associated shoaling of the thermocline have been suggested as a cause for reduced EEP SSTs (Philander and Fedorov, 2003; Ravelo et al, 2004).

In general, tropical Pacific circulation is relatively under-studied, and therefore there is a relative lack of understanding of the tropical Pacific throughout the MPT. Within studies of the EEP, the presence of SST cooling across the MPT has been well documented (McClymont and Rosell-Melé, 2005; Liu and Herbert, 2004; Lawrence et al, 2006; Wara et al, 2005, Dekens et al, 2007), but the causes for this are unresolved. Studies have focused mainly on SST changes, although other indicators of circulation change could be informative. Given the potential for tropical ocean and atmospheric circulation to affect high latitudes and thus global climatic change, as described above, further research on tropical Pacific surface and deep ocean dynamics are fundamental to understanding the MPT in full.

2.4 The tropical Pacific Ocean

The Pacific Ocean has been proposed as the instigator, amplifier and/or moderator of global climate change on timescales from inter-annual to glacial-interglacial (Cane, 1998). Studies have shown that the tropical Pacific ocean-atmospheric system has changed in strength at glacial-interglacial and millennial timescales (Lea et al, 2000; Tudhope et al, 2001; Koutavas et al, 2002; Stott et al, 2002). The tropical Pacific ocean is an important locus of atmospheric convection and supplies heat and moisture to higher latitudes (Rahmstorf, 2002; Lea, 2002; Cane, 1998), and has been proposed as a region capable of driving expansion or contraction of the northern hemisphere ice sheets (Kukla and Gavin, 1992; McClymont and Rosell-Melé, 2005; Lea et al, 2000). The tropical latitudes also emit a vast amount of water vapour into the atmosphere, which as a greenhouse gas has the potential to amplify global climate change (Peterson et al, 2000).

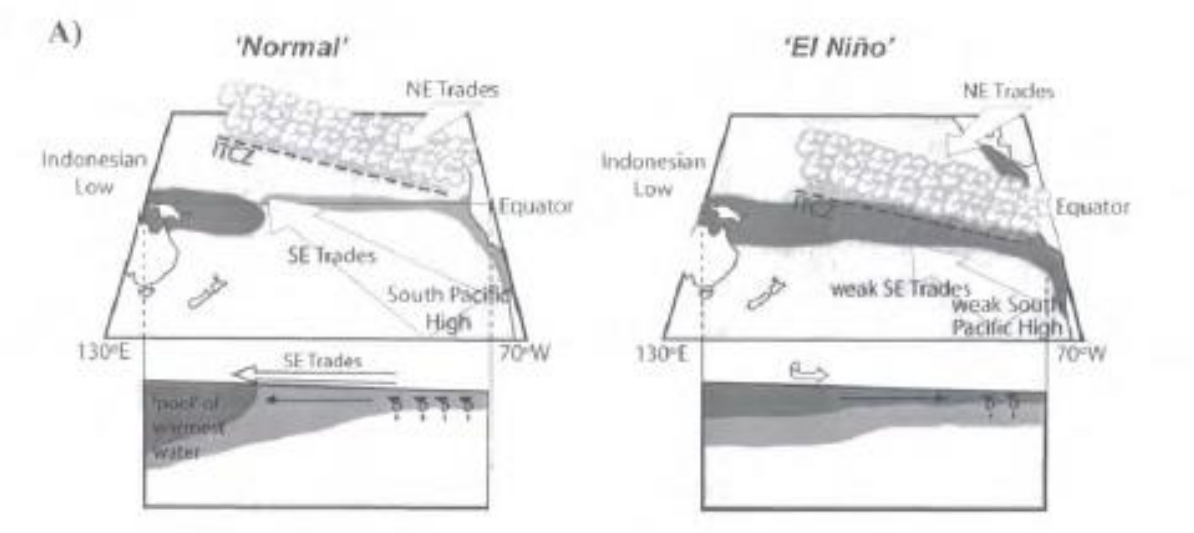

Figure 2.5: The El Niño Southern Oscillation (ENSO). A comparison of ocean-atmosphere circulation during 'Normal' and 'El Niño' conditions. Dark shading indicates warm surface waters; light grey shading indicates eastern Pacific cold tongue. Source: Wilson et al (2000, p.34)

In the late Quaternary and Holocene, the inter-annual El Niño Southern Oscillation (ENSO) and seasonal and millennial-scale shifts in the Inter-tropical Convergence Zone (ITCZ) modify global climate, often through strong feedbacks (Peterson et al, 2000; Stott et al, 2002; Koutavas et al, 2002; Benway et al, 2006; Trenberth et al, 1998; Ropelewski and Halpert, 1987; 1989; Barry and

Chorley, 2003: 303, 308). Today, ENSO is the most dominant process governing inter-annual variability in climate, specifically in the eastern Pacific (Tudhope et al, 2001, Rahmstorf, 2002). ENSO is essentially a positive feedback within the ocean-atmosphere system over the tropical Pacific; and an example of the ocean and atmosphere system acting as one (Clement et al, 1999). During the warm phase of ENSO (El Niño), a decreased zonal Pacific SST gradient causes a relaxation of trade winds, reducing upwelling in the EEP and deepens the EEP thermocline (figure 2.5) (Clement et al, 1999). During the cold phase of ENSO (La Niña), the feedbacks do the reverse (i.e. an extreme version of the 'normal' mode in figure 2.5) (Clement et al, 1999). ENSO modifies the intensity of the zonal atmospheric Hadley circulation, which has been argued to alter the rate of ice sheet growth in high latitudes through variations in the poleward transport of moisture and heat (Lindzen and Pan, 1994; Kukla and Gavin, 1992). Modelling studies show that during the last glacial-interglacial cycle, ENSO-related freshwater fluxes in the tropical latitudes may have considerably influenced deep and intermediate water formation in high boreal latitudes (Schmittner and Clement, 2002). The hypothesis that ENSO operates over glacial-interglacial cycles leads to the suggestion that ENSO could be responsible for reduced or collapsed upwelling in the tropical Pacific; hence ENSO could explain the lower atmospheric concentrations of CO_2 and CH_4 (the main, preindustrial source of CH_4 and CO_2 is from the tropics, partly from upwelling), which were documented in the Greenland ice cores (Stauffer et al, 1998; Flückiger et al, 1999). The eastern Pacific cold tongue is particularly sensitive to regional oceanographic influences, such as thermocline depth during ENSO variations (Fiedler, 2002; Cane, 2005; Philander and Federov, 2003). The latitudinal movement of the ITCZ affects wet and dry seasons of the tropical regions, and therefore knowing its glacial position is incredibly important when reconstructing the climate (Denton et al, 2010). The location of the ITCZ over glacial-interglacial timescales has been shown to be affected by high-latitude events, such as the expansion of the Laurentide Ice Sheet and sea ice in the North Atlantic (Denton et al, 2010).

The role played by circulation systems in the tropics during glacial-interglacial cycles is a continuing discussion within the climate research community. In 1976, members of the CLIMAP project predicted only a ~1ºC SST decrease during the LGM, and so argued that glacial cycles had very little effect on the tropics. However, Rosell-Melé et al (2004) found that tropical SSTs at the LGM fell by up to 4ºC (average 2ºC), using alkenone analysis and general circulation models. Studies using coral records and Mg/Ca ratios of planktonic foraminifera have predicted similar temperature changes (Lea et al, 2000; Koutavas et al, 2002; Stott et al, 2002; Visser et al, 2003; Guilderson et al, 1994; Gagan et al, 2000). Most interpretations of tropical Pacific Ocean circulation changes argue for an atmospheric driver i.e. that as wind systems strengthen or weaken, so the east Pacific upwelling and ocean circulation changes as observed during modern ENSO events. For example, in the north-east tropical Pacific (Gulf of California) it has been suggested that due to the proximity to the Laurentide Ice Sheet during glacial periods of the late Quaternary, there was a likely influence on local atmospheric circulation (and upwelling intensity) by the ice sheet (Cheshire et al, 2005; Ganeshram and Pedersen, 1998; McClymont et al, 2012). From an ocean circulation perspective, the southern hemisphere and tropical Pacific are intimately linked; it has been argued that during the Pleistocene the tropical Pacific was connected to the southern high latitudes via an

oceanic pathway (“oceanic tunnel”) through the EUC; conveying climate signals from the extratropics to the tropics (Koutavas and Sachs, 2008).

In the modern Pacific Ocean, there is a pronounced temperature gradient from east to west, with a tilted thermocline, and an atmospheric limb known as the Walker circulation (figure 2.5). During the Pliocene, ca.4.3 Ma, a previously non-existent slight equatorial Pacific temperature gradient emerged, in the location of the present day EEP cold tongue (Lawrence et al, 2006). The most pronounced change however, occurred between ca.1.8-1.2 Ma, during which both subpolar and EEP SSTs experienced distinct cooling (Wara et al, 2005; Martinez-Garcia et al, 2010). The inferences from this are twofold; firstly it suggests an expansion of polar oceans towards the well-developed Pacific warm pool, as well as an associated formation of Antarctic sea ice being probable, drawing on comparable SST drops at the LGM (Gersonde et al, 2005). Secondly it implies the EEP cold tongue expanded to its present day form, strengthening the zonal Pacific temperature gradient, ahead of the main MPT (Wara et al, 2005; Martinez-Garcia et al, 2010). Martinez-Garcia et al (2010) found that as the meridional gradient in SST between subpolar and the equatorial Pacific increases, the zonal gradient between east and west Pacific also increases. This correlation depicts the close connection between subpolar and equatorial oceanic regions and the capacity for subpolar ocean surface temperature to affect equatorial Pacific thermocline shoaling. The cause for this development is unknown, since during this time period global ice volume was relatively stable (Lisiecki and Raymo, 2005). However, since Martinez-Garcia et al (2010) draw only on evidence for SST change, it is difficult to deduce exactly how the ocean-atmosphere interactions occurred (e.g. more EEP upwelling or changing properties of the upwelling waters). This is motivation for a multi-proxy analysis focusing not only on equatorial SST change, but also productivity and upwelling, which will be undertaken in this thesis.

2.5 The east equatorial Pacific

The EEP exhibits significant seasonal and interannual climate variabilities unparalleled in the rest of the Pacific; it is particularly sensitive to small changes in the ocean-atmosphere system (as demonstrated in figure 2.5). Slight changes in the temperature difference across the thermocline, or to the depth of the thermocline, can significantly affect surface ocean conditions; for example if the thermocline in the EEP deepens, trade winds bring warmer water to the surface ocean, lessening the zonal temperature gradient and further weakening the Walker circulation (Philander and Federov, 2003).

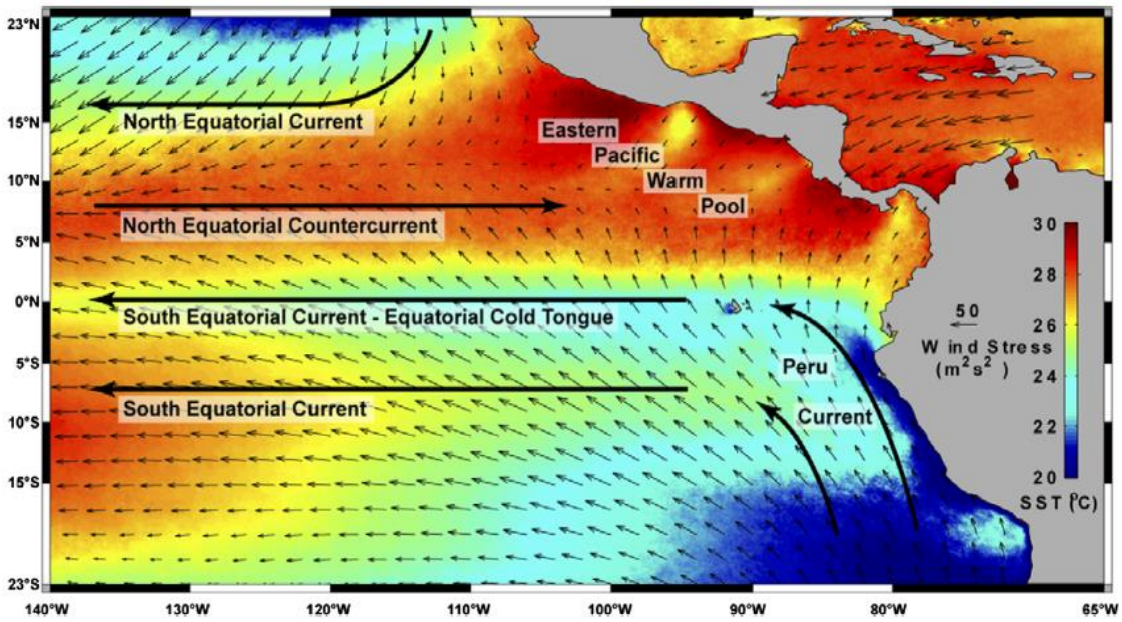

Figure 2.6: Average SST, wind stress and major surface currents in the EEP. Thick black lines denote major currents, thin black lines are a wind stress climatology (1999-2003), colours are a SST climatology (1997-2003). Source: Pennington et al (2006)

The equatorial Pacific Ocean circulation system consists of three major surface currents and one subsurface current (figure 2.6) (Pickard and Emery, 1990, p.235). The circulation of the equatorial Pacific is determined by its location between two anti-cyclonic gyres, and it is driven by regional trade winds (Le et al, 1995). The north equatorial current (NEC) and south equatorial current (SEC) are westward-flowing and extend from 8°N to 20°N and 10°S to 3°N, respectively. The north equatorial counter-current (NECC) flows eastward between the two equatorial currents, transporting low-salinity water (Wyrtki, 1981; Delcroix et al, 1987). The subsurface equatorial undercurrent (EUC) is eastward flowing (between 2°S to 2°N); its source waters are formed north of the sub-Antarctic front (sub-Antarctic mode water) (Toggweiler et al, 1991). The EUC ascends with the thermocline in the east Pacific, and so decreases in depth from ~150-200m at 165°E (Delcroix et al, 1987) to 30-50m to the west of the Galapagos islands (Wyrtji, 1981).

The EEP is dominated by the east Pacific cold tongue (SEC); a low-temperature, nutrient-rich extension of the eastern boundary Peru Current, extending 130°W into the Pacific (Wyrtki, 1981). The cold tongue lies within the high-productivity equatorial divergence zone, produced partly by advection of eastern boundary waters and partly by equatorial divergence (of coreolis-forced southeasterly trade winds) causing Ekman transport and upwelling (Chaisson, et al, 1995; Wyrtki, 1981; Fiedler and Talley, 2006). The equatorial front in the EEP, situated between the east Pacific warm pool (EPWP) and the east Pacific cold tongue, exhibits a globally-renowned steep SST-gradient (figure 2.6) (Deser and Wallace, 1990). The core site chosen for this study, ODP site 849, is located in the heart of the modern EEP cold tongue.

2.6 The biological carbon pump

In this study, both the physical (SST, thermocline depth) and biological (primary productivity) properties of the east Pacific will be examined across the MPT. This will allow interpretation of the role played by upwelling in this region, but will also provide information of the activity of the marine biota.

Biological activity enables the absorption of atmospheric CO_2 into the upper ocean as phytoplankton perform photosynthesis and lower the partial pressure of CO_2 in the surface ocean, enabling CO_2 drawdown (Falkowski et al, 2000). This is known as the biological carbon pump. High levels of primary productivity are capable of strengthening the pump, and it is this, along with higher preservation potential, that increases the flux of carbon to the deep ocean (Shaffer, 1993; Falkowski et al, 2000). The limiting factor for primary productivity is nutrient availability. This is determined by the strength of upwelling (the upward limb of the physical carbon pump), the nutrient content of the upward-cycling water, ocean circulation, wind intensity, and aeolian or fluvial input of terrestrial (nutrient-bearing) sediments.

A strengthened biological pump in the tropical ocean may play a vital role in the MPT. Sarnthein et al (1988) found that an increase in the strength of the biological carbon pump during glacials leads to a drawdown of pCO_2 in the late Pleistocene. During glacial periods, moisture is locked up within glaciers and continental ice sheets, so aridity and strengthened atmospheric circulation increases aeolian dust flux, and therefore the supply of iron, to surface waters. Iron from continental sources is a known limiting factor for productivity in the EEP, as well as the Southern Ocean (Martin, 1990; Chavez et al, 1991; Martin et al, 1991). Thus, an input of the limiting nutrient during periods of cooling may enable a positive feedback cycle whereby enhanced production ultimately lead to pCO_2 drawdown and continued declining temperatures. Ruddiman (2003) proposed that this mechanism may have been key in pushing the planet into 100 kyr cycles, with the proposition that the pCO_2 feedback is strongest at the obliquity frequency. Continental ice sheet size affects trade wind strength, and thus aeolian dust flux in the tropics, and so when precession and eccentricity are also low, this is when greater glacial-interglacial cycles with durations of 100 kyr may have been encouraged (Ruddiman, 2003).

An understanding of productivity is therefore vital to understanding the exchanges between carbon cycling and climate (Harris et al, 1996). The dominant primary producers in the EEP are indicative of subtropical gyres; dinoflagellates, diatoms and blue-green algae, as well as coccolithophores (Chavez, 1989; Chavez et al. 1990, 1991, 1996; Landry and Kirchman, 2002; Mayer et al, 1992). It is the combination of the tilted east-west Pacific thermocline, thermocline shallowing at oceanic gyre boundaries, and small-scale wind-driven upwelling that dictate the levels of productivity in the EEP (Pennington et al, 2006). Therefore ideal settings for high surface ocean productivity require a shallow thermocline within the euphotic zone (Pennington et al, 2006). Biological productivity is also dependent on the macronutrient supply from beneath the thermocline, with the EUC being an important source of nutrients for equatorial upwelling in the EEP (Pennington et al, 2006). Waters sourced from the EUC are upwelled in both the equatorial divergence zone whilst flowing eastward,

and along the eastern boundary Peru Current (then transported via advection to the EEP) (Pennington et al, 2006; Wyrtki, 1981; Toggweiler et al, 1991).

2.7 Proxies for paleoclimate

Arguably, the best-defined direct record of 100 kyr cycles of the late Quaternary is found within the $\delta^{18}O$, pCO_2 and pCH_4 records from Greenland and Antarctic ice cores (Petit et al, 1999). The $\delta^{18}O$ of deep-sea sediments (Shackleton and Opdyke, 1976; Keigwin, 1978; 1979; Lisiecki and Raymo, 2005) is also a reliable and prolific indicator of past ice volume, salinity and temperature. Deep-sea sediments also record aeolian dust particle flux (Janecek, 1985), and changes in marine fauna (Chaisson, 1995) and flora. More recent biogeochemical methods, including the analysis of biomarkers, have provided past SST records (Brassell et al, 1986; Prahl and Wakeham, 1987; Eglinton et al, 2001), alongside indicators of salinity (Rosell-Melé, 1998, Sikes and Sicre, 2002), primary productivity (Budziak et al, 2000), and pCO_2 (Jasper and Hayes, 1990). In this section, the key proxies to be analysed in this thesis will be discussed, focusing on foraminifera stable isotopes and the alkenone and chlorin biomarkers.

2.7.1 Foraminiferal stable isotopes

Calcareous marine organisms secrete their carbonate shells or skeletons from the surrounding seawater. The isotopic ratio of oxygen and carbon within the seawater at the time the marine organism existed will therefore be imprinted within their carbonate structure (Lowe and Walker, Ch. 3, pg. 150). The main cause of changes to the global oxygen isotope signal in seawater is fluctuating polar ice mass (Loubere and Austin, 2007) but temperature and salinity are also important contributors. Carbon isotope shifts are harder to interpret, since they reflect local ocean changes in photosynthesis and upwelling, global shifts between ocean and land, and a range of foramininferal habitat factors (Ravelo and Hillaire-Marcel, 2007).

Of all the micro-marine organisms that preserve the isotope ratio of their oceanic habitat, it is benthic and planktonic foraminifera that are the most widely used as climatic reconstruction proxies. This is largely due to their abundance and variety in marine sediments extending back to the Cambrian, their high preservation potential and easily identifiable form (Boersma, 1980; Dowsett, 2007; Pearson, 2012). Benthic foraminifera tests can be composed of secreted calcite, aragonite, or agglutinated sediment, whereas planktonic tests are exclusively made up of secreted calcium carbonate (Loubere and Austin, 2007; Dowsett, 2007).

2.7.1.1 Stable oxygen isotopes ($\delta^{18}O$)

The use of stable oxygen isotope analysis on deep ocean sediments has had the biggest effect on Quaternary science (Lowe and Walker, Ch. 3, pg.148). The $\delta^{18}O$ of benthic foraminifera is widely used as an indicator of past ice volume changes, and played a huge role in the discovery and demonstration of Milankovitch cycles throughout paleoclimatic history (Lowe and Walker, Ch. 3, pg. 149). Likewise, stable isotope analysis of planktonic foraminifera are a common component to paleoeanographic reconstructions (Stott et al, 2002; Behl and Kennett, 1996; Hendy et al, 2002)

and reflect changes to conditions close to the sea surface. It should be noted that the annotation $\delta^{18}O$ reflects the ratio of ^{18}O and ^{16}O in a measured sample against a known international standard:

$$\delta^{18}O = \frac{(^{18}O/^{16}O_{sample} - {}^{18}O/^{16}O_{standard})}{(^{18}O/^{16}O_{standard})} \times 1000$$

The units for $\delta^{18}O$ are ‰. A sample enriched in ^{18}O relative to the standard will show a positive value. Since the common standard Pee Dee Belemnite is no longer available, various comparative standards are used in its place, monitored by the National Institute of Standards and Technology and the International Atomic Energy Agency.

The application and interpretation of the $\delta^{18}O$ signal relies on the discrimination between the common ^{16}O and more rare ^{18}O isotopes within an environment. The quasi-cyclicity of the benthic $\delta^{18}O$ signal (figure 1.1) over glacial-interglacial cycles reflects the preferential evaporation of ^{16}O, which becomes stored in the ice sheets (and thus removed from the seawater) during glacial periods, in turn increasing the $\delta^{18}O$ ratio in seawater (Lowe and Walker, Ch. 3, pg. 150). Both temperature and salinity also control $\delta^{18}O$ in seawater, especially close to or at the sea surface, where inflows of fresh water tend to provide more ^{16}O, and where warmer SSTs also tend to cause preferential evaporation of ^{16}O. In the deep sea, temperature and salinity change very little, so that the dominant control over benthic $\delta^{18}O$ is global ice volume. The global signal of $\delta^{18}O$ led to the application of marine isotope stages (figure 1.1), enabling global stratigraphic parallels to be drawn (Lowe and Walker, Ch. 3, pg. 151).

Foraminifera are adapted to all marine environments, however, different species have different requirements and so their geographic distribution, and/or dominance, varies depending on these. Their preferred habitat is determined primarily by temperature and salinity, but also nutrient concentration, water density, oxygen and carbon dioxide gas concentration, substrate (if benthic), community members and food source (Dowsett, 2007; Loubere and Austin, 2007). Planktonic species diversity increases in the tropics, due to a lack of distinct seasons (Chaisson, 1995). In these low latitude environments, depth zonation is observed (Be, 1960; Fairbanks and Wiebe, 1980; Gasperi and Kennett, 1992; 1993). This is likely a product of the temperature gradient downward throughout the water column, as well as the decreasing nutrient supply associated with it (figure 2.7) (Loubere and Austin, 2007).

As a result of the different habitats and life-cycles of planktonic foraminifera, the $\delta^{18}O$ difference between shallow- and deeper-dwelling species is a valuable indicator of temperature gradients, and in turn of surface water stratification and subsequently thermocline depth (Farrell et al, 1995; Chaisson and Ravelo, 2000; Cannariato and Ravelo, 1997; Wara et al, 2005). Although the textbook trend of high latitudes being dominated by precipitation and low latitudes being dominated by evaporation would presume the tropics would have more saline waters and therefore higher $\delta^{18}O$, tropical precipitation has a higher $\delta^{18}O$ and therefore the gradient between $\delta^{18}O$ and the salinity of seawater is less steep. This means the $\delta^{18}O$ values of open-ocean tropical and sub-

tropical surface water is relatively uniform; between 0.2-0.5% in the Pacific (Ravelo and Hillaire-Marcel, 2007). In the modern-day EEP, the $\delta^{18}O$ of ambient water (or d_w) is near-constant throughout the year, as the salinity is relatively stable and given no evidence to assume the salinity changed greatly during the MPT, this is considered unlikely to have a large effect on the planktonic $\delta^{18}O$ here (Farrell et al, 1995). This is demonstrated in the weak modern day salinity gradient in figure 2.7 [B]. In summary, a difference in $\delta^{18}O$ between species is an indicator of the difference in temperature (ΔT) between the depth ranges for different foraminifera species (Wara et al, 2005).

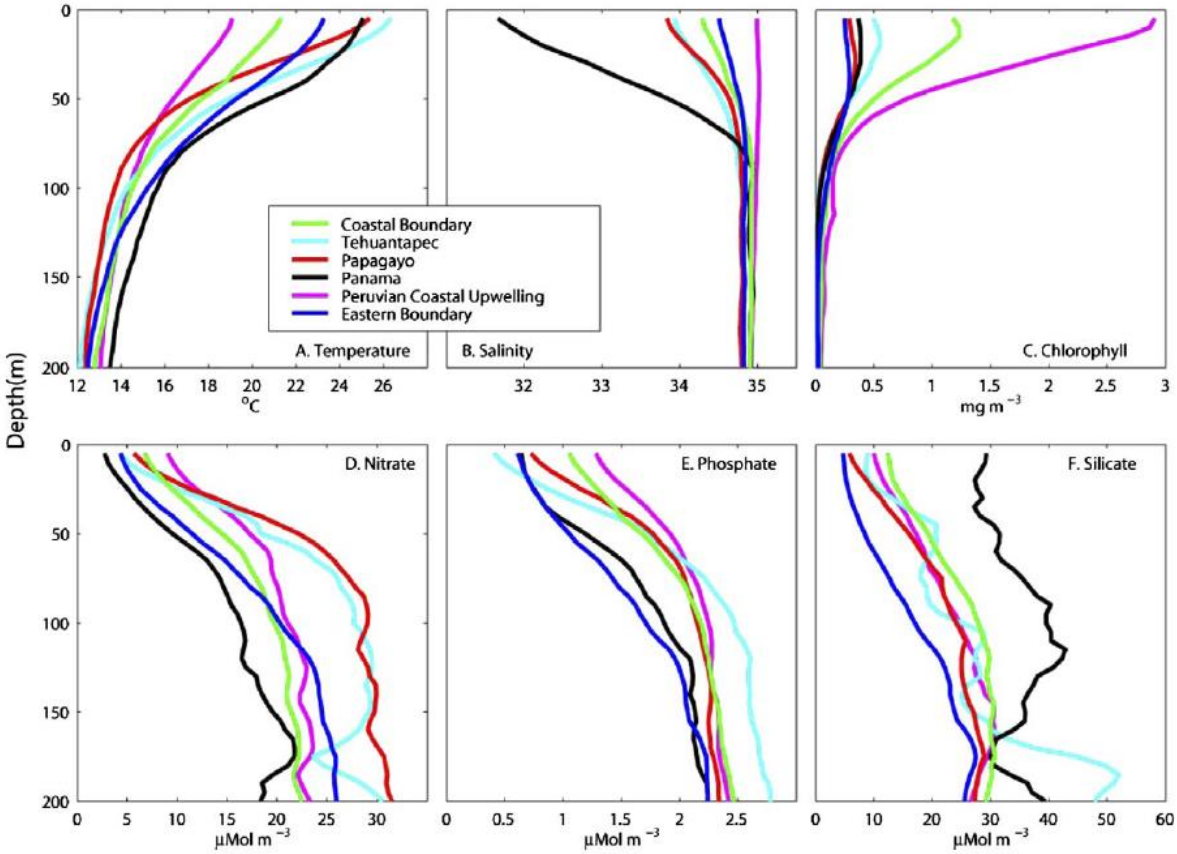

Figure 2.7: Mean profiles of physical, nutrient and chlorophyll values from oceanographic stations in the EEP (0-200m). Source: Pennington et al 2006

Tropical Pacific foraminiferal assemblages are dominated by two or three main species; two of these dominant species, *Neogloboquadrina dutertrei* (*N.dutertrei*) and *Globigerinoides ruber* (*G.ruber*), are the planktonic formainifera species used in this study (Chaisson, 1995). *G.ruber* is a shallow-dwelling species which exists in the surface mixed layer, whereas *N.dutertrei* exists in the subsurface waters of the shallow thermocline (10-40m); it is also found in high-productivity and nutrient-rich regions and in upwelling zones such as the eastern equatorial cool-tongue (Farrell et al, 1995; Fairbanks et al, 1982; Douglas and Savin, 1978). *N.dutertrei* tend to dominate the tropical foraminifera assemblage when the thermocline shoals due to upwelling (Farrell et al, 1995; Chaisson, 1995). Conversely, during interglacials in the tropical Pacific, evidence has pointed to an increase in the abundance of tropical surface-dwellers such as *G.ruber*, *G.sacculifer* and *G.glutinata* (Le et al, 1995, Chaisson, 1995).

There are a number of factors to consider when reconstructing $\delta^{18}O$ from both planktonic and benthic foraminifera species. Previous studies in the east equatorial Pacific have documented a lack of correlation between *N.dutertrei* abundance and glacial-interglacial cycles, whereas *G.ruber* abundance has shown a strong correlation (Le et al, 1995). However, it is noted that species can survive glacial-interglacial cycles with their isotopes recording the cycles. It is understood that benthic and planktonic foraminifera $\delta^{18}O$ primarily record ice volume signal (Loubere and Austin, 2007). However benthic $\delta^{18}O$ values are not immune to changes in deep water temperature; every $\delta^{18}O$ signal is affected partly by temperature as the precipitation of carbonate depends on temperature changes (Lowe and Walker, 1994; Elderfield et al, 2012). Equally, planktonic $\delta^{18}O$ values may be affected by other environmental factors such as SSTs and salinity (e.g. Duplessy et al, 1992; Maslin et al, 1995). The 'vital effects' of the species themselves may have played a minimal part in the $\delta^{18}O$ signal preserved in the fauna shell, caused by photosynthesis of algal symbionts, carbonate ion concentrations and changes in test growth rate during the foramininferal life cycle (Ravelo and Hillaire-Marcel, 2007). It is probable that *N.dutertrei* does not have algal symbionts (Ravelo and Fairbanks, 1992), and so any vital effects to this species are due to changes in size (Ravelo and Fairbanks, 1995). The combined analysis of both benthic and planktonic $\delta^{18}O$ analyses, as well as the addition of independant proxies for SST (the approach undertaken here) allows these different factors to be assessed in the interpretation of the proxy records. The $\delta^{18}O$ from the planktonic foraminifera species, *G.ruber* and *N.Dutertrei,* are used here to reconstruct surface water stratification and complement alkenone-derived SSTs.

2.7.1.2 Stable carbon isotopes ($\delta^{13}C$)

Carbon in a marine environment is known as dissolved inorganic carbon (DIC), and is made up of aqueous ($CO_2(aq)$), bicarbonate (HCO_3^-) and carbonate (CO_3^{2-}) ions; of which the bicarbonate form contributes ~90%, carbonate ~10% and aqueous CO_2 ~1%. Of the two stable carbon isotopes, ~ 1.1% is the heavier ^{13}C isotope; 98.9% is the lighter ^{12}C isotope (Marchitto, 2007). The relative proportion of ^{13}C within marine organism carbonate is determined by primary productivity, ocean circulation, the global carbon cycle and degradation of organic carbon (see figure 2.8) (Hönisch and Hall, 2007). The relative accumulation of this carbon is also affected by a number of constraints; planktonic foraminifer test size, biological processes, pH of seawater, and growth temperature (Hönisch and Hall, 2007).

The calcite tests of both benthic and planktonic foraminifera are made up of bicarbonate ions, and thus translate the ^{13}C signal of DIC (Hönisch and Hall, 2007). Changes in the $\delta^{13}C$ of DIC of seawater in the *global* ocean depend on the size of the terrestrial biosphere and/or a change in the sink/sources to the global carbon cycle, for example carbon release and growth in the lithosphere and biosphere (Ravelo and Hillaire-Marcel, 2007). Whereas changes in the DIC $\delta^{13}C$ of the *local* ocean include the balance between photosynthesis and respiration, changes in the relative contribution of water masses, and the signature of the source water for the locality (Ravelo and Hillaire-Marcel, 2007).

Benthic foraminifera have been shown to closely record $\delta^{13}C$ values of deep water DIC (Duplessy et al, 1984) and reconstructions have been used to assess deep water extent and reorganisations,

and atmospheric CO_2 (Duplessy et al, 1988; Curry and Oppo, 2005; Sigman and Boyle, 2000). Planktonic foraminifera record $\delta^{13}C$ with more difficulty as more factors can affect their $\delta^{13}C$ signal; for example symbiotic relationships, photosynthesis/respiration and carbonate chemistry (Keigwin and Boyle, 1989; Spero, 1998). Many studies have used $\delta^{13}C$ to indicate the ratio of respiration to photosynthesis as an indicator of paleoproductivity during glacials and interglacials (e.g. Zahn et al, 1986; Sarnthein et al, 1988). Atmospheric CO_2 levels can also be reconstructed by modelling the difference in $\delta^{13}C$ between surface and deep waters as a proxy for nutrient concentration, which determines productivity, and associated atmospheric CO_2 levels (Shackleton et al, 1983).

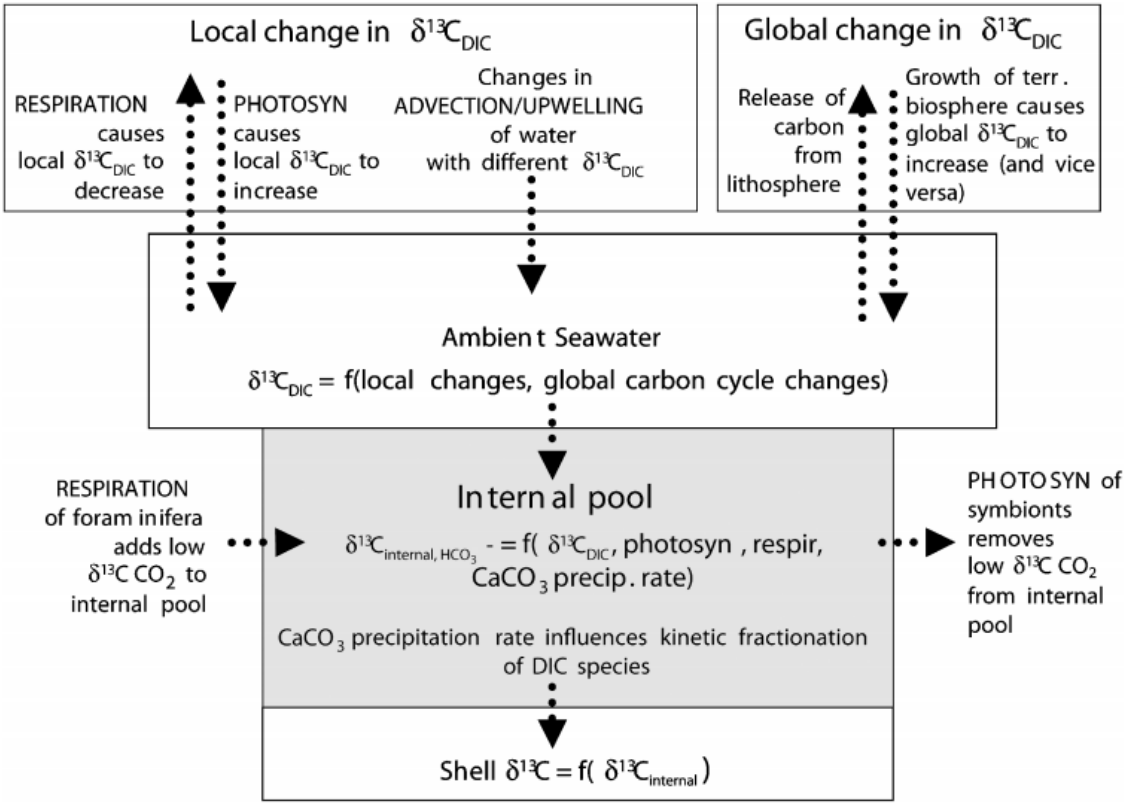

Figure 2.8: Factors that influence the $\delta^{13}C$ of foraminifera shells. Source: Ravelo and Hillaire-Marcel (2007)

Surface waters are generally enriched in ^{13}C compared to their deep water counterparts. This is due to a number of factors. As surface water become more highly productive, during photosynthesis organisms preferentially take up ^{12}C, and so ^{13}C levels proportionally increase. As organic matter decays and falls through the water column, ^{12}C is regenerated along with essential nutrients such as phosphate and nitrate. Nutrient levels tend to be reversely correlated with ^{13}C levels for this reason. This process is termed 'biogeochemical cycling' (Hönisch and Hall, 2007). Secondly, the extent of air-sea exchange determines the isotopic composition of surface waters. If the carbon content in ocean and atmosphere were at isotopic equilibrium, the proportion of $\delta^{13}C$ in DIC could theoretically be enriched by atmospheric CO_2, due to the dominance of bicarbonate ions in surface waters (Lynch-Stieglitz et al, 1995). In reality, isotopic equilibrium takes a longer period of time to complete than is available for surface ocean mixing to take place. Therefore surface water $\delta^{13}C$ may be enriched through longer air-sea contact times, or high wind strength, in addition

to the biogeochemical cycling process (Hönisch and Hall, 2007). Another factor is that as $CO_{2(aq)}$ and atmospheric CO_2 are isotopically light compared to the bicarbonate (HCO_3^-)and carbonate (CO_3^{2-}) ions that make up the remainder of DIC. Due to latitudinal variations in ocean temperature, and therefore partial pressures of CO_2, some oceans are net absorbers of atmospheric CO_2 (e.g. North Atlantic) and have lower $\delta^{13}C$ values than areas which emit CO_2 (e.g. EEP) (Kroopnick et al, 1977; Lynch-Stieglitz et al, 1995).

2.7.2 Chlorin pigments

Chlorophyll is a photosynthetic pigment produced by all phytoplankton, and an essential component for photosynthesis to occur. Therefore the concentration of chlorophyll in surface waters is an indicator of total marine primary productivity and algal biomass (e.g. Harris et al, 1996; Jeffrey et al, 1997) with the most productive surface oceans overlying the most organic matter-dense marine floors (figure 2.9).

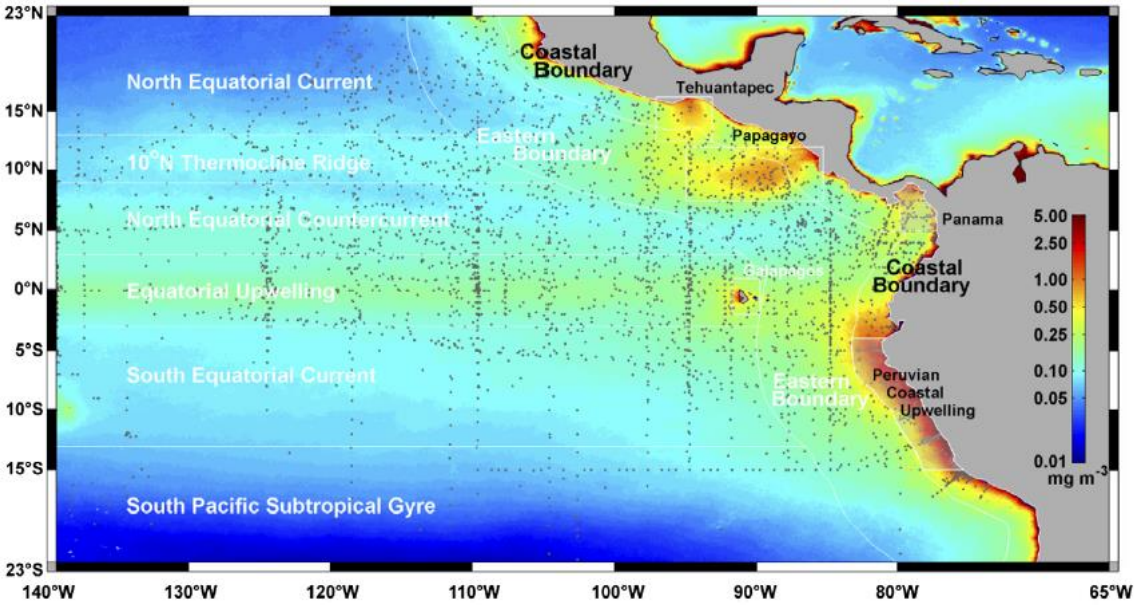

Figure 2.9: EEP chlorophyll (in colour) and locations of ship-collected measurements (grey dots). Source: Pennington et al (2006)

Chlorins are the diagenetic (transformation) products of chlorophyll, and are therefore biomarkers for past productivity. Chlorins are analysed in marine sediments because chlorophyll is not preserved, due to the fast rate at which chlorophyll degrades in the water column following production due to exposure to oxygen, heat and light (Louda et al, 1998; Harris et al, 1996; Jeffrey et al, 1997). Muller and Suess (1979) pioneered the use of chlorins as primary productivity indicators. Despite the fact that less than 1% of chlorophyll produced is preserved in marine sediments as chlorins, several studies have determined good correlations between chlorin accumulation rates and modern surface water productivity levels (Harris et al, 1996; Higginson, 2000; Shankle et al, 2002). Other paleoproductivity/biomarker proxies such as biogenic Opal (Harris et al, 1996) and total organic carbon (TOC) (Gebhardt et al, 2008; Harris et al, 1996; Zhao et al, 2006) have correlated well with chlorin abundances (Summerhayes et al, 1995; Harris et al,

1996; Ishiwatari et al, 2009). Studies have been conducted in the South Atlantic (Summerhayes et al, 1995), North Atlantic (Higginson, 2000), North-east and -west Arabian Sea (Schubert et al, 1998; Altabet et al, 2002; Higginson et al, 2004), and in the SCS (Higginson et al, 2003).

The study of chlorins as an indicator of carbon transfer from the euphotic zone is most valuable when used as part of a multi-proxy approach (Zhao et al, 2006). Schubert et al (1998) studied the paleophytoplankton community in the North Arabian Sea over the past 200 kyr, using a multi-biomarker-proxy based approach, one of the first to do so. They tracked inputs from haptophytes (alkneones), diatoms (brassicasterol), dinoflagellates (dinosterol) and total phytoplankton (chlorins) to determine community structures. They advocate the multiple biomarker technique due to the ability to determine different productivity contributors; this becomes important over glacial-interglacial timescales where contributors and their assemblage structures vary due to different nutrient limitations and environmental changes, as well as selective preservation of certain phytoplankton species (Prahl et al, 1989; Zhao et al, 2006). Harris et al (1996) found that their study site, in the strong upwelling zone off north west Africa, demonstrated a large variation in chlorin/carbon transfer rate over glacial-interglacial timescales (in the past 350 kyr) indicating that perhaps other areas of the oceans which are sensitive to changes in the trade wind system, such as the EEP, can benefit from using chlorins as a primary productivity proxy too.

The chlorin mass accumulation rate (MAR) is affected by both changes in surface productivity and the extent of preservation in underlying sediments, which in turn are affected by the local depositional environment (Furlong and Carpenter, 1988; Calvert and Pedersen, 1992). Shankle et al (2002) promoted the use of chlorins for paleoproductivity reconstructions, with the caveat that chlorin degradation rate is not “fully understood” (Zhao et al, 2006). For example, elevated levels of primary production and increased sedimentation rate both result in high accumulation of chlorins in the sediment, and a high proportion of chlorins being preserved (Shankle et al, 2002). Although there is a lack of detailed knowledge of factors that affect chlorin preservation, Shankle et al (2002) provide a useful summary of studies that have identified potential factors that affect chlorin concentrations in marine sediment. These factors include surface productivity (Guilizzoni et al, 1983; Pedersen and Calvert, 1990), water depth and sedimentation rate (Stein et al, 1986; Henrichs and Reeburgh, 1987); whereas sediment grain size (Orr et al, 1958; Mayer, 1994a), oxygen concentration and changing oxygen minimum zone depth (Swain, 1985; Hedges and Keil, 1995) have been suggested to affect chlorin preservation rates. However, these factors do not rule out the use of chlorins as proxies: since chlorin MARs in sediments reflect the balance between production in the surface ocean and preservation during transport to sediments (i.e. ‘export productivity’) as well as changes in sedimentation, chlorin variability can be used to qualitatively assess the operation of the biological carbon pump (Rosell-Melé and McClymont, 2007).

Finally, porphyrins are created when chlorins undergo thermal diagenetic and maturation processes. They are associated with shales with high organic content (Callot, 1991; Eckardt et al, 1991; in Rosell-Melé and Koc, 1994). Autochthonous porphyrins have not been discovered in sediments younger than the Pliocene (Keely et al, 1994). Presence in younger sediments is taken to indicate deposition of reworked terrigenous sediment, for example ice rafted debris in the North

Atlantic (Rosell-Melé and Koç, 1997; Rosell-Melé et al, 1997), fluvial, or dust inputs (Keely et al, 1994). The presence of porphyrins in ODP site 849 is taken to indicate terrestrial dust flux.

2.7.3 Alkenones

The alkenone biomarkers are used in two ways in this project: to understand changes in productivity through time, and to reconstruct SST. Alkenones are long-chain C_{37} to C_{39} (methyl and ethyl) unsaturated ketones, produced (or biosynthesised) by Haptophyte algae; mainly the coccolithophore *Emiliani huxleyi* and *Gephyrocapsa oceanica* (Brassell et al, 1986; Marlowe et al, 1990; Volkman et al, 1980a,b, 1995; Marlowe et al, 1984; Conte et al, 1994, 1995; Prahl et al, 2006a,b). In response to environmental temperature changes, Haptophyte algae modify the unsaturation ratio of ketones, thus preserving a record of past temperatures and making them a valuable paleotemperature thermometer (Prahl et al, 1988; Muller et al, 1998; Brassell et al, 1986; Prahl and Wakeham, 1987; Eglinton et al, 2001). U^{K}_{37}' and SST exhibit a strong linear relationship (Rosell-Melé et al, 1995b; Muller et al, 1998; Herbert et al, 1998). The U^{K}_{37}' index [$C_{37:2}/(C_{37:2} + C_{37:3})$] is the expression of this relationship (Prahl and Wakeham, 1987) and is calibrated against SST using global core-top calibrations and culture studies (Muller et al, 1998; Prahl and Wakeham 1987). *Emiliani huxleyi* is the most widespread coccolithophore in the global ocean (Okada and Honjo, 1973; Okada and Mclntyre, 1977; Conte et al, 1994). The application of the alkenone paleothermometer relies on the assumption that fossil alkenone biosynthesisers have a similar relationship to temperature as *E.huxleyi*, since *E.huxleyi* only appeared in the sedimentary record in 260 ka (Hay, 1977; Thierstein et al, 1977; Jordan et al, 1996). McClymont et al (2005) show that between 1500-500 ka in the south-east Atlantic, the U^{K}_{37}' record is unaffected by changes in coccolithophore species dominance and evolution, and it reflects a similar sensitivity to SST as in the present day. As marine biomarkers, in addition to SST, alkenones are used to reconstruct primary productivity, (Budziak et al, 2000) partial pressures of CO_2 (Jasper and Hayes, 1990) and salinity (Rosell-Melé, 1998, Sikes and Sicre, 2002). Primary productivity of coccolithophores is reconstructed by calculating total alkenone concentrations ('K37'), which are affected by the same processes of degradation as outlined above for chlorins. To account for the influence of changing sedimentation rates, alkenone concentrations are also corrected for mass accumulation rate ('MAR K37'), as detailed in the Methods chapter below.

Alkenone-derived SSTs have been shown to correlate well with other temperature proxies, such as foraminiferal calcite $\delta^{18}O$ (Brassell et al, 1986), radiolarian assemblages (Prahl et al, 1995) and Mg/Ca planktonic foraminifera ratios (Bard, 2001a). Alkenones are abundant in marine sediments, and are less affected by the type of preservation issues that may hinder microfossil recovery and analysis, such as carbonate dissolution (Herbert et al, 2001; Rosell-Melé and McClymont, 2007). However the degradation of alkenones in both sediments and the water column has been shown not to alter the U^{K}_{37}' index (Conte et al, 1992).

There are three potential issues with alkenones: seasonality effects, the extent to which alkenone unsaturation is controlled by temperature, and the calibration equation recording warm temperatures above a threshold of ~ 29ºC.

The U^{K}_{37}' index is calibrated to mean annual SST (Muller et al, 1998) and usually interpreted as such. However, some studies have argued that alkenones capture surface water temperatures during productivity maxima (Chavez et al, 1990) therefore the resulting SSTs could be greatly seasonal (e.g. Prahl et al, 2000; 2003a; 2005; Wakeham et al, 2002; Conte et al, 1992; Schneider et al, 2010). This may be the case in locations near to major fronts in SST and/or nutrients (Rosell-Melé and Prahl, 2013), however Rosell-Melé and Prahl (2013) found that for U^{K}_{37}' values from 34 sites across the global oceans, the majority closely correlated to mean annual SST, suggesting seasonality appears to be cancelled out once sediments are deposited. Specifically in the EEP, Kienast et al (2012) found no seasonal bias for 129 data points.

Recently, studies have explored potential biotic and abiotic factors that may have an effect on the preservation of alkenones within marine sediments (Rontani et al, 2013). Studies have shown that the degree of alkenone unsaturation and therefore the paleotemperature signal can be affected by factors other than temperature changes, for example: the extent of oxygen exposure and bacterial decomposition, (Rontani et al, 2013; Hoefs et al, 1998, Gong and Hollander, 1999), alkenone degradation during transport through the water column and subsequent deposition (e.g. Prahl et al, 2000; Wakeham et al, 2002), changing Haptophyte algae community structures, nutrient concentrations, and finally light accessibility (Conte et al, 1998; Epstein et al, 1998, 2001; Yamamoto et al, 2000; Prahl et al, 1995; 2006a,b; Sikes and Volkman, 1993). Conte et al (2006) studied a global compilation of U^{K}_{37}' against growth temperature and find an unequivocal agreement between samples in the open ocean, collected during different seasons, concluding that any genetic or physiological factors must exert minimal control on alkenone unsaturation. Kienast et al (2012) tested the effect phosphate concentrations and salinity had on alkenone samples from the EEP, and found there to be no evident effect on unsaturation.

Warm temperature bias is also a factor of concern. Muller et al's (1998) calibration equation has been used extensively to reconstruct temperature ranges from 0-29ºC. However it has been suggested that the temperature reliance of the alkenone unsaturation index is compromised in either extreme warm or cold conditions. This seems to apply in isolated regions; for example off the coast of Peru, a warm bias of up to 4ºC has been recorded (Kienast et al, 2012). Whereas studies in the equatorial Atlantic (Müller and Fischer, 2003; Schneider et al, 1995) and SCS (Pelejero and Grimalt, 1997) do not record an unusual response at the warmer end of the temperature curve. Kienast et al (2012) find no systematic warm bias in the EEP (aside from near-coastal Peru).

Finally, as with all biomarkers, measurement and subsequent interpretation is affected by the fact that only a small proportion of the total biomarkers produced are preserved in the marine sediment (Prahl et al, 1989). Therefore, changes in biomarker concentration can reflect both changes in production and/or changes in organic matter preservation.

2.8 Relevant research in the EEP

McClymont (2004) found that SST at ODP site 849 followed the $\delta^{18}O$ ice volume glacial-interglacial cycles with similar amplitudes to the LGM; and biomarker ARs tended to be high during glacial intervals (Rosell-Melé et al, 2004). McClymont and Rosell-Melé (2005) found EEP SST cooling

(from ODP site 849) beginning 1.17 Ma and intensifying towards the severe cooling event during MIS 22 (ca.900 ka). A coarsening of grain size during this time also indicates strengthening atmospheric circulation (McClymont, 2004). These were concurrent with stable SSTs in the WEP; increasing the zonal Pacific gradient and therefore strengthening Walker circulation. McClymont (2004) and Mcclymont and Rosel-Melé (2005) therefore hypothesise that this increased moisture transport and reduced heat flux to high latitudes enabled the growth of more extensive ice sheets indicative of the 100-kyr world. In addition to this, high biomarker ARs beginning 1.17 Ma and leading up to the severe SST cooling at MIS 22 (and subsequent expansion of high latitude ice sheets) is argued to reflect a strengthened biological pump, enabling $_{p}CO^{2}$ reduction and acting as a possible driver for global cooling (McClymont, 2004). Following MIS 22, ODP 849 reflects reduced biomarker ARs and higher amplitude SST variability at the 100-kyr period.

Farrell et al (1995) use the $\delta^{18}O$ and $\delta^{13}C$ difference between *N.dutertrei* and *G.sacculifer* during 0-1.15 Ma at ODP site 847 (see figure 1.2) to infer variations in temperature and nutrient concentration. Smaller vertical contrasts were found during glacials, ascribed to enhanced upwelling. This agrees well with stable isotope data at ODP site 851 (Ravelo and Shackleton, 1995), the primary aim of the research being to reconstruct past wind field strength between 0-2 Ma. Ravelo and Shackleton (1995) found that during glacials, the thermocline was slightly deeper and SSTs (calculated from $\delta^{18}O$) cooler. The deeper thermocline during this time was hypothesised to be caused either by a lower average wind strength (due to a decrease in the strength of the EUC), or strengthened southeasterly trade winds (due to an increase in the ECC).

2.9 Conclusion

In summary, this thesis seeks to explore the role the EEP plays in the development of the MPT. This will be possible through the reconstruction of a number of key characteristics of the surface ocean, known to play a role in significant paleoclimate changes. The focus of analysis here will be to reconstruct SSTs (using the alkenone U^{K}_{37}' index), productivity (using alkenone and chlorin biomarkers, and $\delta^{13}C$) and changes to water column structure related to stratification and upwelling (using $\delta^{18}O$).

Chapter 3: Methodology

3.1 Introduction

This research project uses two main research methods; biomarker analysis (alkenones and pigments) and planktonic foraminiferal stable isotope analysis. This chapter describes these methods, the age model used, and the statistical analysis of the data.

3.2 Sample preparation

All samples analysed in this project are from ODP site 849 (figure 1.2). All samples were refrigerated below 4°C prior to analysis, at both the ODP Core Repository (College Station, Texas) and at Durham. All glassware was cleaned and furnaced at 450°C before use. All solvents used were high purity (high performance liquid chromatography [HPLC] grade). The original wet sediments were split into two aliquots using an approximate ratio of 2:1, for biomarker and stable isotope analysis, respectively. Sample size was in part dictated by the availability of sediment from the core, which has been heavily-sampled by previous workers.

3.3 Sampling strategy

Previous biomarker (alkenone and pigment) analyses have been performed on ODP site 849, spanning timescales 500-1500 ka, to a resolution of ca.5 kyr (McClymont, 2004). This existing SST and productivity data is used as a framework within which to develop higher resolution data points. The data within this thesis spans 600-1150 ka. The average sampling resolution between biomarker (alkenone and pigment) data points was ~2.5 kyr. Although higher resolution sampling of planktonic stable isotopes was undertaken between ca.740 ka and ca.1000 ka, the average resolution is overall slightly lower at ~3.3 kyr (0.7 – 29.7 kyr). This high variation in sample resolution was in part due to multiple 'no returns' from stable isotope analysis. This work is the first high resolution analysis of temperature and isotopes across this time window from this region, enabling surface ocean productivity, relative stratification and upwelling, and circulation changes in the EEP to be constrained surrounding the '900 kyr' event.

Although some of our samples are spaced relatively closely in time, it is important to note the potential influence of bioturbation, which affects the upper layers of sediment up to 20 cm depth (Patience and Kroon, 1991; Mix et al, 1995), by re-working and mixing the sediment post-deposition. Bottom currents re-distributing sediment, and biological mixing, is exaggerated in finer-grained sediments over coarser, sandy sediment (Bard, 2001b). Sedimentation rates are on average 25-30 m/my at ODP site 849 (Mayer et al, 1992). ODP site 849 has experienced moderate bioturbation (Mayer et al, 1992); however the noteworthy areas of burrowing in ODP site 849 bypass the depths dated ca.840 ka – ca.1220 ka. An average estimate of smoothing via bioturbation is 5-10 cm (Mix et al, 1995). Based on the sedimentation rates for ODP site 849 and the estimate of depth bioturbation affects in ODP 849, it is calculated that bioturbation may have smoothed climatic signals by 1.9 – 3.8 kyr.

3.4 Biomarker analysis

Alkenones are used as a proxy for SST and *Prymnesiophyceae* primary productivity whereas chlorin and porphyrin pigments are used here as a proxy for the total phytoplankton productivity.

3.4.1 Biomarker extraction

In this study, 141 deep ocean sediment samples with weights ranging from 0.9g to 6.1g were analysed. Comparison between sediment samples from McClymont (2004) and this thesis was not deemed necessary given that the methods of extraction and biomarker equations used are exactly the same between studies; as well as the issue of shortage of core samples at key depths. Distinction between sources of SST data is made clear in the results (see figure 4.2). The microwave-assisted extraction (MAE) method of Kornilova and Rosell-Melé (2003) was used to extract the biomarkers, since it is widely recognised as a more efficient solvent extraction technique than the more traditional method of sonication extraction, due to the lower volumes of solvent required and shorter extraction time (Kornilova and Rosell-Melé, 2003). Microwaving at 70°C is the optimum temperature for maintaining both high alkenone and high chlorin yields (Kornilova and Rosell-Melé (2003). Within each batch of 14 samples, one blank and one mixed sediment ("JB sd") were included, the latter for monitoring procedural reproducibility.

3.4.2 MAE

Samples were freeze-dried to remove all moisture, homogenised using an agate pestle and mortar, and weighed into 100 ml Teflon vessels. A known quantity of internal standards (C_{36} *n*-alkane, $C_{19}O$ ketone) was then added, plus magnetic stirrers and 12-15 ml Dichloromethane:Methanol (DCM:MeOH) (3:1, v/v). The samples were microwaved by increasing sample temperatures to 70˚C over 1.5 minutes, after which they were held at 70˚C for 5 minutes, following the method of Kornilova and Rosell-Melé (2003). The samples were then allowed to cool to below 30˚C, to ensure the solvents were below their boiling points (DCM is 39-40˚C, Me:OH is 64.7˚C). The cooled sediment-solvent samples were decanted into 12ml Pyrex test tubes, and centrifuged for 5 minutes at 2500 rpm. The supernatant was decanted into round-bottomed flasks, and taken to dryness using the BUCHI Rotavap. The samples were transferred into vials, taken to dryness under a stream of nitrogen, and stored in the freezer until further analysis.

3.4.3 Clean-up of lipid extracts

To remove any sediment particles that may have remained during the extraction process, lipid extracts were filtered through Pasteur pipettes filled with extracted cotton wool, and eluted with DCM. If any residual water was present in the total lipid extracts, the above step was performed with the addition of anhydrous sodium sulphate within the pipette. Filtered extracts were again taken to dryness under a stream of nitrogen, and stored in the freezer until further analysis.

3.5 Pigment analysis

This thesis uses UltraViolet-visible spectrophotometry (UV-Vis) to identify and quantify the wavelength absorbance spectra of each total lipid extract in the range 350-850 nm. The dry total lipid extracts were dissolved in 400 µl acetone, thoroughly mixed, and an aliquot of the sample (35-40 µl) injected into a Dionex PDA-100 Photodiode Array (PDA) detector attached to a Dionex P580 Quaternary pump. The wavelength absorbance spectra of each sample were compared to those of the standard pigments (chlorophylls *a, b* and *c*): peaks at 410 nm and 665 nm are indicative of chlorophyll derivatives (Jeffrey et al, 1997).

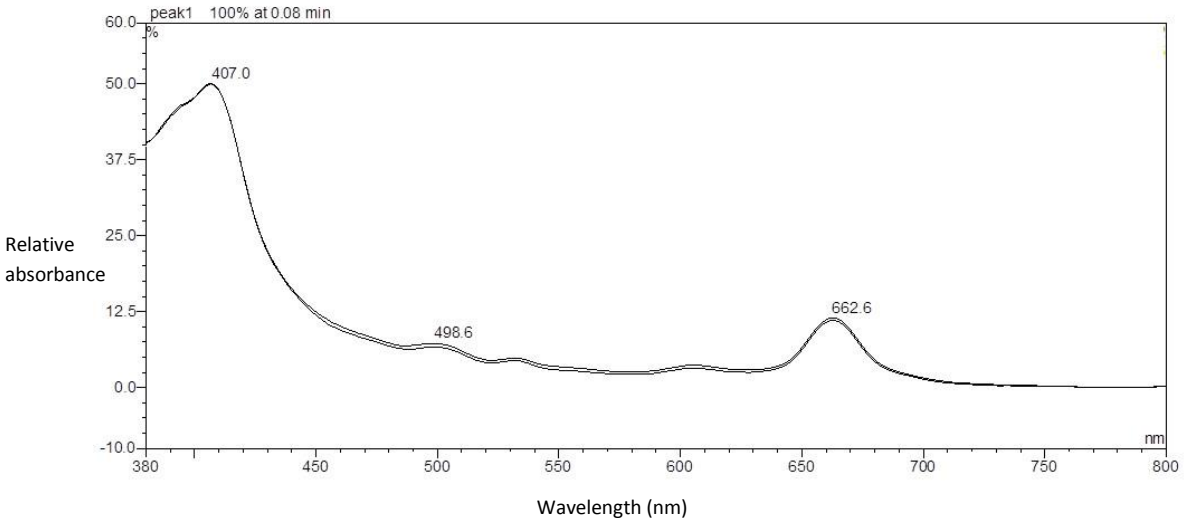

Figure 3.1: UV-Vis absorbance spectrum of the mixed sediment standard "JB sd" with peaks at ~410 nm and ~665 nm

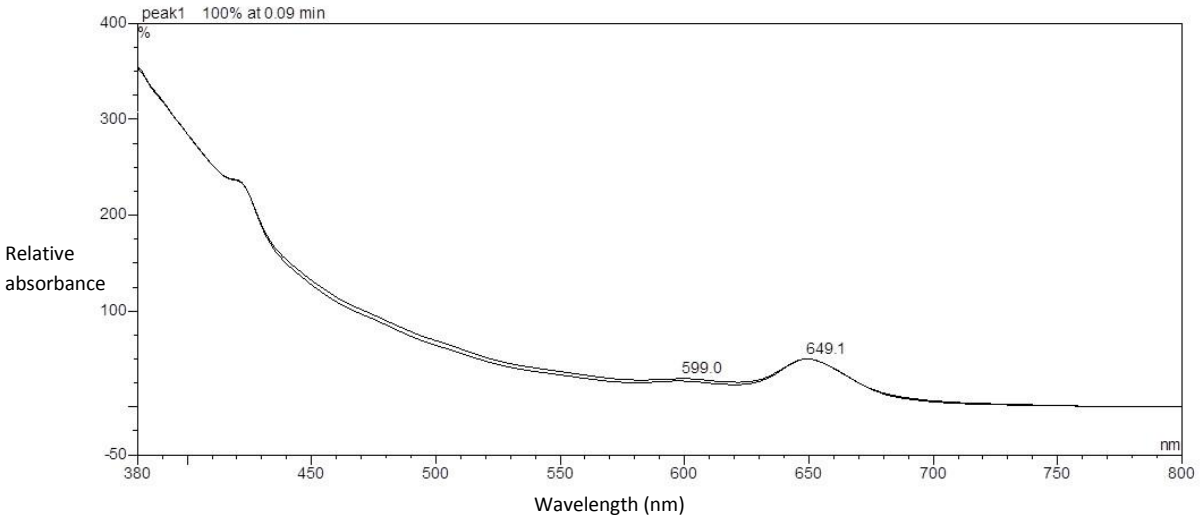

Figure 3.2: UV-Vis absorbance spectrum of sample 849D-2H-6W, 43-44 cm (~893 kyr) with peaks at ~410 nm and ~665 nm

The absorption of chlorophyll (and its diagenetic products) is linearly proportional to concentration, abiding by the Beer-Lamberts law. Therefore a calculation was required to quantify values relative to the sample mass (McGowan, 2007). To quantify the absorbance at 410 nm (indicating

porphyrins, the Soret ['S'] band) and 665 nm (indicating chlorins, the Satellite ['I'] band), the following equation was used to determine relative pigment abundances:

$$P\lambda = (A\lambda \times DF) / M$$

Where Pλ = relative magnitude of absorbance for a given wavelength (λ), as 'area units'/g dry sediment; Aλ = integrated area for that wavelength; DF = dilution factor; the volume of acetone used to dissolve the sample divided by the aliquot size injected; and M = mass (g) of dry sediment extracted.

The ratio of Soret to Satellite band absorbance spectra is expressed as the S/I ratio.

Each sample, standard, and acetone blank was injected three times. At regular intervals throughout the sample sequence, a sediment standard ("JB sd", see section 3.4.1) was injected in order to monitor the reproducibility of the PDA detector. Average reproducibility was around 9.9%, calculated using the standard deviation between "JB sd" in multiple batches. No considerable drift was recorded during use. Due to essential maintenance to the Dionex P580 Quaternary Pump between the two batches of injections, a slight change in the sensitivity of the PDA detector was noted. A standardisation calculation was performed on the wavelength values from the second batch of injections, based on the "JB sd" sediment standard.

Having passed through the PDA detector, samples were collected in Pyrex test tubes and taken to dryness using a LABCONCO Centrivap rotary concentrator, before being added to the total extract in the original vials. Samples were then taken to dryness under a stream of nitrogen, and stored in the freezer until further analysis.

3.6 Gas chromatography analysis

3.6.1 Derivatisation

Prior to gas chromatography (GC) analysis, total extracts were derivatised to remove polarity from compounds which would otherwise not elute through the GC column. To each sample, 50 µl DCM and 50 µl bis(trimethylsilyl)trifluoracetamide (BSTFA) were added, the samples were heated to 70 °C for 1 hour, and allowed to cool to room temperature overnight. The extracts were then taken to dryness under a stream of nitrogen.

Total lipid extracts were analysed with a Thermo TraceUltra gas chromatograph (GC) and DSQ quadrapole mass spectrometer (MS). Samples were dissolved in 30 µl DCM, and aliquots injected by an AS3000 autosampler. The PTV splitless (with silicosteel liner) isothermal injector injected a volume of 1 µl at 280°C. The carrier gas was helium, at a constant flow rate of 1 ml/min. The column was an SGE BP1 5% phenyl column measuring 60m in length, 0.25 mm internal diameter and 0.25 mm film thickness. The initial program temperature was 50°C for 3 minutes, which ramped up to 150°C at a rate of 10°C/min and then immediately up to 310°C at a rate of 4°C/min, at which it was held for 30 minutes. The source temperature of the MS was 220°C, and the transfer line temperature 310°C. The software used to analyse the GC-MS results was Xcaliber version 2.2.

Due to weak alkenone concentration in samples, data points were created using the GC-MS SIM mode scan, enabling the detection of specific analytes with known mass spectra: 55,57,81,83,85,299,313,341,528,530 (all m/z).

Alkenone identification was based on studying previous total lipid extract gas chromatographs from the same core in the EEP (McClymont, 2004), comparison of the "JB sd" sediment standard alkenone chromatographs and their retention times, and the molecular ion of each peak. To quantify the alkenone peaks and calculate the alkenone abundance, the integrated peak areas of the internal standard *n*-alkane C_{36} were compared to those of the samples using the equation:

$$\mathbf{BM = \frac{(IS\ /\ \{IS\})\ x\ \{BM\}}{M}}$$

Where BM = abundance of biomarker per gram of dry sediment; IS = mass of internal standard; {IS} = integrated area of internal standard; {BM} = integrated area of biomarker; M = dry weight of sediment extracted.

The relative peak areas of the unsaturated C_{37} alkenones $C_{37:3}$ and $C_{37:2}$ were used to determine the U^{K}_{37}' index:

$$\mathbf{U^{K}_{37}' = [C_{37:2}]\ /\ [C_{37:3}] + [C_{37:2}]}$$ **(Prahl and Wakeham, 1987)**

This index was then applied to the global sediment core top calibration of Müller et al (1998) to determine SST:

$$\mathbf{U^{K}_{37}' = 0.033T + 0.044}$$ **($r^2 = 0.958$)**

3.7 Biomarker accumulation rates

Biomarker accumulation rates (ARs) are calculated using the bulk mass accumulation rates of the sediment core, in order to account for changes in sedimentation rate and bulk density which could change biomarker concentrations in the absence of a change in productivity. Bulk mass accumulation rates (MAR) are calculated from linear sedimentation rates and sediment dry bulk density (Emeis et al, 1995):

Bulk MAR = linear sedimentation rate x dry bulk density

g/cm^2kyr^{-1} = cm/kyr x g/cm^3

Linear sedimentation rates were interpolated using the new age-depth model created here (section 3.9). Dry bulk density data were taken from the ODP Initial Reports for ODP site 849 (Mayer et al, 1992).

Biomarker accumulation rates (AR) are calculated from the Bulk MAR and biomarker abundance (Emeis et al, 1995):

Component AR = Bulk MAR x component abundance

component abundance/cm^2kyr^{-1} = g/cm^2kyr^{-1} x area units or concentration/g

E.g: pigment AR = Bulk MAR x pigment abundance

AU/cm^2kyr^{-1} = g/cm^2kyr^{-1} x area units/g

3.8 Foraminiferal analysis preparation

Initially, foraminiferal analysis was conducted on 12 evenly spaced sediment samples from ODP site 849. Whole specimens were identified and counted, the purpose of which was twofold: to identify common species down-core for stable isotope analysis, and to determine whether the assemblage was predominantly planktonic or benthic. Overall, ~94% of the assemblages were planktonic.

Sediment samples were diluted in 300 ml tap water and 10 ml Sodium hexametaphosphate dispersant and left for 2 days. The samples were very clay-rich and required a lengthy time to anti-coagulate. Samples were then washed through 500 µm and 63 µm mesh sieves, both fractions were re-mixed and dried down in a 40°C oven until dry. Foraminifera were identified and counted dry under a binocular microscope.

3.8.1 Carbon and oxygen stable isotopes

Neogloboquadrina dutertrei (*N.dutertrei*) (355-425 µm) and *Globigerinoides ruber* (*G.ruber*) (250-350 µm) were consistently present down-core in ODP site 849. 60 samples of *G.ruber* and *N.dutertrei* were selected for stable carbon and oxygen isotope analysis. Where *G.ruber* was not present in high volumes, *Globigerinoides sacculifer* (*G.sacculifer*) (300-355 µm) was substituted, based on their similar depth habitats in the surface mixed layer (0-50 m) (Fairbanks et al, 1982). However, poor comparison of *G.ruber* and *G.sacculifer* $\delta^{18}O$ on two samples resulted in *G.sacculifer* $\delta^{18}O$ being excluded from analyses. $\delta^{13}C$ was more comparable between the two species and so two *G.sacculifer* $\delta^{13}C$ values have been used in the analysis (see data in the appendix).

G*.ruber* and *N.dutertrei* specimens weighing approx. 30 mg were picked using ethanol, loaded into glass vials and sealed with septa. Due to small sample weights, this was on the lower end of the recommended amount of 30-100 mg. Samples were loaded into an IsoPrime dual inlet mass spectrometer plus Multiprep device. The automated system evacuates vials and delivers anhydrous phosphoric acid to the carbonate at 90°C. The evolved CO_2 is cryogenically cleaned and passed to the mass spectrometer. Isotope values ($\delta^{13}C$, $\delta^{18}O$) are reported as per mille (‰) deviations of the isotopic ratios ($^{13}C/^{12}C$, $^{18}O/^{16}O$) calculated to the Vienna Pee Dee Belemnite (V-PDB) scale using a within-run laboratory standard calibrated against NBS-19 standards. Analytical reproducibility of the standard calcite (KCM) is < 0.1‰ for $\delta^{13}C$ and $\delta^{18}O$.

3.9 Age model

The initial shipboard age model for ODP site 849 was generated during ODP leg 138 using both extinctions and emergences of calcareous organisms (such as nannofossils and foraminifera) to produce a biostratigraphic framework, and GRAPE density measurements (Mayer et al, 1992). The density values were used to compare ODP site 849 to others along the Leg 138 transect and to assign events to epoch boundaries or known ages, since high productivity at the site prevented the more commonly applied paleomagnetic reversal stratigraphy (Mayer et al, 1992; Shackleton et al, 1992; Mix et al, 1995). This preliminary age model was then updated by Mix et al (1995) using benthic foraminifera (*Cibicidoides wuellerstorfi*) oxygen isotope stratigraphies from the continuous sedimentary record at ODP hole 849C spanning 0-5 Ma at ca.4 ka resolution. The ODP site 849 $\delta^{18}O$ record was then correlated to ODP site 677 (Panama basin) $\delta^{18}O_{benthic}$ record using a Fourier mapping function.

The new age model used in this study is created by tuning the existing $\delta^{18}O_{benthic}$ data (Mix et al, 1995) to the LR04 benthic stack; an orbitally-tuned compilation of benthic foraminifera $\delta^{18}O$ values, extending back to 5.3 Ma (Lisiecki and Raymo, 2005). The LR04 model was created by aligning $\delta^{18}O_{benthic}$ data from 57 globally-distributed deep ocean core sites using an algorithm, and tuning this stack to a simple ice volume model using insolation values at 65°N (Lisiecki and Raymo, 2005). The LR04 age model has been successfully used within numerous paleoclimate studies over the past decade. Stacked records improve the signal-to-noise ratio of individual sites, which could perhaps be biased by local or regional factors (Lisiecki and Raymo, 2005). One of the longest most consistent $\delta^{18}O_{benthic}$ records employed within the LR04 benthic stack is the ODP site 849 Mix et al (1995) sequence (figure 3.3). Figure 3.4 compares the Mix et al (1995) and LR04 age models. Differences exist between the two age models due to the “smoothing” of local and regional signals in the LR04 stack, but also potentially due to the different tuning targets of the two studies.

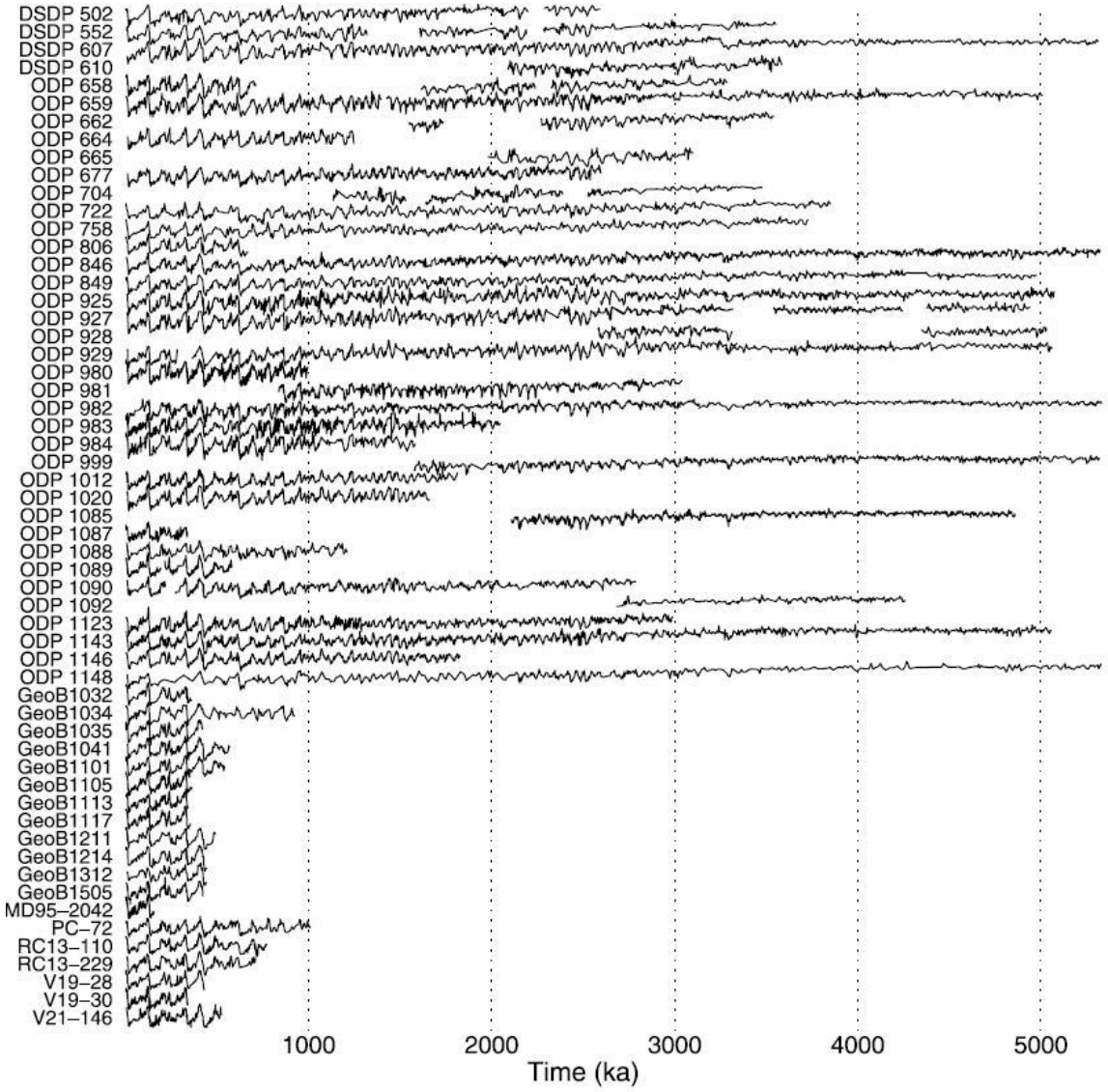

Figure 3.3: Graphically aligned $\delta^{18}O_{benthic}$ data, plotted with their original variance but offset vertically as part of the creation of the LR04 stack. Note the presence of the ODP site 849 $\delta^{18}O$ record within the LR04 data set (Mix et al, 1995b). Source: Lisiecki and Raymo (2005)

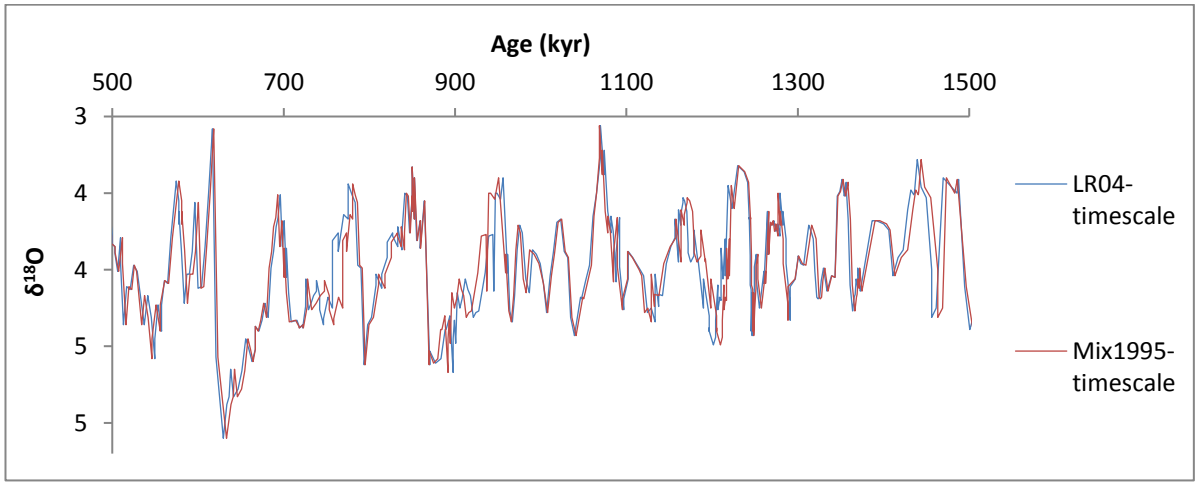

Figure 3.4: Comparison between the original Mix et al (1995) age model for ODP site 849 and the Lisiecki and Raymo (2005) LR04 benthic stack between 1500 – 500 ka (the time interval originally

examined by McClymont (2004)). Both age models are plotted on their original timescales. Between 1150 - 600 ka (the timescale for this thesis' data), maximum shift between datasets is 12.4 kyr.

The composite depth (mcd/Rmcd) of each sample from ODP site 849 was taken from the ODP Initial Reports (Mayer et al, 1992). Linear interpolation was then performed for sample composite depths between LR04 tie points, assuming a constant sedimentation rate, to obtain sample ages. The existing alkenone data from ODP site 849 (McClymont, 2004) was originally plotted using the Mix et al (1995) age model. Here, these data points have been re-plotted on the LR04 age model to ensure consistency between previous and new data within this study.

Chapter 4: Results

4.1 Introduction

The purpose of this chapter is to identify any key patterns within the data from ODP site 849. The LR04 benthic stack is used here as a reference to glacial-interglacial stages (Lisiecki and Raymo, 2005). Although high resolution (<2.5 kyr) sampling was undertaken for all proxy techniques, some samples did not yield data, therefore the final average resolution (3.65 kyr) is lower than the target resolution. Data for all the graphs included in the thesis, and data referenced throughout is included in the appendix.

4.2 SST

The U^{K}_{37}' SST data from ODP site 849 shows glacial-interglacial cycles as recorded in the LR04 stack (figure 4.2 A and B). The SST data here span 10 glacials and 11 interglacials, generally with lower SSTs during glacials (average 24.7°C) and higher SSTs during interglacials (average 25.6°C); shown in figure 4.2. However the SST variability within glacials and interglacials increases the standard deviation (also figure 4.2). The average SST spanning the entire record between 600-1150 ka is 25.2°C with a range of 5.9°C (between 21.9°C and 27.8°C). The coolest glacials occurred ca.1050 ka (MIS 30; 22.6°C), ca.900 ka (MIS 22; 22.5°C) and ca.740 ka (MIS 18; 21.9°C). Notably warm interglacials occurred 970-1000 ka (MIS 27; ~27.4°C), ca.960 ka (MIS 25; 27.8°C) and ca.860 ka (MIS 21; 27.6°C). SSTs show MIS 16 (ca.650-630 ka) to be a very mild glacial. During periods of higher resolution sampling (MIS 28-25, MIS 23 and MIS 18), high resolution sub-orbital (<2.5 kyr) SST changes are observed.

4.3 Chlorin and alkenone accumulation rates

Alkenone (K37) and chlorin (P665) ARs correlate relatively well, with an r^2 value of 0.6 (figure 4.2 C and D; see also figure 4.1). The average P665 is 4.9 AU/cm²/kyr (range 0.7-16.3); average K37 is 157.1 µg/cm2/kyr (range 5.2-1154). McClymont and Rosell-Melé (2005) found that biomarker accumulation rates at ODP site 849 tended to be higher when SSTs were low, during glacial intervals. The creation of higher resolution data points in this study reveals a more variable record of K37 and P665 which is no longer so strongly related to SST. However there is a relationship with glacial-interglacial cycles pre-MIS 21, with moderate to high P665 and K37 values occuring during glacials (defined as values higher than the average, and greater than or equal to the upper 75% of values, respectively). Post-MIS 21, P665 and K37 values are variable with no apparent link to glacials, interglacials or SST. Maxima of K37 and P665 occur ca. 1045 ka (MIS 30), between 990-960 ka (MIS 27-25), ca.930 ka (MIS 24), and 705-690 ka (MIS 17). Prolonged periods of minima in both K37 and P665 which span both glacials and interglacials occur during 990-1030 ka (MIS 27-29), 750-800 ka (MIS 19/20) and 600-650 ka (MIS 15/16).

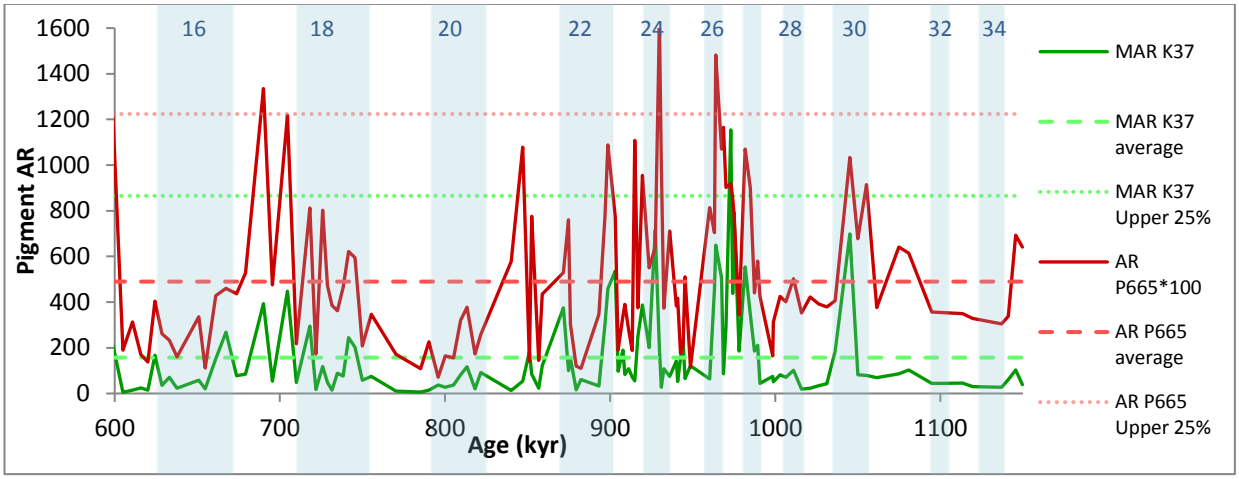

Figure 4.1: ODP 849 MAR K37 plotted against AR P665 (multiplied by 100 for comparable scale); average and upper 25% lines shown to indicate moderate and high values. Blue bands indicate glacial periods, or high $\delta^{18}O$ (e.g. MIS 27).

4.4 Planktonic $\delta^{18}O$

G.ruber and *N.dutertrei* $\delta^{18}O$ values are offset throughout the majority of the time interval (figure 4.2 C); the average offset (*N.dutertrei-G.ruber*) is 0.98 ‰. *N.dutertrei* values are predominantly higher than *G.ruber*, consistent with their position in the water column. In the sections where *G.ruber* and *N.dutertrei* have the same sampling resolution, their signatures are broadly similar. This trend changes at the beginning of the interglacial stage MIS 25 (ca.955 ka), MIS 24 (ca.930 ka) and MIS 22 (ca.880 ka), where the offset is reduced (0.02 ‰; 0.45 ‰) or reversed (-1 ‰), respectively. Looking at figure 4.2, there appears to be little to no pattern between the degree of offset during glacials and interglacials. The maximum offset throughout the time window is 1.87 ‰ and occurs ca.963 ka (MIS 26); the minimum is -1 ‰ at ca.880 ka (MIS 22).

Figure 4.2 (overleaf): All results from ODP site 849. Faded grey lines indicate separation of Stages A, B and C. Blue bands indicate glacial periods, or high $\delta^{18}O$ (e.g. MIS 27). See section 4.8.1 for description of the phases 2a, 2b and 3 (A) LR04 $\delta^{18}O$ benthic stack with labelled marine isotope stages (MIS); (B) U^{K}_{37}' SST. Red points indicate new data from this thesis added to existing data from McClymont and Rosell-Melé (2005) (C) mass accumulation rate of alkenones 'K37'; (D) accumulation rate of chlorins 'P665'; (E) $\delta^{18}O$ of planktonic foraminifera G.ruber and N.dutertrei. Error bar (880 ka) shows the difference between two values, as discussed in Chapter 5 (F) $\delta^{13}C$ of planktonic foraminifera G.ruber and N.dutertrei; (G) S/I values. S/I = 10 shown by black dashed line.

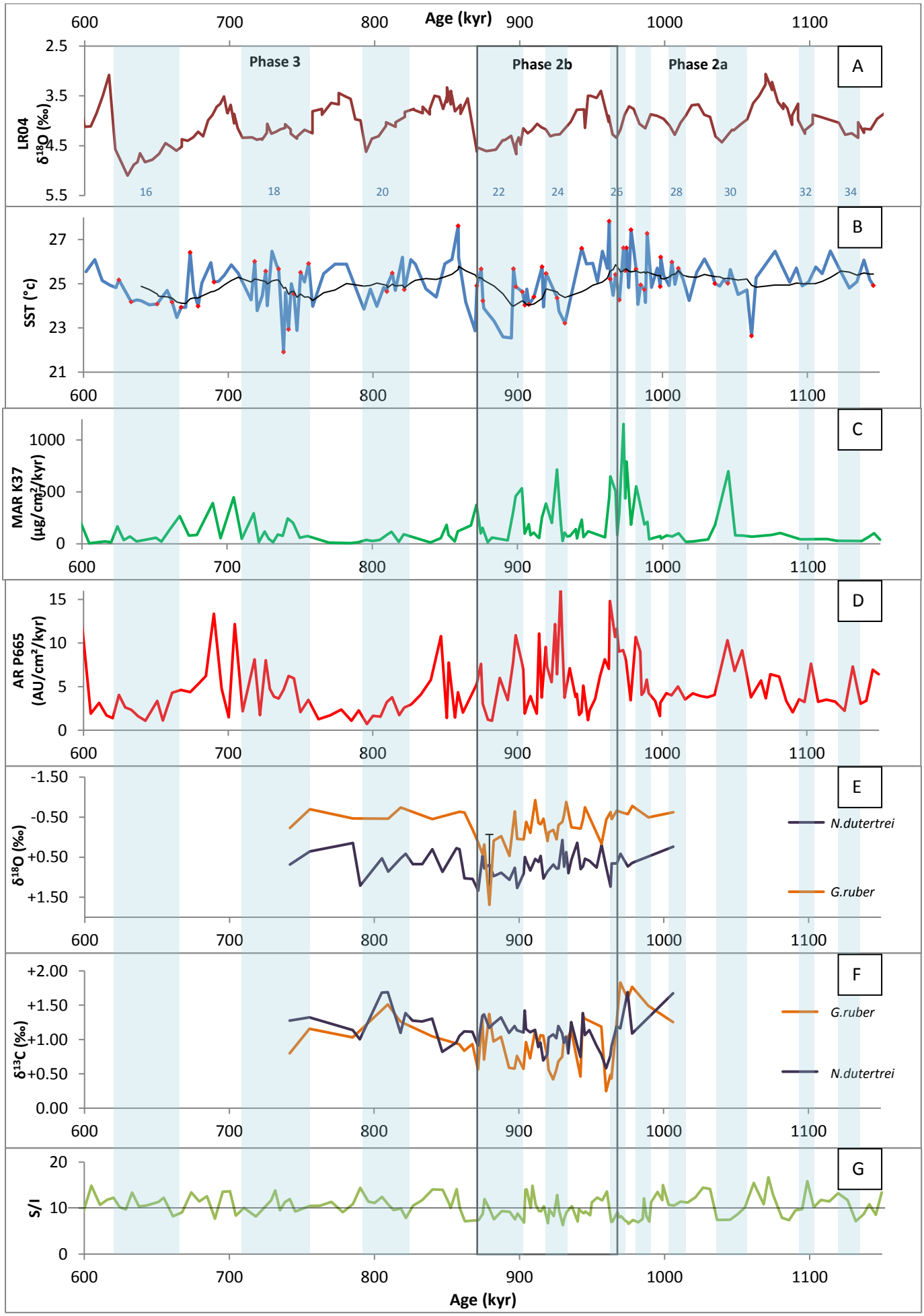
Age (kyr)
600
700
800
900
1000
1100
Phase 3
Phase 2b
Phase 2a
A
LR04 δ18O (‰)
2.5
3.5
4.5
5.5
16
18
20
22
24
26
28
30
32
34
B
SST (°c)
27
25
23
21
C
MAR K37 (µg/cm2/kyr)
1000
500
0
D
AR P665 (AU/cm2/kyr)
15
10
5
0
E
δ18O (‰)
-1.50
-0.50
+0.50
+1.50
N.dutertrei
G.ruber
F
δ13C (‰)
+2.00
+1.50
+1.00
+0.50
0.00
G.ruber
N.dutertrei
G
S/I
20
10
0
Age (kyr)

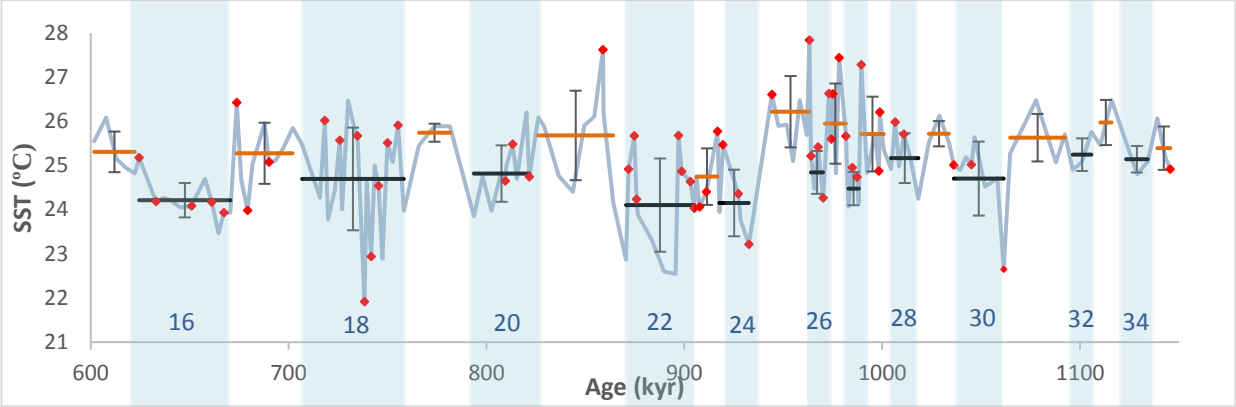

Figure 4.3: ODP 849 U^{K}_{37}' SST with error bars and averages per glacial/interglacial. Red points indicate new data from this thesis added to existing data from McClymont and Rosell-Melé (2005). Orange lines show average SST during interglacials, black lines show average SST during glacials. Error bars show standard deviation per glacial/interglacial. Blue bands indicate glacial periods, or high $\delta^{18}O$ (e.g. MIS 27).

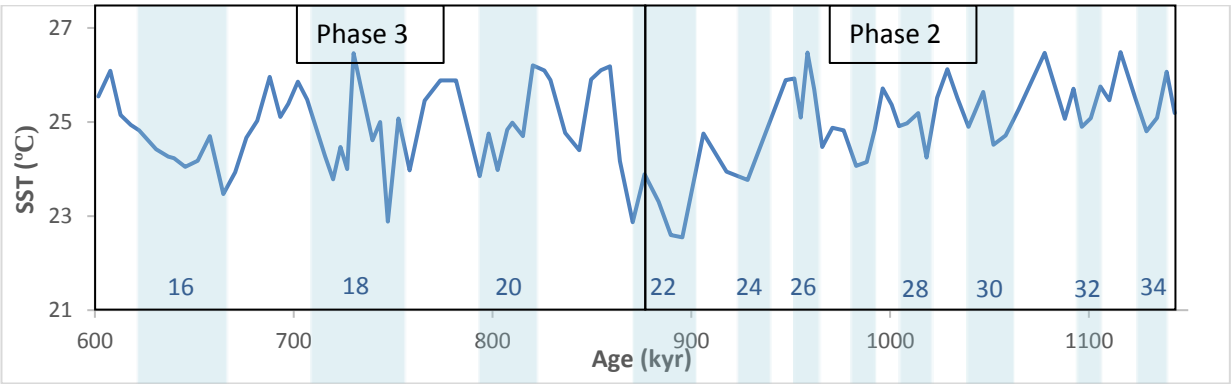

Figure 4.4: Original McClymont (2004) SST from ODP 849. Blue bands indicate glacial periods, or high $\delta^{18}O$ (e.g. MIS 27). Black boxes indicate original phases, discussed in section 4.8.1.

4.5 Planktonic $\delta^{13}C$

G.ruber and *N.dutertrei* $\delta^{13}C$ values are broadly similar and rise and fall together throughout the time window (figure 4.2 F). This is not consistent with their position in the water column; *G.ruber* is expected to have a higher $\delta^{13}C$ value than *N.dutertrei.* Two periods of noticeable offset occur between ca.920-930 ka (MIS 24) and ca.875-910 ka (MIS 22/23), where the average offset is 0.48 ‰ and 0.4 ‰, respectively, compared to an average offset of 0.24 ‰ elsewhere in the time window. During these two periods, *N.dutertrei* values were higher than *G.ruber;* an unusual finding. The maximum difference between species' values (*N.dutertrei-G.ruber*) is 0.66 ‰ at 875 ka (MIS 22), and -0.68 ‰ at 978 ka (MIS 27); the minimum is 0.01‰ at 910 ka (MIS 23). The average offset throughout the entire time window is 0.29 ‰.

4.6 S/I

ODP site 849 exhibits high S/I ('Soret'/'Satellite' ratio) values throughout 1500-500 ka; on average 10.4 (figure 5.1 G). This demonstrates that the contribution by pigments with absorbance at the 410 nm wavelength exceed those with at 665 nm, suggesting that porphyrins are present in the sediment in high concentrations relative to chlorins (see section 3.5). In pre-Pliocene sediments, the presence of porphyrins is taken to represent contribution of reworked sediment from elsewhere, for example terrigenous dust input (as discussed in section 2.7.2). At this site however, high S/I values (above 10) are not considered to represent the presence of terrigenous material, as aeolian dust only contributes ~2.5% of sediments in ODP hole 849B, due to the high productivity in the EEP region (Hovan, 1995). This indicates that there is a contribution to the 410 nm wavelength (the "S" band) from another source. McClymont (2004) found that in ODP site 849 the ~471 nm wavelength was high due to the presence of carotenoid-like pigments which distorted absorbance at ~410 nm. In the modern ocean, these carotenoid pigments are found in blue-green algae, prymnesiophytes, dinoflagellates and diatoms, and could be the source. This is consistent with diatom abundance in the Pacific (Jeffrey et al, 1997). Taking this into account, only the 665 nm absorbance spectra, indicative of the chlorins, will be used as a proxy for total primary productivity.

4.7 Summary of ODP site 849 new data

In conclusion, at ODP site 849 cooler SSTs occur during glacials. The chlorin and alkenone accumulation rates agree well with each other, with high accumulation rates during glacials pre-MIS 21. SST does not show a relationship with the biomarker accumulation rates, given intervals of high biomarker accumulation rates with both warm (27.8°C, ca. 960 ka) and cold (23.7°C, ca. 928 ka) SSTs. Planktonic $\delta^{18}O$ values are offset throughout the record, with *N.dutertrei* consistently heavier than *G.ruber*, except during MIS 25, 24 and 22. In contrast, both species' planktonic $\delta^{13}C$ signatures were similar throughout the record, except during MIS 22/23 and MIS 24. The data here indicates that a climate threshold has been crossed ca.870 ka, and that there may be a more complex relationship between changes in SST and productivity, challenging the traditional view of 'low temperature - high production' for upwelling systems.

4.8 ODP site 849: Comparison with McClymont (2004) data

There are two directly comparable proxies between McClymont (2004) and this study: SST and biomarker (chlorin and alkenone) accumulation rates (ARs). This section will focus on the similarities and differences between the original dataset (>5 kyr resolution) and new higher resolution dataset (av 3.65 kyr resolution).

Within McClymont (2004), the original data from ODP site 849 spanning 1500-500 ka was separated into three phases (see figure 4.4): phase 1 (1500-1170 ka), dominated by glacial-interglacial variability in SST at the obliquity period, and relatively high glacial biomarker accumulation rates between 1345-1200 ka; phase 2 (1170-875 ka), characterised by declining SSTs and increasing biomarker accumulation rates towards severe cooling in MIS 22; and phase 3

(875-500 ka), characterised by lower average SSTs compared to phase 1, and comparable to the late Pleistocene. Eccentricity begins to dominate the period at which SSTs vary, and biomarker accumulation rates are relatively low.

The new data presented here covers only phases 2 and 3 of McClymont's (2004) record. Therefore we may expect to observe an initial decline in SSTs and increase in biomarker ARs (phase 2), until ca.875 ka where average SST becomes more stable and biomarker ARs maintain low concentrations (phase 3). However, the generation of new data in this thesis has changed the previous SST pattern in three ways.

Firstly, the SST amplitude across both glacials and interglacials (MIS's 18, 21, 24, 25, 30) in both phases has increased. Most notably, at the beginning of MIS 30, SST drops to 22.6°C; a decline of 2.7°C whereas the original data showed a drop of just 0.5°C, and during MIS 25, SSTs increased by 3.3°C; compared to a previous 1.2°C rise (see figure 4.4). Also, at the beginning of phase 3, at ca.860 ka, (MIS 21) a SST increase of 4.8°C is recorded (22.8°C to 27.6°C), whereas previously the amplitude was 1.5°C less (22.8°C to 26.1°C). Although new SST data points during the MIS 22 glacial have increased the average temperature slightly, the introduction of a higher MIS 21 interglacial peak temperature has maintained the sharp increase in temperature across the glacial-interglacial transition. McClymont (2004) states that the temperature range in phase 3 reflects the modern day range more closely (23-26°C, Conkright et al, 2002). Although the average temperature during this time window has not changed, within the 22 new data points in phase 3, the increased SST variability has produced ~5 high temperature values, 3 of which lie above 26°C.

Secondly, the new SST data show suborbital variability (<2.4 kyr) where the sampling resolution permits (MIS 28-25; 23; 18). During phase 2 (875-1150 ka), new data increases the range in SST from 3.9°C to 5.3°C. High resolution sampling between 940 and 1010 ka (2.2 kyr) exhibits large fluctuations in temperature and is responsible for the majority of this variance.

Finally, McClymont and Rosell-Melé (2005) originally noted a period of SST cooling and thermocline shoaling at this site beginning ~1.2 Ma. This studies' data supports a much shorter 65 kyr period of SST cooling prior to the MPT; the 50-kyr running mean does not exhibit cooling until 965 ka, 235 kyr later than McClymont and Rosell-Melé (2005). SST between 1050-960 ka varies in accord with the glacial-interglacial cycles, with the 50-kyr running mean predicting a long term warming with ~1°C amplitude (see figure 4.2B). This increasing mean is largely due to the increase in SST amplitudes and average SSTs from MIS 27 to 25.

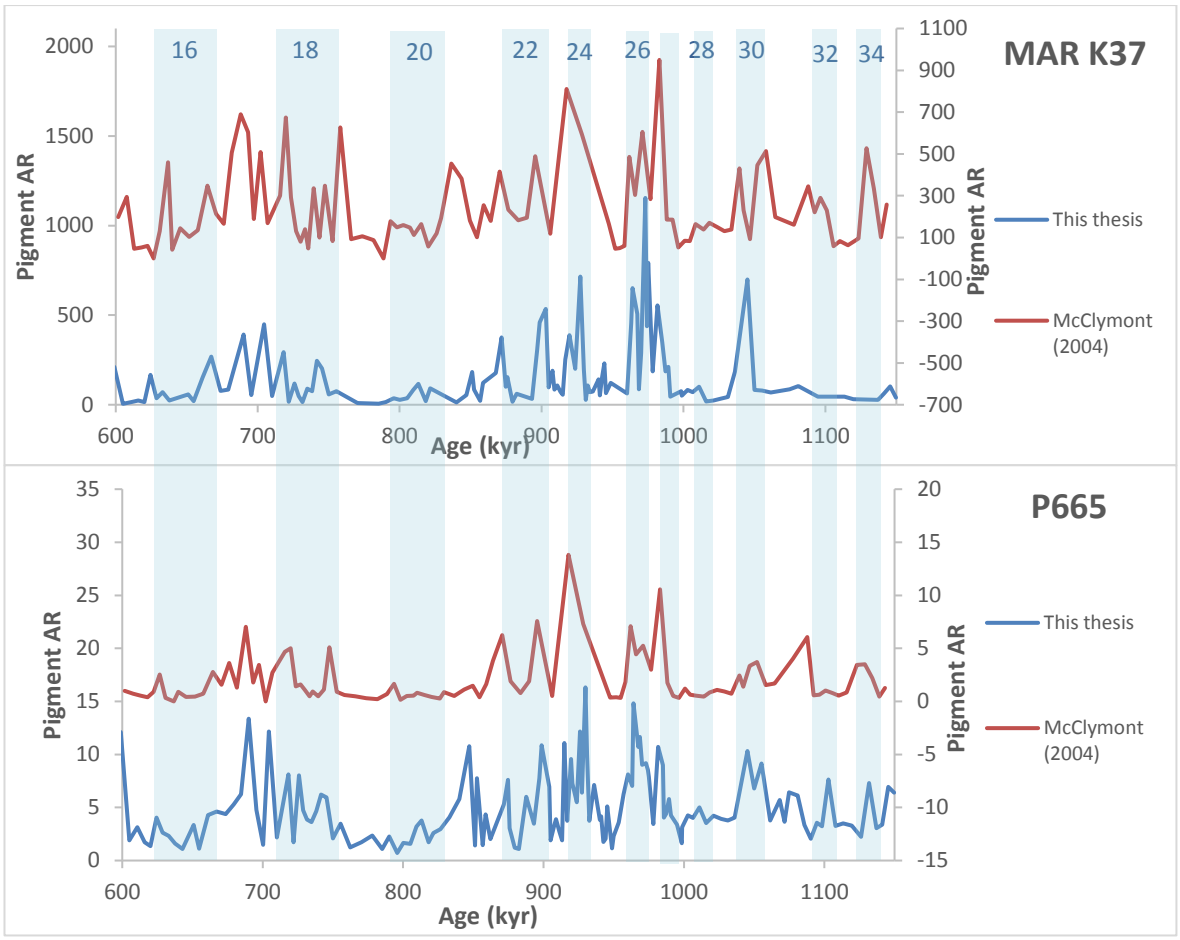

Figure 4.5: Comparison of biomarker ARs in this thesis and McClymont (2004). This thesis data is plotted against the primary axis (left); with McClymont (2004) data plotted against the secondary axis (right). Blue bands indicate glacial periods, or high $\delta^{18}O$ (e.g. MIS 27).

New biomarker ARs have not been synthesised with McClymont (2004) data as the order of magnitude of values between studies are different (see figure 4.5), most likely due to differences in PDA detector sensitivity (outlined in section 3.5). In the original data, biomarker ARs began to increase from ca.980 ka, remaining high until ca.850ka (figure 4.5). The new data presented here supports this trend; the higher resolution sampling shows clusters of peaks during the glacials MIS 26, 24 and 22, correlating well with lows in SST. During MIS 30 a period of high biomarker ARs occurs, which is noticeable in the original P665 record. The new record detects a few high P665 values during MIS 21 P665, later than in the original data, going against the cool SST-high biomarker AR trend during glacials seen across phase 2. The new biomarker data also picks up more isolated high values between ca.690 and ca.710 ka, whereas McClymont's (2004) data showed moderate values. In conclusion, the biomarker accumulation rates broadly support those from McClymont (2004), with the exception of the moderate peak in chlorins during MIS 21. The agreement between McClymont (2004) and this studies' MAR K37 data indicates consistency and therefore reliability in the new SST data points.

4.8.1 Three phases of the MPT

Following the discussion of McClymont's (2004) three 'phases' above, it is clear that there is the need for an additional 'phase' within the existing phase 2, separating the long-term gradual warming SST trend and intermittent productivity from MIS 34 to 26 from the decreasing SST trend and high amplitude productivity peaks between MIS 26 and 22. Phase 2 is therefore split into 2a and 2b, to enable structured analysis of the proxies during each stage of the MPT. Phase 2a spans 1150 ka-965 ka (MIS 34-26); phase 2b spans 965-870 ka (MIS 26-22) (figure 4.2). Note that the transitions between phase 2b and 3 have been altered from 875 to 870 ka to fall in line with the termination of MIS 22, and the culmination of the SST cooling (this is independent of the change in age model between McClymont (2004) and this study).

4.9 Harmonic analysis of ODP site 849 SST and productivity

The solar radiation/insolation value for any latitude is modulated by the orbital parameters eccentricity, obliquity and precession, as discussed in section 1.1. Harmonic analysis, a method of time series analysis, can be used to identify the dominant periodicities (i.e. Milankovitch frequencies) in paleoclimatic data. The presence or absence of these periodicities enables interpretations into the drivers and pacers of climatic change. Here, harmonic analysis has been performed on SST and biomarker AR data using the SPECTRUM programme; procedures are the same as outlined in Schefuβ (2003) [also in McClymont, 2004 - level of significance is 0.05; oversampling factor is 4; high-frequency factor is 1; 1-2 frequencies expected] (see figure 4.6). The advantage of the SPECTRUM harmonic analysis method is the applicability with unevenly spaced datasets (Schulz and Stattegger, 1997) such as this one.

Both statistical tests "gf" and "gs" detect whether periodic components are present which exceed background white noise; with Fishers test ("gf") identifying a single periodicity, and the Siegel test ("gs") identifying up to three (Schulz and Stattegger, 1997). The only statistically significant peak against Fishers test in all three datasets is that of the 128 kyr peak in SST (see figure 4.6 A). This is most likely related to eccentricity forcing. P665 also detects a Siegel-significant peak at an obliquity frequency of ~41 kyr. Both P665 and K37 identify a number of statistically significant peaks (against the Siegel test) at non-orbital frequencies. No significant periodicities below 29 kyr (P665) are identified.

Notably, a ca.30 kyr period in the P665 chlorin productivity indicator is statistically valid against the "gs" test. A 30-kyr period has been found in equatorial Pacific late Pleistocene SST series (Pisias and Mix, 1997; Beaufort et al, 2001). The cause of this non-orbital period is unclear; theories include links to the boreal summer monsoon and ENSO dynamics (Beaufort et al, 2001). This 30-kyr signal has not been found in the tropical Atlantic, only indo-Pacific sites (Clemens et al, 1991; Bassinot et al, 1994; Reichart et al, 1998) adding weight to the idea that ENSO is a controlling factor. Despite this, a 30-kyr cycle has been found in the Vostok ice core (Petit et al, 1999); and low CO_2 values are correlated to high productivity in the Indo-Pacific (Beaufort et al, 2001), argued to

suggest a strengthened biological pump in the tropical Pacific and Indian oceans, with an ENSO-like regulator, was responsible for carbon drawdown and further lowering of atmospheric CO_2.

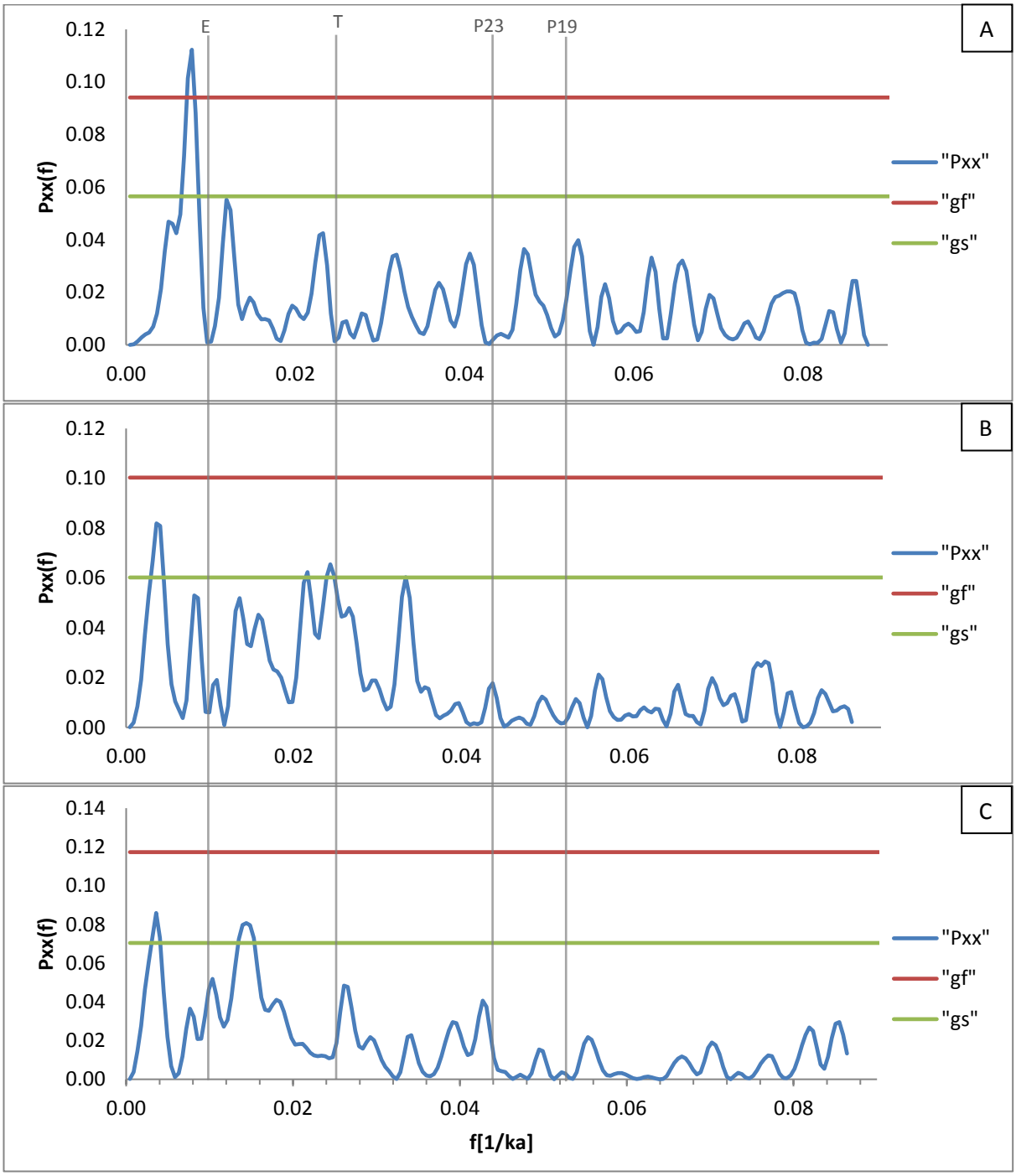

Figure 4.6: Harmonic analysis of ODP site 849 for the following proxies: (A) U^{K}_{37}' SST; (B) accumulation rate of chlorins 'P665'; (C) mass accumulation rate of alkenones 'K37'; "gf" = Fishers test (1929); "gs" = Siegels test (1980) (see text for description and discussion); vertical grey lines show Milankovitch frequencies E = eccentricity (ca.100 kyr); T = tilt ('obliquity'; ca.41 kyr); P = precession (ca.23- and 19-kyr).

The lack of dominant Milankovitch frequencies in ODP site 849 paleoclimate data could be explained in a number of ways. One key disadvantage associated with the SPECTRUM harmonic

analysis is that it is difficult to identify changes within one time series dataset; the entire time window is split into overlapping windows (or 'segments') which are then averaged (Schulz and Stattegger, 1997). This means that in this study, where the total number of proxy data points ranges from 115-149, the number of data points within each segment may be below 100; the minimum value for statistically significant periodicities to be determined (Schulz and Stattegger, 1997). Secondly, in theory, higher resolution sampling enables the detection of higher frequency variations such as precessional (19-23 kyr) variations above background "white noise" (Schulz and Stattegger, 1997). McClymont (2004) noted that it was not possible to identify precession-related variations in a record with >5 kyr temporal spacing. Although the average SST resolution from this study is 3.65 kyr; this is clearly not sufficient to observe sub-29 kyr statistically significant variations in the data using this method; as the strong visual correlation between precessional insolation forcing in both SST, biomarkers and subsurface oxygen isotope data proves (discussed below). This inability to identify high resolution orbital forcing via Harmonic analysis has also been noted in similar studies (Liu and Herbert, 2004; Pisias et al, 1995b).

As a supporting analytical technique, the SST, biomarker AR and carbon and oxygen isotope data have been visually compared to Berger and Loutres (1991) record of orbital parameters and 15°N (July) insolation for the past 10 million years, based on numerical and analytical calculations. This also provides the advantage of identifying any lead/lag relationships.

4.10 Insolation and precession signals at ODP site 849

There is a strong precessional (19- 23-kyr) spectral component to seasonal insolation forcing at tropical latitudes (Cane, 1998; Berger, 1978), as visible on figure 4.7; when precessional forcing is low, the perihelion (the point closest to the sun) is in the northern hemisphere during boreal summer, and so 15°N insolation is higher (Clement et al, 2004). For this reason insolation and precession signals are discussed here together.

Here, 15°N insolation is highly correlated to SST between 1150-950 ka, as precession and SST are inverse to one another; after which SST begins to trace precession and insolation is inverse to SST (figure 4.7 A, B). Liu and Herbert (2004) also found that between 1.8-1.2 Ma, EEP SST varied inversely to local insolation. SSTs are low amplitude during MIS 23, and ca.840-730 ka and 670-630 ka, P665 and K37 productivity is low; all during a period of waning precessional amplitude (figure 4.7). It is clear that precession has a strong influence on tropical SSTs and productivity at ODP site 849. Many late Pleistocene studies have made links between precession and tropical surface ocean proxies (Lyle et al, 1992 [SST]; Perks et al, 2002 [productivity]; Rostek et al, 1997 [productivity]; Molfino and MacIntyre, 1990 [nutricline]; Budziak et al, 2000 [productivity]). Although the way in which precession alters basin-scale tropical ocean-atmosphere feedback processes is not yet fully understood (Koutavas et al, 2002), it is generally accepted that precession modifies seasonal wind and upwelling strength; through altering pole to equator temperature gradients which subsequently expand and contract the trade wind belts (Clement et al, 1999; 2000; Lyle et al, 1992). Indeed, the studies above all concluded that a change in trade wind strength, affecting wind-

driven upwelling (argued to be similar to the modern-day La Niña-like state in the tropical Pacific [Perks et al, 2002]) was responsible for the precessional-scale productivity and SST fluctuations.

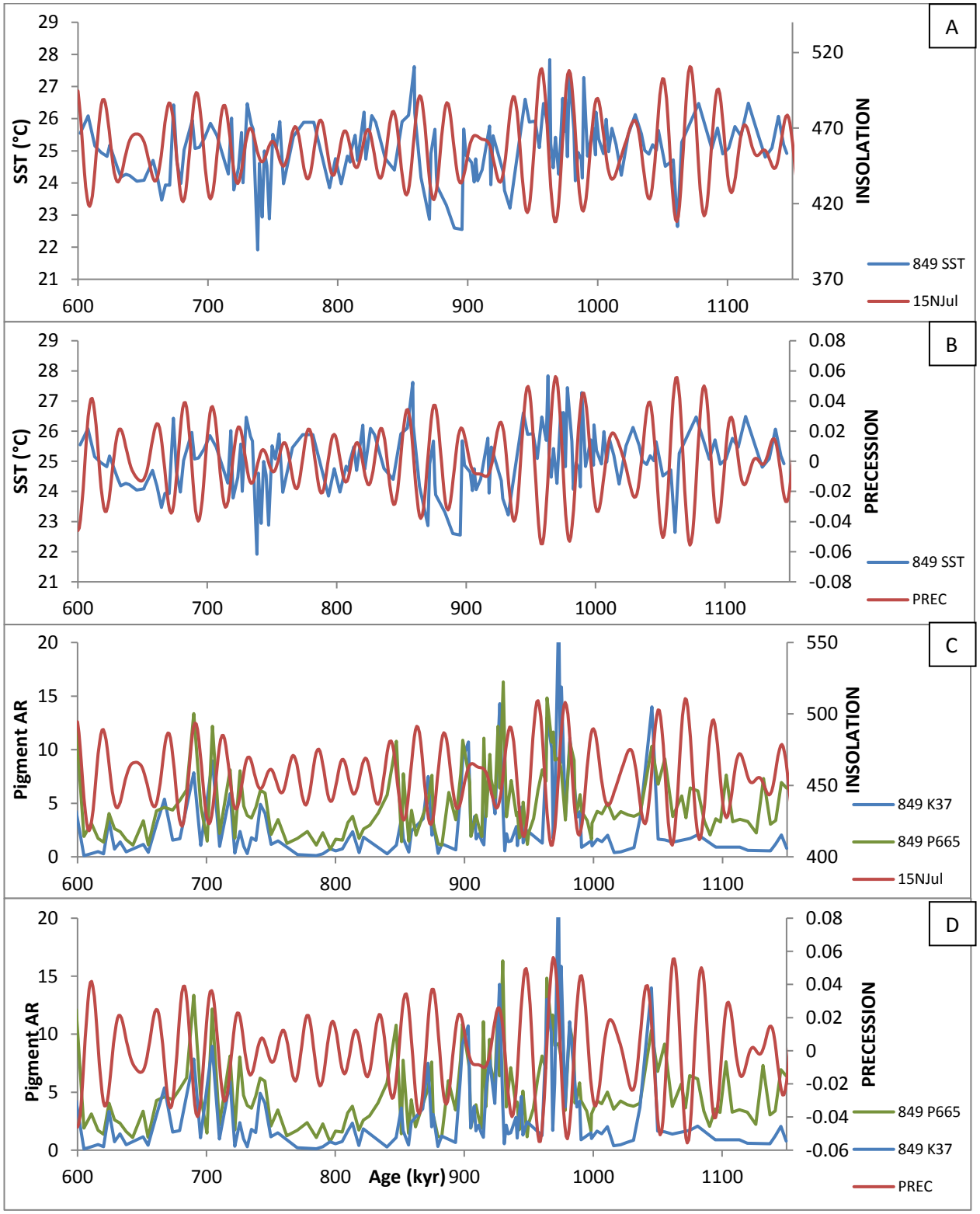

Figure 4.7: ODP site 849 SST and biomarker ARs plotted against Berger and Loutre's (1991) values of 15°N (July) insolation (A, C) and precession (B, D)

The data presented here suggests that prior to and during the MPT, productivity and SST has a strong precessional periodicity, agreeing with the inferred upwelling as a control over the surface ocean at this site as justified throughout this discussion.

Between ca.1000-960 ka, SST fluctuates on a semi-precessional basis, peaking once or twice as precessional power is low and vice versa (figure 4.7 A). During this time precessional amplitude is strong, and SSTs are abnormally high. As discussed in section 5.4, a semi precessional (9-12 kyr) signal in tropical paleoclimate records is hypothesised to be capable of driving the MPT through ocean-atmosphere feedbacks (Hernandez-Almeida et al, 2012). As this correlation is during a key period of the MPT, just prior to the onset of severe SST changes during MIS 24-22, this indicates that the EEP may play a key role in the progression of the MPT.

4.11 Eccentricity and obliquity signals at ODP site 849

Overall, there is little correlation between eccentricity and SST (figure 4.8 A). Regarding biomarker ARs, there is also negligible correlation with eccentricity; although it could be argued that from ca.750 ka increases in productivity during MIS 17/18 occur during a peak in eccentricity. Although the glacial-interglacial cycles operate on a ~100-kyr timescale post-MPT, the majority of variance in solar radiation is dominated by obliquity and precession, especially in low to mid latitudes (Berger et al, 1993). There is little change in the direct insolation forcing at the eccentricity component, hence the '100-kyr problem' of the MPT (Imbrie et al, 1992; 1993). Some studies have identified a significant 100-kyr component (Anderson and Prell, 1993; Emeis et al, 1995; Lea et al, 2000; Beaufort et al, 2001; Medina-Elizalde and Lea, 2005). However the majority of studies, as with ODP site 849 here, note there is a negligible or nil eccentricity aspect to tropical late Pleistocene climate records (Clemens et al, 1996; Perks et al, 2002).

SST appears to trace the obliquity insolation pattern very well between 1150-800 ka, after which SST tends to lag obliquity variations by an increasing amount, until there is no discernible correlation (figure 4.8 B). There does not appear to be any consistent relationship between obliquity and productivity (figure 4.8 D). The presence of obliquity SST cyclicity suggests a remote connection with the higher latitudes; as local isolation is completely dominated by precession in the equatorial region. It could be argued that the connection between high and low latitudes would be more pronounced in the late Pleistocene following the development of more extensive ice sheets; however the reverse is seen here, from 800 ka onwards there is little to no correlation with 41-kyr cycles. A similar response in the EEP has been noted by Liu and Herbert (2004); accredited to a stronger northern hemisphere ice-albedo feedback whilst the climate was highly attuned to obliquity forcing.

McClymont (2004) found (only) prominent obliquity peaks in both SST and K37 at ODP site 849. Although the method of analysing orbital periodicities is different between the two studies, the addition of higher-resolution data appears to have enabled clearer correlations between precessional forcing, however arguably less clear later eccentricity forcing in the dataset.

In summary, visual comparison of orbital cycles against ODP site 849 paleoclimate proxies show that the key time period when the MPT shift from 41-kyr to 100-kyr dominant cycles became unequivocal at this site was ~800 ka; and there was a noticeable transition at ca.950 ka as SST became out of phase with insolation and began tracing precession.

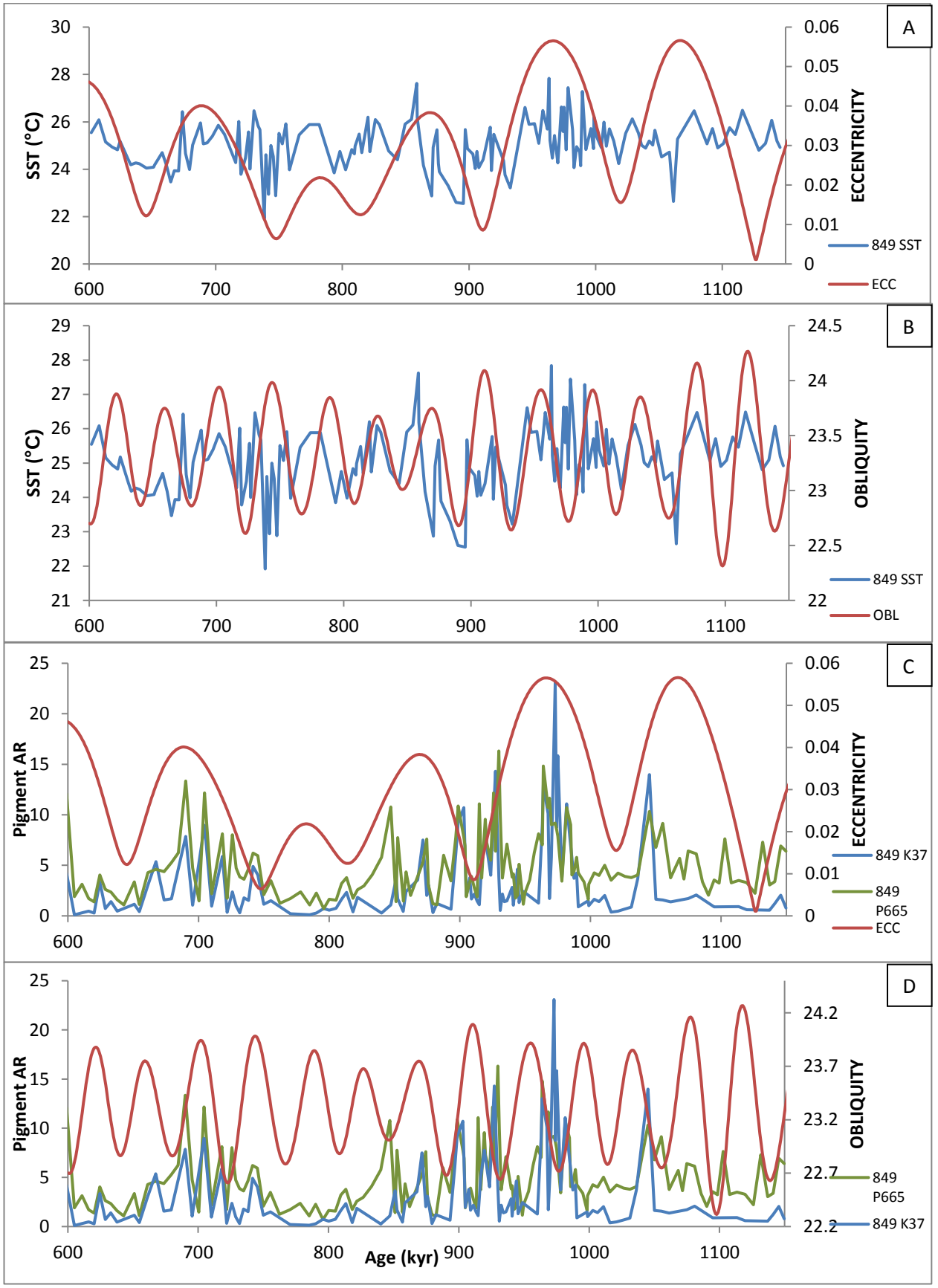

Figure 4.8 (overleaf): ODP site 849 SST and biomarker ARs plotted against Berger and Loutre's (1991) values of eccentricity (A, C) and obliquity (B, D)

Chapter 5: Discussion and Wider Implications

5.1 Introduction

The aim of this chapter is to explore the themes and events outlined in the results, and reconstruct the activity of the ocean-atmosphere system during each of the three 'phases' of the MPT, as defined above. The findings will then be discussed with reference to the theories of how the MPT evolved; and the role the EEP might have played.

5.2 Stratification vs upwelling in the EEP

5.2.1 Evidence from plankonic foraminifera assemblages

Based on the preliminary analyses, on average throughout the record, *G.ruber* made up less than 10% of the assemblage, whereas *N.dutertrei* tended to dominate the assemblages with 37%. Farrell et al (1995) found that at ODP site 847 *N.dutertrei* averaged 45% of the core species (*G.sacculifer* was never more than 13% of the total count); high production of *N.dutertrei* is accredited to optimal ecological conditions, perhaps caused by high levels of upwelling. Considering *N.dutertrei* is resistant to dissolution, this value is more likely due to increases in production rather than changing levels of dissolution (Farrell et al, 1995). The dominance of *N.dutertrei* is encouraging when considering the validity of carbon and oxygen isotope interpretation as Reynolds-Sauter and Thunell (1991) found that *N.dutertei* provides accurate signal of depth distribution, except when the flux of the species is low.

5.2.2 Evidence from oxygen isotopes

Upon visual inspection of the individual planktonic $\delta^{18}O$ records (see figure 4.2E), the $\delta^{18}O$ of *G.ruber* is consistently lighter than *N.dutertrei*, indicating a higher habitat temperature (a higher calcification temperature produces a lighter $\delta^{18}O$ and vice versa [Rohling, 2007; Ravelo and Hillaire-Marcel, 2007]). This suggests that between the surface mixed layer and the thermocline there is some stratification in the water column. There is no clear trend that both species follow, which suggests that as well as ice volume, temperature fluctuations are responsible for changes in $\delta^{18}O$ in one or both species. It must be noted that because no species-specific correction for foraminiferal 'vital effects' has been carried out (aside from those discussed in section 5.2.3.1 below), these may play a small role in the fluctuations of stable isotope values (Ravelo and Hillaire-Marcel, 2007).

Ideally the effect of ice volume on seawater $\delta^{18}O$ will have affected both species' foraminiferal $\delta^{18}O$ equally. The difference between $\delta^{18}O$ of both species ($\Delta\delta^{18}O_{(N.d\text{-}G.r)}$) will in theory remove this ice volume signal, leaving changes in temperature the main signal; from which the thermal gradient, and extent of stratification or upwelling can be estimated. A reduced thermal contrast ($\Delta\delta^{18}O$) between species during glacials indicates a reduced or absent thermal gradient, therefore (strengthened) upwelling. A larger temperature difference between the surface ocean (*G.ruber*) and the thermocline (*N.dutertrei*) indicates a steeper thermal gradient and a well stratified water column. Thermocline depth cannot be estimated in this study as *N.dutertrei* calcifies within the

thermocline and so as the thermocline migrates to a deeper or shallower position, the calcification temperature and therefore the *N.dutertrei* $\delta^{18}O$, remains the same.

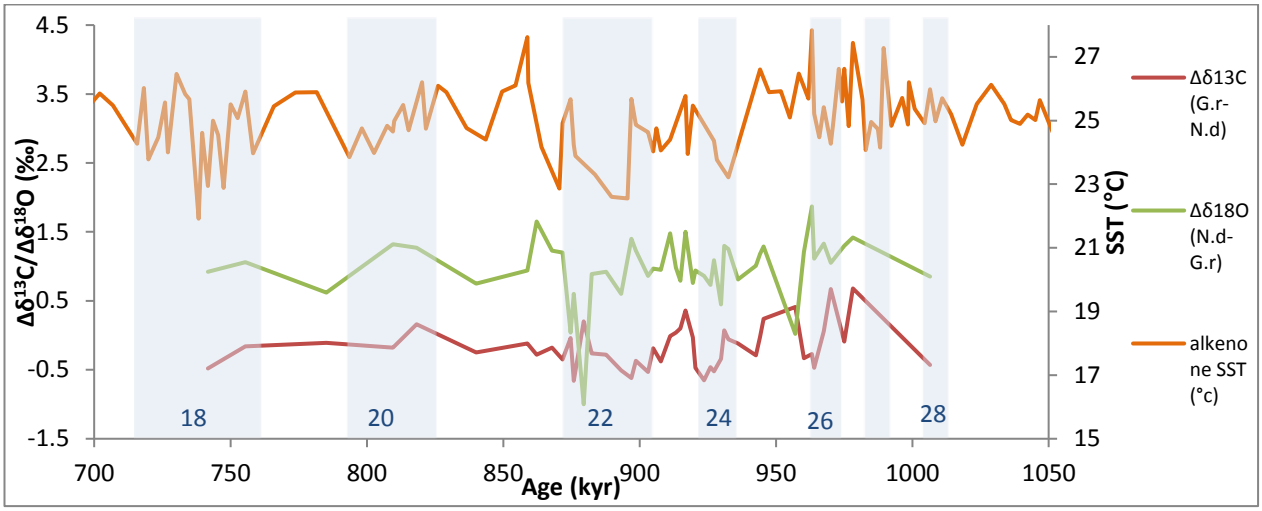

Figure 5.1: ODP site 849 $\Delta\delta^{18}O$, $\Delta\delta^{13}C$ and SST. Blue shading indicates glacial stages or periods of heavier LR04 $\delta^{18}O_{benthic}$; numbers refer to marine isotope stages.

Across the entire time window, three events occur which go against the aforementioned trend of a consistent offset between the species. *G.ruber* and *N.dutertrei* values coincide (low $\Delta\delta^{18}O$) towards the end of the glacials MIS 24 and 22, and interglacial MIS 25 (figure 5.1). It appears that during MIS 25 and 22 *G.ruber* $\delta^{18}O$ deviates from its average signal, becoming heavier (see figure 4.2E), this not only suggests intense upwelling but also surface cooling, corroborated by low or declining U^{K}_{37}' SSTs. A much smaller amplitude dip in $\Delta\delta^{18}O$ occurs during MIS 24.

During MIS 22 (ca.880 ka), the $\delta^{18}O$ signature of *G.ruber* is much heavier than *N.dutertrei*, suggesting the surface ocean temperature was much cooler than the thermocline. Farrell et al (1995) also produced temperature 'inversions' using a complex estimation of temperature difference between G.*sacculifer* (a surface dweller) and *N.dutertrei* $\Delta\delta^{18}O$ at ODP site 847 (see figure 1.2 for site location). Farrell et al (1995) comment that these inversions are unlikely in reality, however during MIS 22 they too found a low $\Delta\delta^{18}O$, equating to a 0°C change in temperature between the surface and the thermocline (see figure 5.2). As discussed in section 2.7.1.1, changes in salinity, capable of affecting $\delta^{18}O$ values, are negligible in the EEP therefore changes in salinity at either the surface or thermocline is not an adequate explanation for this inversion. The data point at ODP site 849 responsible for this 'reversal' was repeated for reliability, and returned a value much lighter (from +1.69‰ to -0.07‰). Even with this lighter second-run value, a dip in the $\Delta\delta^{18}O$ would still be produced as the *G.ruber* $\delta^{18}O$ value at 875 ka is also close to that of *N.dutertrei* (figure 5.1). With two data points indicating a noticeable inflection or reduction in thermal gradient whilst U^{K}_{37}' SST is low and during a particularly cool glacial known to be key in the tipping point of the MPT, this may mean a considerable change in surficial temperature - an extreme upwelling event, occurred ca.875-880 ka.

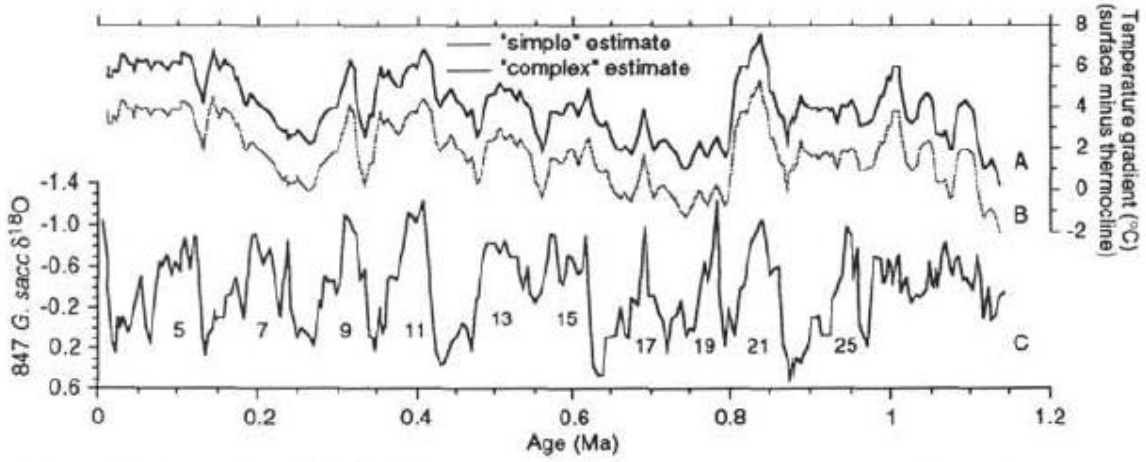

Figure 5.2: ODP site 847 temperature difference between upper thermocline and surface mixed layer in the EEP ($\Delta\delta^{18}O_{(N.dutertrei\text{-}G.sacculifer)}$); A) "Simple" estimate calculated using Erez and Lutz (1983) equation; B) "Complex" estimate is corrected for species 'vital effects'; C) G.sacculifer $\delta^{18}O$ record. Source: Farrell et al (1995).

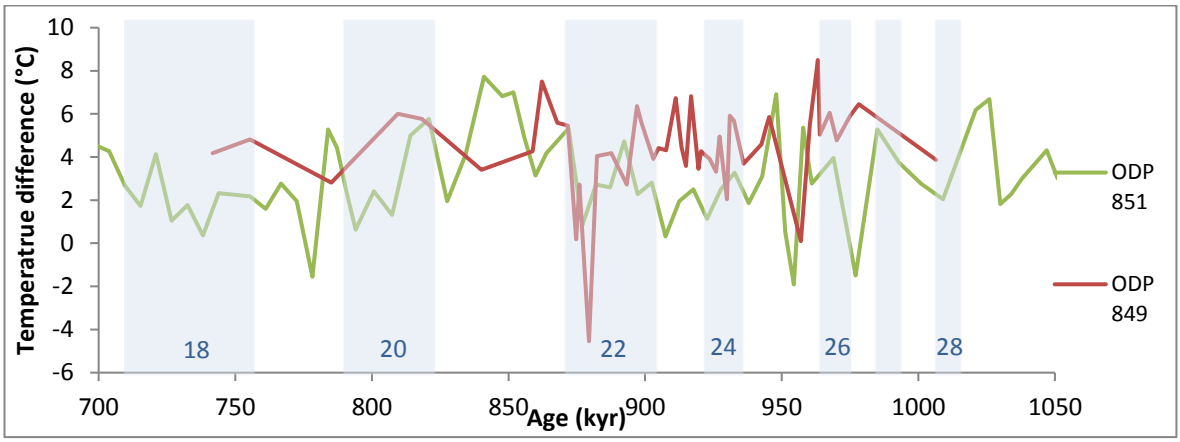

Figure 5.3: Comparison of temperature differences between upper thermocline and surface mixed layer in the EEP ODP site 849 (this thesis - $\Delta\delta^{18}O_{(N.dutertrei\text{-}G.ruber)}$) and ODP site 851 (Ravelo and Shackleton, 1995 - $\Delta\delta^{18}O_{(N.dutertrei\text{-}G.sacculifer)}$). Both calculations use the Erez and Lutz (1983) equation. Blue shading indicates glacial stages or periods of heavier LR04 $\delta^{18}O_{benthic}$; numbers refer to marine isotope stages,

Previous studies on planktonic foraminifera *G.sacculifer*, *N.dutertrei* and *G.tumida* (which calcifies at the base of the photic zone) in the EEP at ODP site 847 and 851 (Farrell et al, 1995; Ravelo and Shackleton, 1995) have found that the $\Delta\delta^{18}O$ between *G.sacculifer* and *G.tumida,* and *G.sacculifer* and *N.dutertrei* was smaller during glacials and greater during interglacials, indicating a tendency towards glacial upwelling. However, Farrel et al (1995) does note this is not seen throughout the entire 1.2 Ma record. This trend at both sites is particularly clear between MIS's 8-18, whereas from MIS onwards the pattern is not as distinct (see figure 5.3) (Ravelo and Shackleton, 1995; Farrell et al, 1995). These findings are somewhat consistent with ODP site 849; in two of the possible four glacials the record spans (MIS 20-26) upwelling events are observed; although this trend is not

consistent, with one event occurring during the interglacial MIS 25, as noted also by Farrell et al (1995).

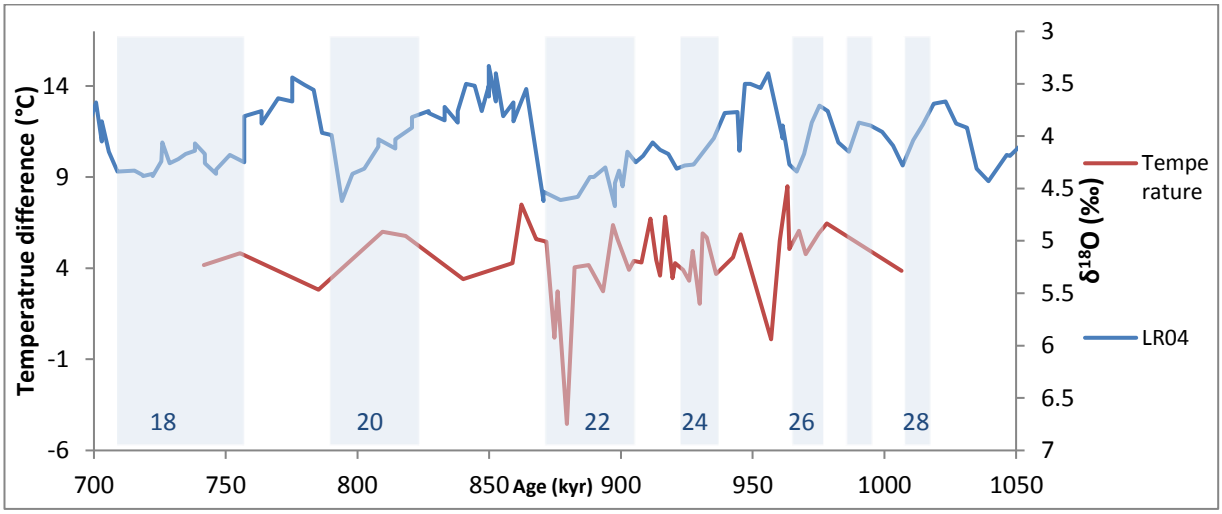

Figure 5.4: The ODP site 849 temperature difference between the surface ocean and thermocline (N.dutertrei-G.ruber), against LR04. Blue shading indicates glacial stages or periods of heavier LR04 $\delta^{18}O_{benthic}$; numbers refer to marine isotope stages.

Studies have produced an equilibrium fractionation calculation to determine the approximate temperature at which the foraminifera calcified its shell based on the oxygen isotope value. This ranges from 0.21-0.23‰ depletion in carbonate $\delta^{18}O$ per 1°C (Erez and Lutz, 1983; Bemis et al, 1998). Erez and Lutz (1983) based their equation on *G.sacculifer* whereas Bemis et al (1998) studied the planktonic species *O.universa* and *G.bulloides*. All three species reside in the surface mixed layer (0-50m), as with *G.ruber*, studied here. Although the difference in temperature between *N.dutertrei* and *G.*sacculifer is analysed here, and not the individual $\delta^{18}O$ values, it is acknowledged that the incorporation of *N.dutertrei* (it's habitat being in the variable-depth thermocline), introduces some uncertainty as publications applying this equation to this exact species are not profuse.

$$\frac{\Delta\delta^{18}O\ (N.dutertrei - G.ruber)}{0.22} \qquad \textbf{(Erez and Lutz, 1983)}$$

Using the value 0.22‰ equal to each 1°C (as above), during the upwelling events in MIS 22, 24 and 25 the surface-thermocline temperature difference is predicted to be -4.55°C (including the ca.880 ka reversal; 0.18°C without), 2.05°C and 0.09°C respectively (see figure 5.4). This is compared to an average $\Delta\delta^{18}O$ of 0.98‰ representing a warmer surface ocean compared to thermocline by an average of 4.45°C (range -4.55 to 8.5°C). ODP site 847 had a temperature difference of between 0.2-7.6°C, with an average of 4.2°C, using the Erez and Luz (1983) equation, and ODP site 851 had a temperature difference of 3°C during glacials and 5°C during interglacials using the Epstein et al (1953) equation (Farrell et al, 1995; Ravelo and Shackleton, 1995). Therefore average temperature contrasts in the EEP across the MPT were similar. However specific glacial upwelling events at ODP site 849 exhibited much smaller thermal contrasts with an

average of 0.7°C (not taking into account the 880 ka reversal). The interglacial temperature difference at ODP site 849 however is 4.9°C, comparable to ODP site 851. Whilst the time period covered by this study from ODP site 849 is relatively short, it appears that site 849 experienced more severe upwelling than either sites 847 and 851.

5.2.3 Evidence from carbon isotopes

Planktonic carbon isotope changes are governed by a number of different factors (as discussed in section 2.7.1.2); here the difference in $\delta^{13}C$ ($\Delta\delta^{13}C$) between the surface and thermocline is used to infer nutrient gradients, and therefore the degree of vertical mixing, in much the same way as $\Delta\delta^{18}O$ infers thermal gradients.

The weak trend in $\Delta\delta^{13}C_{(G.r\text{-}N.d)}$ (*N.dutertrei* has been subtracted from *G.ruber* simply to produce peaks in the same direction of $\Delta\delta^{18}O$, enabling easy comparison), visible on figure 5.1, is one of lower $\Delta\delta^{13}C$ during glacials, indicating high levels of mixing caused by upwelling. This finding agrees somewhat with the $\Delta\delta^{18}O$, particularly during MIS 24. Approaching the severe glacial during MIS 22 (ca.880 ka), $\Delta\delta^{13}C$ and $\Delta\delta^{18}O$ diverge. $\Delta\delta^{13}C$ increases, indicative of a more stratified vertical water column, as $\Delta\delta^{18}O$ decreases dramatically suggesting severe upwelling. At this time both SST and biomarker ARs seem to go against the previous trend of low SST-high productivity (figure 4.2); with low values for both, followed by high values for both some 5 kyr later. At ca.875 ka, $\Delta\delta^{13}C$ and $\Delta\delta^{18}O$ once again appear inverse, with $\Delta\delta^{13}C$ indicating upwelling and $\Delta\delta^{18}O$ a highly stratified water column. It is difficult to reconcile this event without further (higher resolution) evidence; although it is clear that between 875-880 ka the EEP surface ocean is highly dynamic suggesting that perhaps a climatic threshold has been crossed. Farrel et al (1995) (ODP Site 847) also identified a clear trend whereby smaller $\Delta\delta^{13}C_{(G.sacculifer\text{-}N.dutertrei)}$ contrasts occurred during glacials, attributed to increased (wind-induced) upwelling along the equator, mixing the low $\delta^{13}C$ thermocline waters with the high $\delta^{13}C$ surface waters and reducing the steep $\delta^{13}C$ gradient (see figure 5.5).

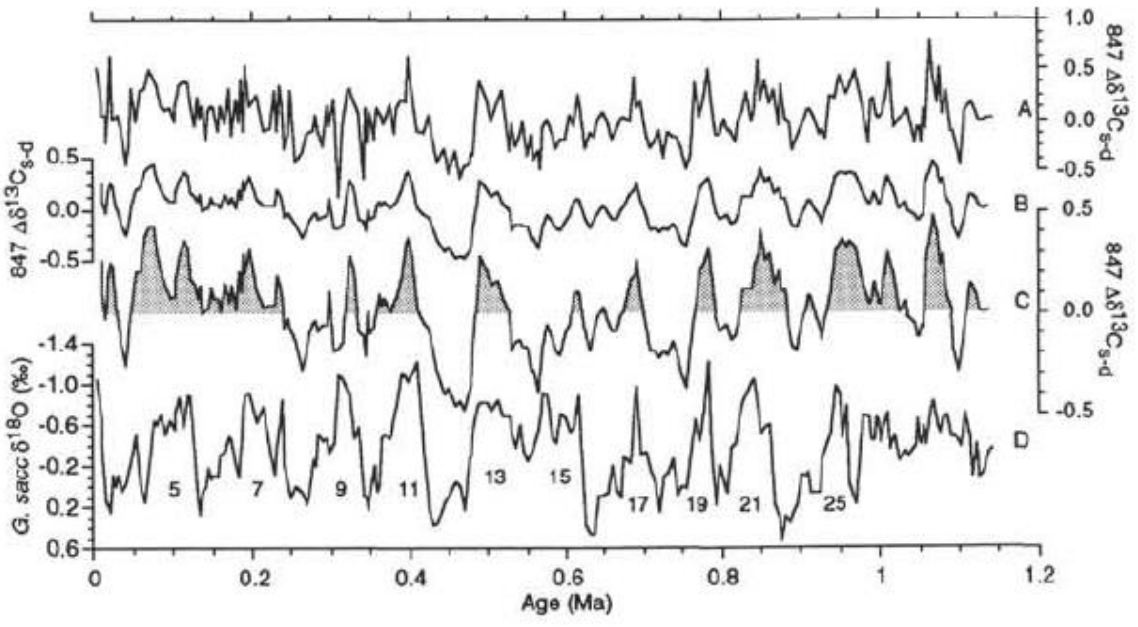

Figure 5.5 (overleaf): Carbon isotope difference between the thermocline and mixed layer at ODP site 847 ($\Delta\delta^{13}C_{(G.sacculifer-N.dutertrei))}$. A) Difference per sample; B) Smoothed version of A; C) Expanded scaling of B; D) G.sacculifer $\delta^{18}O$ shown for comparison. *Source: Farrell et al (1995).*

In summary, carbon and oxygen isotopes from ODP site 849, and supporting evidence from ODP sites 847 and 851, indicate that during phase 2b, glacial upwelling occurred in the EEP.

5.2.3.1 Correcting *N.dutertrei* $\delta^{13}C$

In the surface ocean, photosynthesis dominates over respiration and therefore local $\delta^{13}C$ is high (as discussed in section 2.7.1.2). In the deep ocean, respiration dominates over photosynthesis thus $\delta^{13}C$ values are much lower. Changes in primary productivity would therefore be expected to play a large role in the $\delta^{13}C$ of surface dwelling isotope signals. It would follow that *G.ruber*, as a surface dweller, would be expected to have a higher $\delta^{13}C$ over *N.dutertrei*, due to its position in the photic zone with highest photosynthesis rates. However this is not seen here, and $\Delta\delta^{13}C_{(G.r-N.d)}$ (figure 5.6) produces mainly negative values with an average of -0.16‰. A similar result was noted by Farrell et al (1995) at ODP site 847 whereby their average $\Delta\delta^{13}C$ was 0‰. There are two possible reasons for this. The first is a genuine thermodynamic explanation for heavier thermocline (*N.dutertrei*) $\delta^{13}C$ values (Broecker and Peng, 1982; Charles et al, 1993). Southwest Pacfic surface waters sink to form sub-Antarctic Mode Water (SAMW) which feeds the subsurface EUC and thermocline. If greater gas equilibriation took place between the (southwest Pacific) ocean surface and the atmosphere, caused by cooler temperatures, faster CO_2 exchange rates and longer surface water residence times, the $\delta^{13}C$ of DIC would increase (Farrell et al, 1995; Lynch-Stieglitz, 1995). This heavier $\delta^{13}C$ signal would then be transmitted to the EEP thermocline via the EUC. However, the $\Delta\delta^{13}C$ at ODP site 851 has a positive average value as *G.ruber* $\delta^{13}C$ was consistently higher than *N.dutertrei* (Ravelo and Shackleton, 1995; Cannariato and Ravelo, 1997), and so this explanation seems unlikely given that the EEP would be expected to reflect broadly similar trends.

Alternatively, as discussed in sections 2.7.1.1 and 2.7.1.2, foraminifer size may have affected the calcite $\delta^{13}C$ signal. At ODP site 847, *G.sacculifer* was found to approximate the $\delta^{13}C$ of the surface layer DIC based on previous studies (Farrell et al, 1995), whereas it is known that *N.dutertrei* (355-425 μm) generally calcifies with $\delta^{13}C$ values 0.5‰ heavier than seawater (Ravelo, 1991). Ravelo and Shackleton (1995) comment that *N.dutertrei* calcify within the steepest part of the thermocline, where $\delta^{13}C$ and nutrient gradients are also steep. Therefore small changes in the depth of calcification have a large effect on their $\delta^{13}C$ signature (Ravelo and Shackleton, 1995). Also, algal planktonic species are known to have size-specific $\delta^{13}C$ signals; Farrell et al (1995) found a strong positive correlation between foraminifera size and changes to $\delta^{13}C$, potentially due to the increased rates of photosynthesis (Ravelo and Fairbanks, 1995; Spero and Deniro, 1987). This is a more likely explanation for this 0.5‰ discrepancy. To account for this disparity, a correction of -0.5‰ has been applied to *N.dutertrei* $\delta^{13}C$ values prior to the $\Delta\delta^{13}C$ calculation, shown in figure 5.6 ('corrected $\delta^{13}C$'). This raises the $\Delta\delta^{13}C$ to above 0‰, except for MIS 22 and 24.

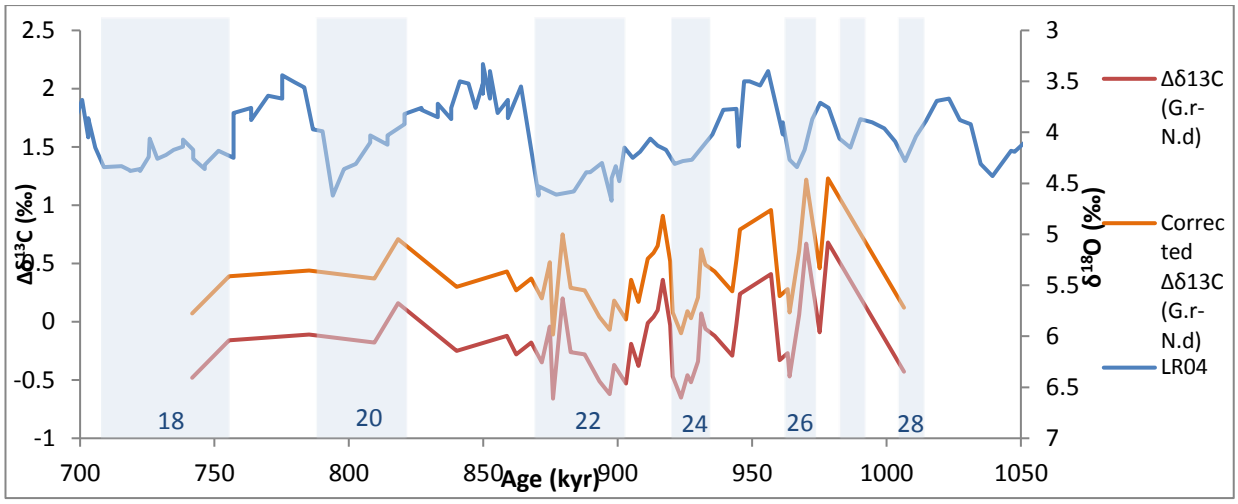

Figure 5.6: ODP site 849 $\Delta\delta^{13}C$ (G.ruber-N.dutertrei) and corrected $\Delta\delta^{13}C$ (G.ruber-N.dutertrei where N.dutertrei - 0.5‰, as discussed in text) against LR04. Blue shading indicates glacial stages or periods of heavier LR04 $\delta^{18}O_{benthic}$; numbers refer to marine isotope stages.

Interestingly, following the *N.dutertrei* $\delta^{13}C$ correction, ODP site 847 had no $\Delta\delta^{13}C$ values below 0‰ (Farrell et al, 1995), unlike ODP site 849. This suggests either the sampled or mean EEP *N.dutertrei* test size was much larger at ODP site 849, or the upwelling events were more severe. ODP site 851 did not experience any negative $\Delta\delta^{13}C$ values (0-2 Ma) and instead their average $\Delta\delta^{13}C$ was 0.33‰ (Ravelo and Shackleton, 1995). As outlined in section 5.2.2, the $\Delta\delta^{18}O$ changes (and inferred temperature contrasts) were also more severe at ODP site 849 than 851; and so this further supports the idea that ODP site 849 experiences more severe upwelling events than both ODP sites 847 and 851.

5.3 Productivity at ODP site 849

On the whole, ODP site 849 exhibits a high degree of correlation between the chlorin and the alkenone ARs, suggesting that coccolithophores make up a substantial part of the marine phytoplankton biota, as observed in the modern-day EEP (Chavez, 1989; Chavez et al, 1990; 1991; 1996; Landry and Kirchman, 2002). Each compound class has different susceptibilities to degradation, suggesting degradation to the core has been minimal as both proxies agree well with each other.

During phases 2a and 2b, high productivity (both alkenone and chlorins) tends to occur during glacial stages. In fact, every glacial period during this time experiences high levels of total primary productivity, with the exception of MIS 28. From MIS 22 onwards (phase 3), there is no apparent relationship between productivity and glacial-interglacial cycles.

5.2.1 *G.ruber* $\delta^{13}C$ and biomarker ARs: productivity vs upwelling and source water contributions

During MIS 22-23, both K37 and P665 display a moderate inverse correlation with *G.ruber* $\delta^{13}C$; with an r^2 value of -0.6 (figure 5.7). K37 has a slightly weaker correlation with *G.ruber* $\delta^{13}C$

between MIS 22-25 (r^2 0.5); whereas elsewhere in the time window both proxies have a negligible statistical correlation with *G.ruber* $\delta^{13}C$; although in some places some visual correlation exists (e.g. coming into MIS 26), suggesting the temporal resolution of samples may be slightly out of sync. During these correlative periods, when P665/K37 is low, $\delta^{13}C$ is high, and vice versa. High $\delta^{13}C$ in surface waters suggests high productivity, as ^{12}C is being preferentially taken up during photosynthesis (Wefer et al, 1983; Dunbar, 1983). However, high $\delta^{13}C$ could also mean a reduction in the supply of ^{12}C-enriched water, if the $\delta^{13}C$ was recording shifting contributions of upwelled water into the surface mixed layer. This would explain the inverse correlation with productivity. Cool, nutrient-rich, ^{12}C-enriched SAMW feeds into both the EUC and the SEC which makes up the thermocline waters at ODP site 849 (Farrel et al, 1995; Ravelo and Hillaire-Marcel, 2007). The ^{12}C-enriched signal relates to higher nutrient concentrations or lower atmospheric CO_2 gas exchange in the zone of SAMW formation (~50°S), in the Southern Ocean. Either an increase in the proportion of SAMW fed into the surface ocean at ODP site 849 or an increase in the rate of upwelling, or both, may account for a lighter *G.ruber* $\delta^{13}C$ signal. Supporting this, low *G.ruber* $\delta^{13}C$ also tends to occur during periods of low SST, and vice versa (such as during the notably high MIS 27 SSTs, *G.ruber* $\delta^{13}C$ is high). Further support for the input of SAMW exists in the $\Delta\delta^{18}O$ and $\Delta\delta^{13}C$-inferred upwelling during MIS 22, 24 and 25, which also occur during periods of moderate to high productivity. Pena et al (2008) studied ODP site 1240, east of the Galapagos Islands, during the past 275 kyr and found negative $\delta^{13}C$ excursions of *G.ruber* during glacials which they attribute to the transport of Antarctic-sourced low $\delta^{13}C$ waters into the EEP via the EUC.

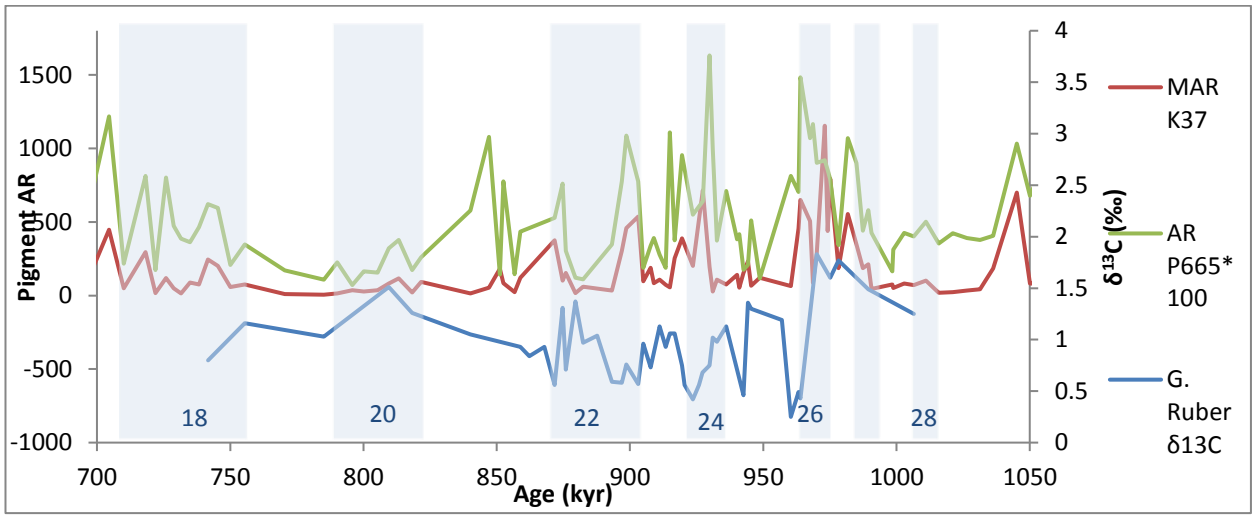

Figure 5.7: MAR K37, P665 and G.ruber $\delta^{13}C$ from ODP site 849. AR P665 has been multiplied by 100 in order to compare to MAR K37. Blue shading indicates glacial stages or periods of heavier LR04 $\delta^{18}O_{benthic}$; numbers refer to marine isotope stages.

5.3.2 Controls over productivity at ODP site 849

A change in the nutrient content of surface waters in the EEP, and therefore a change in productivity, is most likely caused either by upwelling, shifting source water contributions or fluvial or aeolian terrestrial fertilisation (Higginson, 2000). Upwelling and contribution from the equatorial cold tongue (Chavez and Barber, 1987) provides the macronutrients (such as nitrate, phosphate

and dissolved silica) required to sustain productivity levels, whereas aeolian dust provides other nutrients such as iron (Zhao et al, 2006), having an instant fertilising influence in the open ocean (Martin and Fitzwater, 1988; Mills et al, 2004).

In the equatorial upwelling region, upwelled macronutrients are never fully consumed and so productivity never reaches its true maximum (Barber and Chavez, 1991). This is termed the high-nitrate low-chlorophyll state (HNLC). Limiting nutrients such as iron is just one explanation for this (Sorokin et al, 1977; Barber and Chavez, 1991), and in the equatorial upwelling region, iron limitation is known to affect productivity (Chavez et al, 1991; Martin et al, 1991). Farrell et al (1995) refers to the potential for increased input of micronutrients, like iron, (Martin, 1990) as the cause for higher glacial productivity in the EEP. Two potential sources into ODP site 849 region are increased aeolian dust flux and strengthened erosion from the Galapagos Islands due to lower sea level and stronger westward trade winds (Farrel at al, 1995). The EUC has also been suggested to carry iron-rich waters from Indonesia to the eastern Pacific (Wells et al, 1999). Alternatively, Pichevin et al (2009) found that during the LGM, the biological carbon pump was strengthened in the EEP (ODP site 1240, near ODP site 847) but evidence from silicon and nitrogen isotopes indicate that there was no iron, nitrogen or silicon limitation, and instead phosphorous was the only limiting nutrient. Biogeochemical cycling can enable algal blooms to remain in the surface ocean for up to 2 years, and as a consequence annual dust 'storms' can be reflected as continuous productivity in the sediment record (Zhao et al, 2006). In the Southern Ocean, strengthened atmospheric dust transport during the past 2 glacials were found to correlate with enhanced productivity, attributed to this dust fertilization effect (Ikehara et al, 2000).

The presence of glacial upwelling suggests that this is a key control over productivity at this site pre-MIS 22; and the anti-correlated P665 and *G.ruber* $\delta^{13}C$ signals suggest an enhanced contribution of ^{12}C-enriched SAMW; and therefore changing source water contributions may also be considered a controlling factor. Comparison of SST and $\Delta\delta^{18}O$-derived changes in temperature gradients (figure 5.1) indicate that upwelling events occur between 2-4 kyr before (MIS 25, 22), or after (MIS 24) dips in SST. This, coupled with the increasing $\Delta\delta^{18}O$ of *G.ruber* during these events leads to the qualification that there is a link between a cool surface ocean and upwelling. Further to this, during phase 2b, high productivity is strongly linked to cool SSTs, with peaks in biomarker AR productivity occurring on average within 2.6 kyr (P665) or 2.7 kyr (MAR K37) of lows in SST. There is no consistent lead/lag relationship between the two. In summary the multiproxy evidence analysed here suggests ODP site 849 reflects a La Niña-like (section 2.4) glacial EEP prior to, and including, MIS 22. This state is characterised by stronger trade winds, strengthened upwelling, a steeper east-west thermocline tilt, and cooler SSTs. The strengthening glacial-productivity link from phase 2a to 2b may be explained via more severe glacial-interglacial cycles and larger continental ice sheets creating stronger trade winds, and therefore strengthened dust flux (supplying limiting nutrients), as well as enhanced wind-induced upwelling. Supporting this, McClymont (2004) identified a coarsening of sediment grain size in the ODP site 849 core between 1200-900 ka, suggesting an increasing contribution of aeolian dust (figure 5.8) (Janecek and Rea, 1985; Hovan, 1995; Zhao et al, 2000).

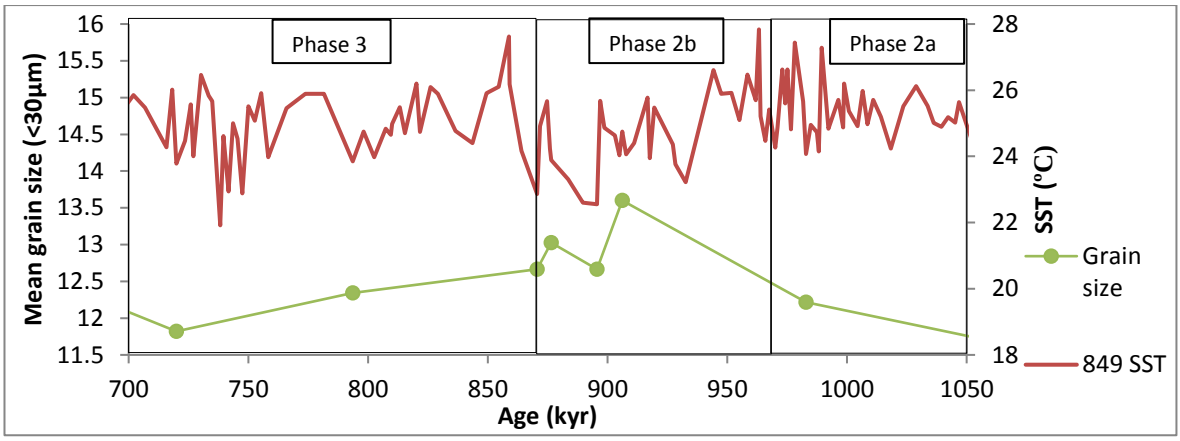

Figure 5.8: Mean grain size at ODP site 849 against SST. Mean grain size data taken from McClymont, 2004. Phases shown for context.

The findings here agree with many studies which call for a more productive glacial EEP over the past few glacial-interglacial cycles (Lea et al, 2000; Beaufort et al, 2001; Pedersen, 1983; Finney et al, 1988; Pedersen et al, 1988; Pedersen et al, 1991; Perks et al, 2002). However, not all studies agree (Koutavas et al, 2002; Stott et al, 2002); this is a burgeoning area of research which requires further study to identify a common hypothesis to explain tropical ocean processes during glacial phases.

The relationship between productivity and glacial-interglacial variations is less clear from ca.870 ka. The most likely reason for this is weakening atmospheric circulation; evidence for this includes an absence of glacial upwelling events and less correlation between P665 and *G.ruber* $\delta^{13}C$ (although low resolution carbon isotope sampling prevents any resolute conclusions). McClymont (2004) also found that EEP wind strength reduced between ca.900-700 ka; and Winckler et al (2005) found that aeolian dust input during the period 560-800 ka in the central equatorial Pacific (140°W, 4°N) was greatly reduced compared to the late Pleistocene (560-100 ka). This is discussed in more detail in section 5.8.2.1, with reference to global-scale climate changes. Further research on dust flux, SAMW nutrient concentration and limiting nutrients in the EEP across the MPT would be valuable to help test this hypothesis further.

5.4 Suborbital-scale SST variations

Suborbital-scale variations in time series data can be any cycle <19 kyr (below the precessional time period), although in the section below, “suborbital-scale” refers to any cycle <2.5 kyr. Although the average resolution of SST data points is 3.65 kyr throughout the time period studied within ODP site 849, areas of higher resolution have enabled the identification of these smaller suborbital cycles. Specifically during MIS 28-25 (2.2 kyr) (figure 5.9B), MIS 23 (2.4 kyr) and MIS 18 (2.4 kyr) (figure 5.9A), which span all three phases (see also figure 4.2B). Focusing on the period between MIS 28-25, SST cycles with an average period of 2.2 kyr occur during both glacials and interglacials, although interglacial amplitude was much higher. Elsewhere in the record, sampling resolution was not sufficient to pick up further suborbital-scale cycles across glacial-interglacial

boundaries and there is insufficient evidence of suborbital-scale fluctuations in either the biomarker AR or isotope records to warrant analysis. The presence of dramatic shifts in the proxy records at a 2.2- to 2.4- kyr resolution from ODP site 849 suggests bioturbation has not significantly affected the core, as this would be expected to smooth climatic signals by 1.9 – 3.8 (section 3.3). Not only this, but during MIS 28-25, notable burrowing was not seen in the core (section 3.3; Mayer et al, 1992), and so it is argued that these <2.5 kyr variations in SST are real and not a function of different resolution sampling.

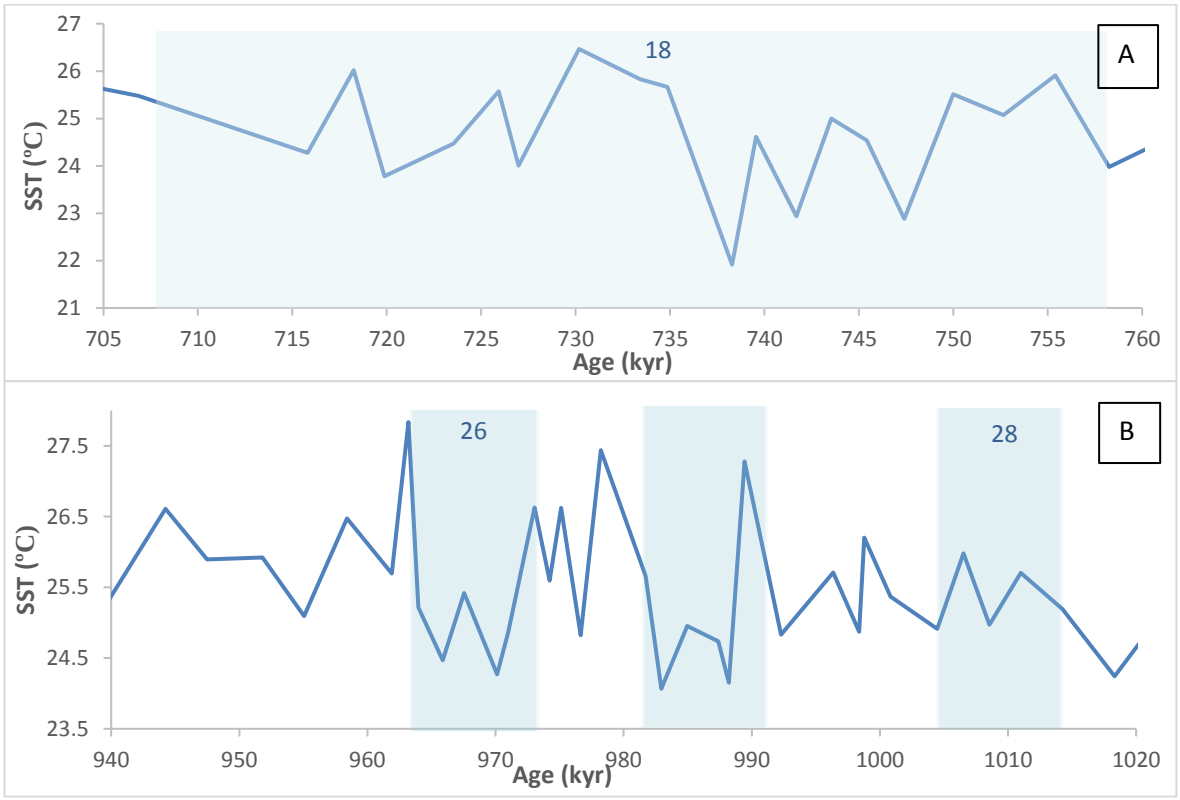

Figure 5.9: Suborbital scale SST variations at ODP site 849 SST of A) MIS 18 (average resolution 2.4 kyr); B) MIS 28-25 (average resolution 2.2 kyr). Blue shading indicates glacial stages or periods of heavier LR04 $\delta^{18}O_{benthic}$; numbers refer to marine isotope stages.

The millennial-scale cycles which occurred during the last glacial cycle and Holocene, Dansgaard-Oeschger (D/O) and Bond cycles (see section 2.1), varied on a ~1.5-3 kyr (Dansgaard et al, 1984; Bond et al, 1997) timescale, and therefore they are temporally comparable to those fluctuations identified here. D-O and Bond cycles have been well-documented globally during the last glacial; and indeed similar scale climate oscillations have been identified for other 100-kyr glacial-interglacial cycles during the late Pleistocene (Stott et al, 2002; Koutavas et al, 2002; Hendy and Kennett, 2000; Leduc et al, 2007; 2009; Oppo et al, 1998; McManus et al, 1999). The most favoured cause for the D-O (and associated Heinrich) events involves the rapid melting of ice sheets reducing the salinity and density of the ocean surface (particularly the North Atlantic), preventing sinking and thus reducing the strength of the THC (Broecker, 1994; Rahmstorf, 1995; Stocker and Wright, 1991; Teller et al, 2002).

Millennial- or suborbital-scale peturbations have also been identified in a range of earlier paleoclimate records (IRD, Mg/Ca SSTs, benthic and planktonic isotopes, foraminifera abundance) ranging from pre-MPT (Raymo et al, 1998; Bolton et al, 2010) to records spanning the MPT (Hernandez-Almeida et al, 2012; Weirauch et al, 2008; Zheng et al, 2005; Elderfield et al, 2012); however records from tropical, and particularly equatorial, latitudes are rare. The presence of lower amplitude millennial-scale cycles in the North Atlantic prior to the intensification of northern hemisphere glaciation (NHG) ca.2.4-2.6 ka (Bolton et al, 2010; and references within), and the marked increase in amplification during MIS 22 and MIS 12 (Mid-Brunhes Cooling Event) suggests the amplification of millennial-scale cycles is related to the development of large-scale ice sheets, having reached a critical size, following the MPT (Weirauch et al, 2008; Bolton et al, 2010), such as via the THC hypothesis as outlined by Broecker (1994). This would explain the greater amplitude glacial SST cycles observed during MIS 18 here. However, the presence of pervasive suborbital-scale shifts prior to MIS 24-22 (the key period in the MPT) in the 41-kyr world shows that the control over these cycles was already established before the onset of the larger 100-kyr-scale glacial-interglacial cycles. Therefore the initial, underlying forcing mechanism is thought to be related to insolation (Hernandez-Almeida et al, 2012; Bolton et al, 2010; Weirauch et al, 2008) which would reconcile their presence pre-MPT and during interglacials.

Some tropical millennial-scale records have shown strong half-precessional (9-12 kyr) signals signifying a relationship with insolation maxima (Weirauch et al, 2008; Rutherford and D'Hondt, 2000; Higginson et al, 2004) however high-latitude records have also recorded these 10-kyr trends (Hernandez-Almeida et al, 2012), suggesting a possible atmospheric/ocean advection of this signal to high latitudes, as with D-O cycles (McIntyre and Molfino, 1996; Hagelberg et al, 1994; Behl and Kennett, 1996). Increases in equinox insolation at the equator increase the equator-pole temperature gradient, strengthening atmospheric circulation and enabling greater moisture transport to the high latitudes, fuelling the growth of larger ice sheets via promoting a positive mass balance (Hernandez-Almeida et al, 2012). So in this way, increased insolation has the potential to cause ice sheet growth. Similarly, in the Pacific, the response of the surface ocean to increased insolation forcing can bring about a lowering of SSTs, with the involvement of ocean-atmosphere interactions. Upwelling is the main control over SST in the EEP and so increased insolation would increase SSTs in the WEP only, thus increasing the Pacific zonal temperature gradient, increasing the strength of Walker circulation and further lowering temperatures in the EEP (Philander and Federov, 2003). Figures 5.10 A and B show that the ODP site 849 SST record has a close relationship with both insolation and precession during MIS 28-25. It is thought for the reasons above that millennial- and semi-precessional-scale variations may play a role in propagating the long-term cooling leading to the development of 100-kyr glacial-interglacial cycles; for example strengthened Walker circulation is capable of reducing the heat flux to the high latitudes, promoting ice sheet growth (Weirauch et al, 2008; McClymont, 2004).

Despite similar sampling resolutions, where high amplitude variations are recorded at ODP site 849, ODP site 846 exhibited much lower amplitude variations, or maintained a stable temperature (see figure 5.11). For example, between 965 and 1000 ka (MIS 28-25), ODP site 849 SST had a temporal resolution of 1.9 ka and a range of 3.4°C whereas ODP site 846 SST resolution was 2.8

ka and had a range of 0.7°C. This suggests that although the general SST trends between EEP sites are very similar (discussed below), there is still a large variation in the ways in which local sites respond to external forcing; and that the need for further high-resolution studies is great.

Existing studies do not agree on the glacial-interglacial timing of pre-/MPT suborbital scale cycles; with some records reflecting pronounced glacial-interglacial trends (Hernandez-Almeida et al, 2012) and some showing none (Weirauch et al, 2008; Bolton et al, 2010; Zheng et al, 2005). This study shows that although suborbital-scale cycles are present in both glacials and interglacials pre-MPT, there is a pronounced shift in amplitude between states. The cycles do not follow the prescribed D-O/Bond cycle trends of high amplitude cycles during glacials and relatively stable interglacials, instead demonstrating the opposite (Bond et al, 1997). Equally, this site differs to the gradual cooling and abrupt warming per cycle described in the North Atlantic across the MPT by Hernandez-Almeida et al (2012) as the this study records abrupt SST cooling as well as warming. In conclusion, ODP site 849 SST data supports the idea that the way in which the ocean-atmosphere system responds to the millennial-scale forcing mechanism may have changed pre- and post- MPT; and tropical suborbital-scale forcing pre-MPT (such as during MIS 25-28) reflects a role for the tropical Pacific in the development of the 100-kyr cycles. Additional high-resolution tropical paleoclimate data consistently spanning the MPT is necessary to further explore the hypotheses outlined above.

5.5 Productivity and SST: A highly dynamic EEP across the MPT

Here, ODP site 849 SST and K37 records are compared to ODP site 846 U^{K}_{37}'-derived SST and K37 (Lawrence et al, 2006) and ODP site 847 Mg/Ca- and U^{K}_{37}'-derived SST (Wara et al, 2005; Dekens et al, 2007, respectively) (figure 5.10). The resolution between data points in the time window 600-1150 ka at ODP site 847 is low; 27.6 (Wara et al, 2005) and 11.2 ka (Dekens et al, 2007). Because of this, it is difficult to draw any reliable conclusions; however certain events are similar, for example the abnormally warm period between MIS 27-25, and prominent MIS 22 cooling. ODP site 846 also agrees with these observations, and apart from the lack of suborbital variability (despite similar sampling resolutions; as discussed above), SST is very similar to ODP site 849 (figure 5.11). McClymont et al (2013) found that ODP site 846 and ODP site 849 displayed a later onset of MPT cooling than ODP site 847. In the higher resolution ODP site 849 SST record here, the same trend is shown.

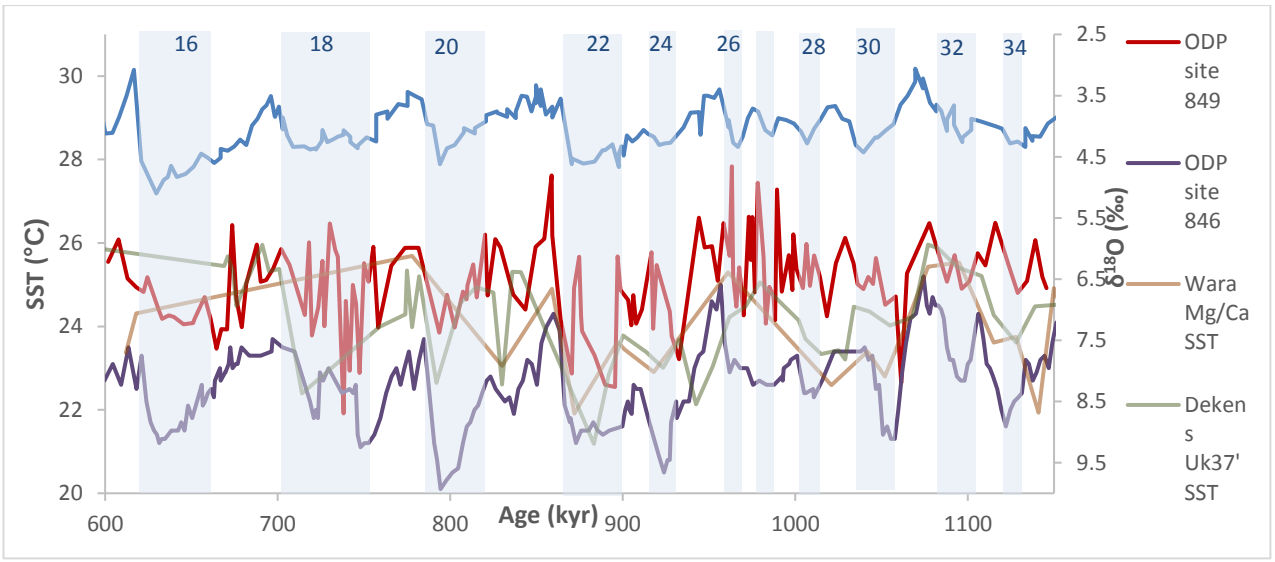

Figure 5.10: A comparison of the SST trends between 600-1150 ka in the EEP. Study sites: ODP site 849 (this study); ODP site 846 (Lawrence et al, 2006); ODP site 847 (Wara et al, 2005 and Dekens et al, 2007). Blue shading indicates glacial stages or periods of heavier LR04 $\delta^{18}O_{benthic}$; numbers refer to marine isotope stages.

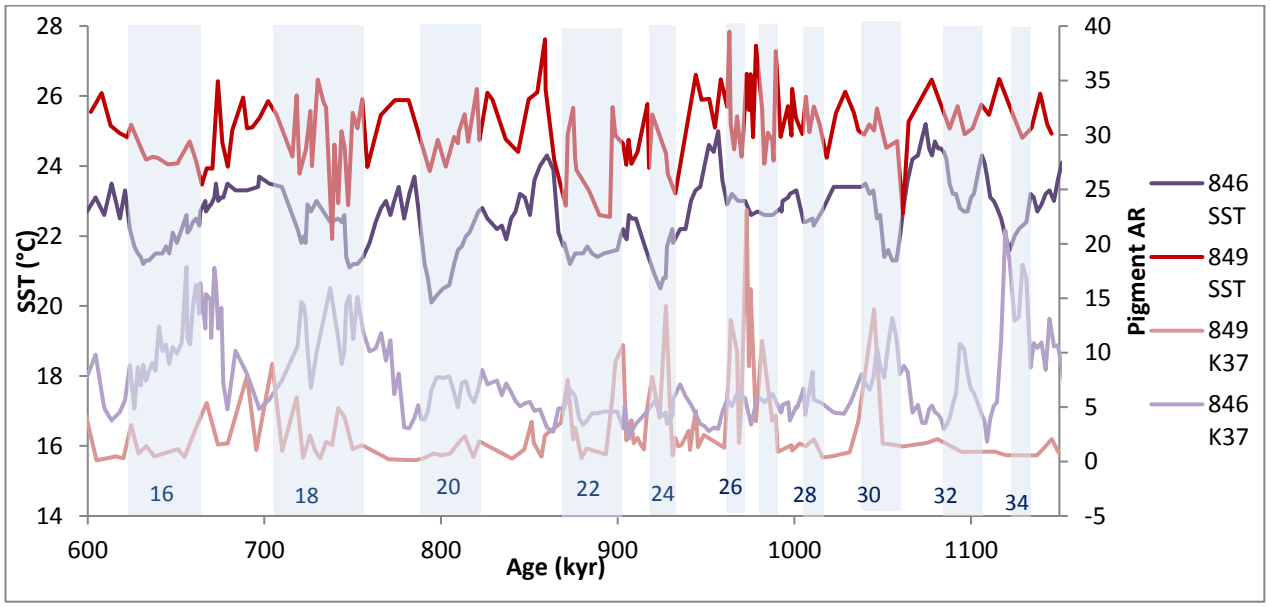

Figure 5.11: Comparison of the alkenone and chlorin accumulation rates from this study (ODP site 849) with the alkenone accumulation rates from Lawrence et al (2006) (ODP site 846). Blue shading indicates glacial stages or periods of heavier LR04 $\delta^{18}O_{benthic}$; numbers refer to marine isotope stages.

The K37 record at ODP site 846 (figure 5.11) has an anti-phase correlation with SST. From MIS 22 onwards, ODP site 846 reflects higher K37 ARs, once again in phase with cool SST, in contrast to ODP site 849. However the most conspicuous difference between EEP sites is across MIS 27-22 as ODP site 846 productivity is low and weakly correlated to SST; whereas ODP site 849 productivity is high and coupled to cool SST. This suggests that the control over productivity at this

time has more of an effect on ODP site 849 than ODP site 846. This is discussed above to be a possible combination of increased upwelling; increased contribution of SAMW, and potential influx of aeolian dust. ODP site 849 is close to the ITCZ during winter conditions in the modern Pacific as it shifts south (figure 1.2) (Mitchell and Wallace, 1992; Amador et al, 2006). If this southerly shift occurs during glacials, conditions analogous to a winter ITCZ position may affect the core site. These include stronger trade winds at the zone of equatorial divergence and therefore increased upwelling. Similarly, an increased contribution of SAMW, carrying recycled nutrients from the Southern Ocean, is transported to the EEP via the westerly-flowing EUC; directly above the (most-westerly-positioned EEP) ODP site 849 core site. In order to test this hypothesis, many more core sites would be required and so the main factor these differences highlight is the potential for a shifting ITCZ as the cause for differing SST-productivity relationships across the MPT in the EEP.

Overall, these findings suggest that the EEP is dynamic and varied spatially as well as temporally across the MPT. Whilst there are broad similarities between SSTs on longer-term timescales, there can also be significant differences; clearly a single record cannot be used as the definitive for the EEP region. McClymont et al (2013) showed that the EEP is a highly variable region where SSTs do not show a consistent pattern in terms of the emergence of long-term cooling and 100-ka cycles. They observed a cooling of ~1-1.7°C between 1.7-0.9 Ma in the EEP; the greatest variability in the same region of all global sites (McClymont et al, 2013).

5.6 EEP SST trends in a global context

The ODP site 849 SST record discussed here draws parallels with existing global SST records across the MPT. At ODP site 849, the highest SST value was experienced at the onset of the MIS 25 interglacial. MIS 25 was a particularly warm interglacial globally. SSTs during MIS 25 were amongst the highest of Medina-Elizalde and Lea's (2005) 1.4 Ma-long tropical Pacific record, and Hönisch et al (2009) find 'exceptionally high' SSTs at ca.950 ka in their study of the past 2.1 Ma in the eastern equatorial Atlantic. In high-latitudes too, Martinez-Garcia et al (2009) found high alkenone-derived SSTs during MIS 25 in the subAntarctic Atlantic. In the North Atlantic, Hernandez-Almeida et al (2012) find that MIS 25 SSTs remained high for ~20 kyr, marking the beginning of more severe glacial-interglacial shifts in their paleoclimate records suggesting ice sheet expansion. Interestingly, after MIS 25, Hernandez-Almeida et al (2012) find that SSTs in the North Atlantic dropped by 12°C at ~935 ka. ODP site 849 similarly records a drop in SSTs (of 3.4°C) at 932 ka. One of the common trends between ODP site 847 and ODP site 849 is a particularly warm period between MIS 27-25. The highest MIS 25 SST value at ODP site 849 was experienced at ca.960 ka, ~10 kyr prior to many of the studies outlined above. ODP site 846 (Lawrence et al, 2006) also exhibited early warming prior to MIS 25, at ca.957 ka (as visible in figure 5.11). The significance of a lead in EEP SSTs over ice volume is discussed in more detail in section 5.7.

The period between MIS 22 and 24 has been noted in globally-distributed SST records as one of severe cooling, marking the culmination of the decreasing SST trend beginning ca.1.2 Ma (McClymont et al, 2013). Between MIS 22-24, both glacial and interglacial cooling is seen at ODP

site 849. Low temperatures were experienced at ODP site 849 during MIS 22: the 50-kyr running mean in SST shows a cooling trend with an amplitude of ~1.7°C between 965 and 895 ka, then SSTs fall abruptly from 25.7°C at 897 ka to 22.5°C at 896 ka; a 3.2°C drop within 1ka. ODP site 847 (figure 5.10) experiences particularly low temperatures during MIS 22. Also, ODP site 849 SST during MIS 22 and 24 exhibit greater oscillations in temperature than before. This observation supports the development of the MPT from ca.940 ka onwards (Hernandez-Almeida et al, 2012); as glacials become longer and more severe, this is reflected in higher-amplitude SST fluctuations (Lawrence et al, 2006; Medina-Elizalde and Lea, 2005; Pisias and Moore, 1981; Clark and Pollard, 1983).

In summary, 1.2-0.9 Ma is viewed as a key period during the MPT; during which the development of larger ice sheets and the onset of the 100-kyr cycles is observed in proxy records globally (McClymont et al, 2013; Clark et al, 2006). The EEP records discussed here support an unusually warm MIS 25, as well as the timing of the onset of the MPT ca.940 ka, with glacial cooling becoming more severe.

5.7 SSTs and productivity lead $\delta^{18}O_{benthic}$

Between MIS 18-31, ODP site 849 SST tends to lead LR04 $\delta^{18}O_{benthic,}$ and consistently leads the ODP site 849 Mix et al (1995) $\delta^{18}O_{benthic}$ record by 0.96 – 12.27 kyr (average 6.04 kyr) (figure.5.7). During MIS 22 and 27, SST leads the Mix et al (1995) $\delta^{18}O_{benthic}$ but lags the LR04 $\delta^{18}O_{benthic}$, during the instances where the LR04 and Mix et al (1995) age models diverge, particularly between MIS 18-19 and MIS 22-25 (figure 5.12). This is because the LR04 model is a stack of numerous global $\delta^{18}O_{benthic}$ records, producing a 'smoothed' signal, whereas the Mix et al (1995) is a local, site-specific record (as discussed in section 3.9). Importantly, there are no clear instances where the Mix et al (1995) $\delta^{18}O_{benthic}$ record leads SST, although there are occasions where values are simultaneous, for example during MIS 18 and 22, highest $\delta^{18}O_{benthic}$ values in both Mix et al (1995) and LR04 were coincident with the coolest SSTs. Overall, this consistent SST lead trend is not an artefact of the tuning of the LR04 stack and is a clear indicator that the surface temperature in the EEP is changing before the $\delta^{18}O_{benthic}$.

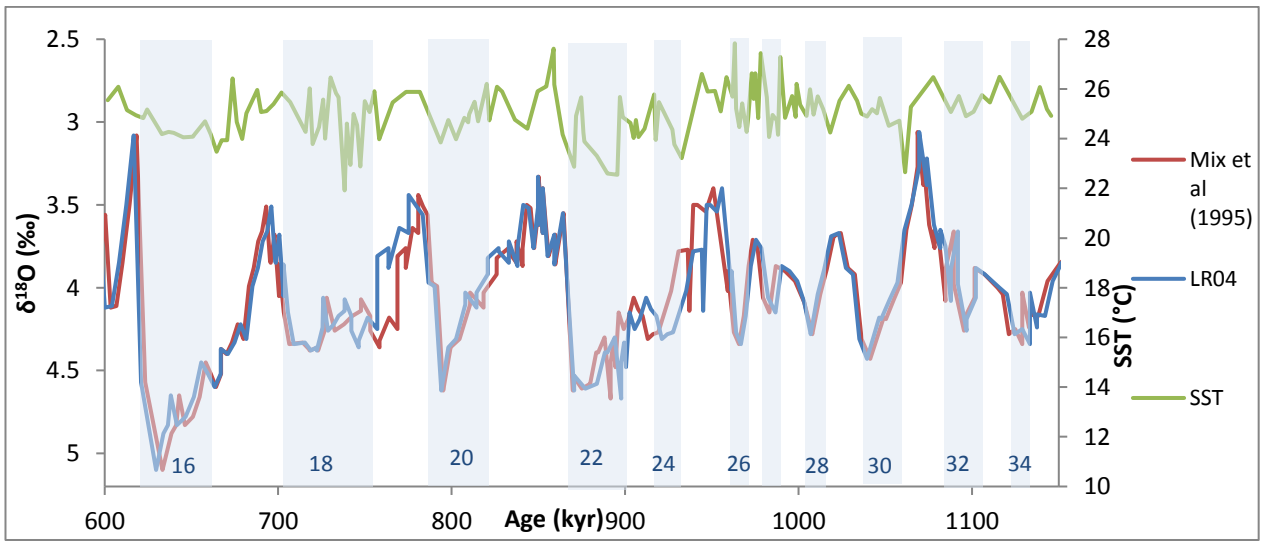

Figure 5.12 (overleaf): LR04 (blue line) and Mix et al (1995) (red line) $\delta^{18}O_{benthic}$ and ODP site 849 SST (°C) (green line). Blue shading indicates glacial stages or periods of heavier LR04 $\delta^{18}O_{benthic}$; numbers refer to marine isotope stages.

Where a relationship exists between the productivity proxies and $\delta^{18}O_{benthic}$, during phases 2a and 2b, P665 and MAR K37 lead (increases in) LR04 $\delta^{18}O_{benthic}$ (but also the original Mix et al (1995) age model) by between 0.98 and 16.89 kyr (average 7.34 kyr), with the one exception of MIS 27 (see figure 5.13). This agrees with the similar lead in SSTs during the same period. The relationship between $\delta^{18}O_{benthic}$ and oxygen and carbon isotopes is not consistent enough to identify a lead/lag relationship.

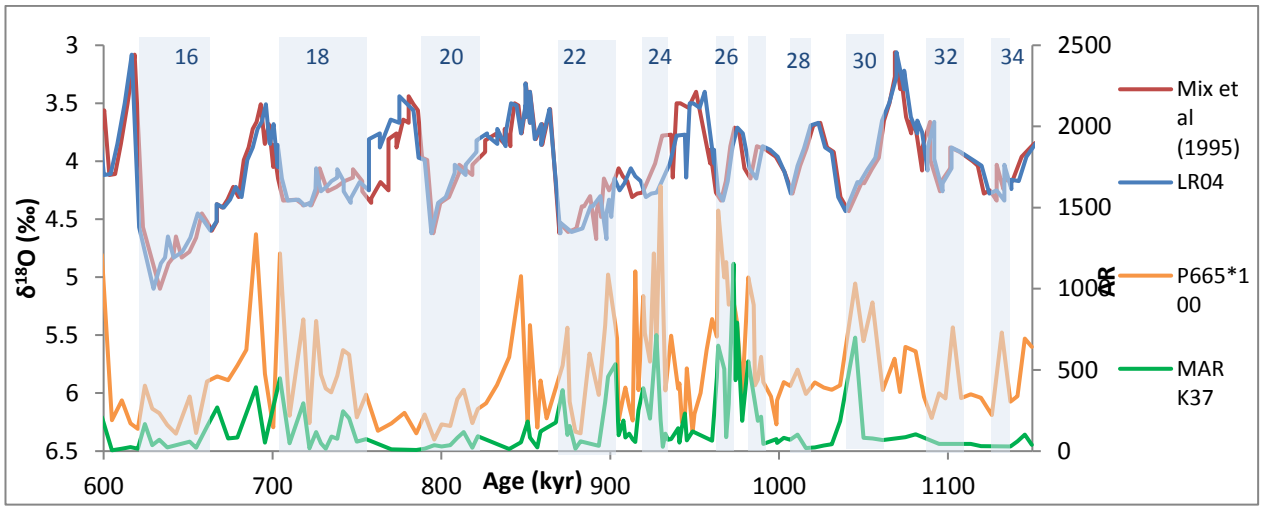

*Figure 5.13: LR04 (blue line) and Mix et al (1995) (red line) $\delta^{18}O_{benthic}$, ODP site 849 P665*100 (AU/cm²/kyr) (orange line) [P665 has been multiplied by a factor of 100 for easy comparison between pigments] and ODP site 849 MAR K37 (µg/cm²/kyr) (green line). Blue shading indicates glacial stages or periods of heavier LR04 $\delta^{18}O_{benthic}$; numbers refer to marine isotope stages.*

5.8 A wider perspective: Global controls over EEP climate and oceanography and causes for the MPT

Whichever hypothesis is invoked to explain the MPT must take into account the ODP site 849 paleoclimate findings discussed above. Key observations include: the lead of productivity and SST over $\delta^{18}O_{benthic}$ and the strengthening La-Nina-like state until MIS 22, followed by a decoupled surface ocean with respect to productivity and temperature. A critical discussion of these hypotheses is below.

5.8.1 Explanations for SST/productivity lead over $\delta^{18}O_{benthic}$: Changes in greenhouse gas concentrations and a strengthened biological pump

At ODP site 849, there is a 6-7 kyr lead in both SST and productivity over $\delta^{18}O_{benthic}$ across 1150-600 kyr and 1150-870 kyr, respectively. Many tropical Pacific sites have noted a SST lead over $\delta^{18}O$ throughout the Pleistocene, ranging from 1-4 kyr (Lawrence et al, 2006 [also K37]; Medina-

Elizalde and Lea, 2005; Lea et al, 2000; Herbert et al, 2010; Emeis et al, 1995). Similarly, high-latitude SSTs have also noted a lead over ice volume; such as Mg/Ca SSTs in the Southern Ocean leading $\delta^{18}O_{planktonic}$ by 1-3 kyr over 300 kyr (Mashiotta et al, 1999), as well as numerous other Southern Ocean studies (Hays et al, 1976; Howard and Prell, 1992; Pichon et al, 1992; Labeyrie et al, 1996). Beaufort et al (2001) also found that over the past 2 glacial-interglacial cycles, estimates of primary productivity from the WEP and EEP and equatorial Indian Ocean led $\delta^{18}O_{benthic}$ by 2 kyr in the precession band. Thus, the data here agrees with the existing, widely acknowledged body of research referring to the "early responder" tropical surface ocean during the MPT (Beaufort et al, 2001).

The observed lead SST has over benthic $\delta^{18}O$ (a portion of which reflects changes in global ice volume) negates the theory that the direct radiative forcing of continental northern hemisphere ice sheets regulates tropical SST changes. Herbert et al (2010) suggest that the $\delta^{18}O_{benthic}$ signal may be weighted towards reflecting the relatively slow process of ice sheet expansion more than the more rapid deep ocean cooling; thus tropical SSTs may be responding to changes in the deep ocean temperature, accounting for this lead. Similarly, Philander and Federov (2003) noted that deep ocean cooling is capable of affecting tropical SSTs on a shorter timescale, rather than high-latitude ice sheet growth initiating polar cell expansion. Lea et al's (2000) EEP SST record which is near synchronous with Antarctic Vostok air temperature records over the past 420 kyr shows a connection with the Southern Ocean (Petit et al, 1999), suggesting these changes may have been transmitted to the EEP via the EUC.

Some studies which noted a SST/productivity lead over $\delta^{18}O_{benthic}$ have put forward greenhouse gas/CO_2 feedbacks as the cause for this (Medina-Elizalde and Lea, 2005; Lawrence et al, 2006). Studies advocating greenhouse gases as the primary forcing mechanism behind the MPT require a long-term cooling prior to the configuration of 100-kyr cycles ca.900 ka (Berger and Jansen, 1994; Raymo, 1997). This is not seen at ODP site 849; with the higher-resolution SST data building on that of McClymont (2004) shifting the onset of long-term cooling from 1170 ka to 965 ka. Also, ODP site 849 and other tropical sites experienced high SSTs during MIS 25 (as discussed in section 5.6). Hönisch et al (2009) used boron isotopes in planktonic foraminifera shells to reconstruct a pCO_2 (partial pressure of CO_2) record spanning the MPT, and found higher than average pCO_2 values during MIS 25 (ca.950 ka); estimated as 308 µatm; and similarly ≥300 ppm by Martinez-Garcia et al (2009). They conclude that interglacial pCO_2 was similar before and after the MPT; and thus the data here supports the findings of Hönisch et al (2009). However, this does not necessarily mean that CO_2 forcing does not play a role as a driver of the MPT.

An increasingly similar SST record in all 4 tropical sites studied by Herbert et al (2010) approaching the MPT suggests there was an influential greenhouse gas constituent of SST forcing, overprinting any regional SST changes. Herbert et al (2010) essentially corroborate Hönisch et al's (2009) findings of very little long-term change in CO_2 across the MPT; with only a slight increase in pCO_2 drawdown during glacials; a measure capable of explaining only modest (1-2 °C) deep ocean temperature cooling (Sosdian and Rosenthal, 2009) and little to no interglacial cooling observed in the tropical SST stack (Herbert et al, 2010). The ultimate cause therefore for the intensifying

glacials during the MPT is argued to be deep-sea glacial high-latitude CO_2 sequestration via high latitude surficial processes such as productivity (including iron limitation), stratification and wind mixing (Archer et al, 2000; Toggweiler, 1999; Sarmiento and Toggweiler, 1984; Watson et al, 2000; Hain et al, 2010). This was demonstrated by Martinez-Garcia et al (2009) in their study of the sub-Antarctic Atlantic over the past 1.1 Ma.

However even in those cases where a substantial change in biological productivity or nutrient concentration is not seen, there is an alternative mechanism which can bring about lower glacial atmospheric CO_2 (Toggweiler, 1999). Toggweiler (1999) suggests that a chemical divide between the mid-depth and deep ocean, rather than the thermocline as is typically represented in models, is the depth of separation between high CO_2 and low CO_2 waters. Toggweiler's biological productivity box model shows a shift of isotopically light CO_2 from the upper/mid to lower ocean enriches the deep ocean with considerably more ^{12}C than a shallower chemical divide.

Herbert et al (2010) conclude that simultaneous tropical SST cooling with a slight fall in atmospheric CO_2 is capable of encouraging further greenhouse gas feedbacks (CO_2 as well as water vapour) (Held and Soden, 2006; Lea et al, 2000). One of these feedbacks is an enhanced biological carbon pump; increasing the export of carbon into the deep ocean and lowering atmospheric CO_2 further (Sarnthein et al, 1998). The argument of a stronger biological pump as the underlying cause for CO_2 draw-down during glacials is popular and oft-cited (Pichevin et al, 2009; Lea et al, 2004; Pichevin et al, 2009). High productivity during glacial periods during phases 2a and 2b at ODP site 849 supports this. However the timings of productivity peaks are harder to explain.

High productivity at ODP site 849 occurred at the terminations of MIS 30 and 26, with moderate values at the terminations of MIS 24 and 22. Increased productivity during terminations would indicate that enhanced carbon drawdown reduces atmospheric CO_2 concentrations just as ice volume is retreating, which goes against the expected response of climate to lower CO_2 (Higginson and Altabet, 2004; Zhao et al, 2006). However, in some upwelling sites the process of deglaciation can renew deep ocean nutrient cycling, triggering blooms in productivity. For example, Harris et al (1996) looked at chlorin accumulation rate over the past 350 kyr and found it varied hugely on glacial-interglacial timescales; with chlorin accumulation rates increasing at the end of terminations, taken to represent high diatom accumulation rate as biogenic opal also increased in their study site in the subtropical Atlantic. One mechanism to explain this is outlined by Marchitto et al (2007); in their study they found a substantial reduction in radiocarbon activity ($\Delta^{14}C$) in the tropical eastern north Pacific during the last glacial period, beginning at the onset of deglaciation. Here $\Delta^{14}C$ is used as an indicator of carbon cycling, used to infer the activity of the deep Southern Ocean. This drop in $\Delta^{14}C$ occurred synchronously with Antarctic atmospheric CO_2 rise (Marchitto et al, 2007). Marchitto et al (2007) therefore hypothesise that Southern Ocean deep waters were separated from the atmosphere through density stratification and/or extensive sea ice cover (Sigman and Boyle, 2000; Toggweiler et al, 2006; Stephens and Keeling, 2000), enabling the steady draw-down of atmospheric carbon during the glacial and pooling into a substantial deep ocean carbon reservoir. This would tie into Hönisch et al's (2009) high-latitude carbon sequestration theory for the cause of the MPT. Supporting this, Ninnemann and Charles (2002) recorded low deep water $\delta^{13}C$

values in the south Atlantic sector of the Southern Ocean during the last glacial period, suggesting a build up of remineralised carbon and/or weak ventilation. During deglaciation, sea-ice retreat encourages upwelling and deep convection bringing sequestered carbon and heat to the surface and atmosphere, transmitted to the eastern north Pacific via the Antarctic Intermediate Water (AAIW) and SAMW, explaining the rise in atmospheric CO_2 (Marchitto et al, 2007; Spero and Lea, 2002). Further, an arguably stronger AAIW during deglaciation (Schulte et al, 1999) would enhance the transportation of $\delta^{13}C$- and $\Delta^{14}C$- depleted water masses to the tropical Pacific (Marchitto et al, 2007). A strongly correlated Southern Ocean $\delta^{13}C_{benthic}$ and $\Delta^{14}C$ record and northern hemisphere climate/NADW (Charles et al, 1996; McManus et al, 2004) suggests changes to the Antarctic climate may have been paced by northern hemisphere ice sheet and meltwater changes.

Thus, if this process of glacial deep water sequestration of carbon followed by deglacial deep water convection and upwelling bringing depleted carbon to the surface was also operating across the MPT, we would expect to see low $\delta^{13}C$ and potentially high productivity (due to remineralised nutrients also brought to the surface) at terminations. Certainly decreases in surface (*G.ruber*) $\delta^{13}C$ are seen at the end of glacials in phase 2b, and there is some evidence for moderate to high productivity during terminations in both phase 2a and 2b. A shorter $\delta^{13}C$ record (compared to the SST and productivity proxies) makes it difficult to draw any strong conclusions as to whether the process of deep ocean nutrient and carbon cycling and deglaciation changed moving into phase 3; however an absence of low $\delta^{13}C$ in MIS 20, and low productivity during glacials MIS 20 and 16 suggest this may be the case.

In summary, although the data here does not support a substantially lower atmospheric concentration of CO_2 prior to the MPT, the tropical Pacific has the potential to drive the initiation and termination of glacials following slight changes in pCO_2 content through a number of positive feedbacks involving greenhouse gases, such as with an enhanced biological pump. If high-latitude ocean surficial processes were the initiator of deep water change, transmitted to the EEP via potentially strengthened ocean currents, this would also explain the lead of tropical surface ocean SST and productivity over ice volume changes.

5.8.2 Understanding the transition between phases 2b and 3: global-scale controls over SST and productivity

5.8.2.1 Phases 2a and 2b

The causes of surface water cooling in the EEP include decreased radiative heating and increased cooling from evaporation, or an increased flux of cool waters into the surface ocean due to increased rates of upwelling and/or changing contributions of source waters (Farrel et al, 1995). Changing atmospheric greenhouse gas composition is also a factor (Lawrence et al, 2006). Productivity is dependent on the nutrient concentration of the surface ocean, affected by terrestrial nutrient transport, increases in rates of upwelling, and in more nutrient-rich upwelled water. Only some of these driving factors cause coupled changes in SST and productivity. A strong correlation between SSTs and insolation suggests that the primary forcer of SST is direct radiative heating,

negating the need for any alternative techniques to explain tropical surface ocean dynamics (such as thermocline tilt or wind strength changes). However ODP site 849 operates a coupled SST-productivity La Niña-like response during phase 2a and 2b on orbital and suborbital timescales, as demonstrated in figure 4.7; suggesting there is a forcing mechanism which alters both temperature and surface ocean nutrient concentration on glacial-interglacial timescales. As discussed in section 5.3.2, the simplest explanation for these coupled productivity-SST results is strengthened trade winds causing increased rates of upwelling (Liu and Herbert, 2004). Wind-induced upwelling is consistent with every aspect of the upper water column found here during phases 2a and 2b; cool SSTs, increased contribution of ^{12}C and nutrients from cool sub-thermocline waters, and potentially enhanced aeolian flux inputting nutrients into the surface ocean.

Martinez-Garcia et al (2011) studied dust and iron inputs into the sub-Antarctic Atlantic over the past 4 Ma and found that dust deposition and glacial terminations were unequivocally linked; across the MPT dust fluxes doubled, comparable to the LGM. This is attributed to a spatial contraction of atmospheric Hadley cells and associated strengthened convection due to the increased meridional temperature gradient following the onset of the MPT (Martinez-Garcia et al, 2010). The sensitivity of the Southern Ocean to the more intense glacials of the MPT also reconciles the lack of a decline in interglacial atmospheric CO_2 concentrations, and associated unchanged SSTs as discussed above. The strong correlation between SST and productivity and precession-driven insolation during phases 2a and 2b suggests a modification of the ITCZ position creating a strong east-west asymmetry as winds diverge in the east and converge in the west. This enhances Walker circulation; strengthening upwelling, and contributes to a La-Nina-like state in the EEP (Clement et al, 1999).

McClymont and Rosell-Melé (2005) suggest on the basis of their data (with EEP SST cooling beginning ca.1.2 Ma) that intensified Walker circulation is responsible for enabling the growth of larger ice sheets (the inertia of which is associated with the onset of the 100-kyr cycles [e.g. Berger and Jansen, 1994; Clark and Pollard, 1998]) through a positive feedback cycle whereby an enhanced east-west Pacific temperature gradient strengthens trade winds, reduces heat transport to higher latitudes, and increases precipitation (see also Martinez-Garcia et al, 2010; Garidel-Thoron et al, 2005). The cause for the strengthened zonal temperature gradient is argued to be a decrease in EEP SSTs, as WEP SSTs remained similar throughout the time series (McClymont and Rosell-Melé, 2005). However, studies have found conflicting evidence for this; for example the Mg/Ca record in Medina-Elizalde and Lea (2005) does not reflect an anti-phased east-west Pacific SST pattern over glacial-interglacial timescales (Herbert et al, 2010). A prolonged cooling from 1150-900 ka is not seen at ODP site 849 here; rather beginning ca.965 ka. Therefore although a strengthened Walker circulation would account for the changes seen at ODP site 849 during phase 2a and 2b, there is little evidence at ODP site 849 for its development in the way of long-term EEP cooling. Further basin-wide SST research in the tropical Pacific would be valuable in exploring this hypothesis further.

5.8.2.2 Phase 3

As identified in numerous other studies, the time period ~900 ka is associated with a number of climatic shifts and extremes in paleoclimate proxies, and so it is likely that this time period is reflecting a number of events or feedbacks crucial to the development of the 100-ka cycles (McClymont et al, 2013; Clark et al, 2006). The data presented here supports the theory that a climate threshold has been crossed following MIS 22; between the phase 2b and phase 3 boundary. Following MIS 22, productivity and SST decouple for the first time in the dataset, suggesting that following MIS 22, the controls over SST and productivity have changed or weakened. It appears that the control over productivity in the EEP during this time is more complex than the 'more upwelling = more productivity' relationship operating during phases 2a and 2b. No upwelling events are recorded during MIS 20, and SSTs do not reflect a strong relationship with glacial-interglacial cycles post-MIS 22. In order to determine the control over productivity in phase 3, we must examine the controls over nutrient concentration in the surface waters. As discussed above, nutrients can be supplied to the surface ocean in three main ways; terrestrial nutrient transport, increases in rates of upwelling, and in more nutrient-rich upwelled water.

Firstly, increases in productivity via flux of terrestrial dust into the ocean is caused by a more arid climate and strengthened atmospheric circulation i.e. as expected to occur during glacial stages. The fact that productivity in phase 3 is not consigned to glacial periods suggests this relationship does not hold for ODP site 849.

Secondly, although the expected surface ocean response to increased rates of upwelling is cooler SSTs, changes to the strength of upwelling and source of upwelled waters can occur independently of temperature. For example, Mulitza et al (1997) found that throughout the Atlantic during the last glacial, a highly dynamic water column, exhibiting $\delta^{18}O$-inferred upwelling events, occurred during a 'stable' SST record. Dekens et al (2007) also found that within upwelling regions (EEP, California and Peru margins) during the early Pliocene, productivity and SSTs were decoupled with upwelling of nutrient-rich waters occurring during warm SSTs. Liu and Herbert (2004) observed a decreasing correlation between (high) K37 and (cool) UK37 SST from the early to the late Pleistocene (r^2=0.46 to 0.04). This may justify the absence of a SST-productivity link at ODP site 849 during phase 3; however, $\delta^{18}O$ values of *G.ruber* and *N.dutertrei* at ODP site 849 do not indicate upwelling events during the first half of phase 3, and so it is unlikely upwelling events are the cause for the spikes in productivity ca.850 ka. Given that there is no evidence to suggest the control over productivity changed throughout phase 3 (no consistent relationship between SSTs, productivity and isotopes), this assumption is applied to the full phase 3 time period.

Thirdly, a change in the source, or composition of the upwelled waters from a portion of the EUC or a change in the SAMW may account for productivity variations. There is debate around whether North Pacific Intermediate Water (NPIW) may have replaced AAIW at depth; which could then have fed into the thermocline. In this case a cooler AAIW could transport cooler, more nutrient-rich waters to the surface despite upwelling intensity remaining stable (McClymont, personal correspondence). However there is a poor understanding of NPIW extent or properties even for the

LGM and so there is little evidence for this (Ono et al, 2005). The composition of the source water however may have changed. Ravelo and Shackleton (1995) suggest that the carbon isotope composition of Pacific Intermediate Water (which sources a portion of the upwelling thermocline water in the EEP) changed over the past 2 Ma. A mechanism described above (in section 5.8.1) outlines how recycled nutrients from the Southern Ocean are transported to the EEP via the AAIW and SAMW (Marchitto et al, 2007; Spero and Lea, 2002). Both of these examples reflect the propensity for changing Southern Ocean source water composition to affect the EEP surface ocean.

Looking at the controls over SST during phase 3, as described above, the causes range from direct radiative heating and evaporative cooling, increased rates of upwelling or changing source water contributions (Farrel et al, 1995). As the relationship between insolation and surface ocean proxies began to change post-950 ka, it suggests that radiative heating is not the sole driver of SST changes. As discussed above, increases in upwelling during glacials is not believed to have taken places during phase 3.

The remaining explanation involves a change in the composition of source waters. The EEP has a shallow thermocline and so changes to the properties of the upwelled deep waters via the EEP have a large effect on the temperature of the surface ocean (Philander and Fedorov, 2003). One explanation put forward to explain the long-term cooling of the EEP from ca.1.2 Ma (incidentally not found at this site) is a cooling of deep ocean waters, as shown by global Mg/Ca temperatures of foraminiferal calcite over past 50 Ma (Lear et al, 2000) and in $\delta^{18}O_{benthic}$ of WEP over past 5 Ma (Tian et al, 2002). Martinez-Garcia et al (2010) show SST cooling in the subantarctic Atlantic occurred during the MPT. However, for this mechanism to work the temperature signal must be transmitted to the upwelling regions via the intermediate and deep ocean (not requiring a change in upwelling strength); however there is currently no data on this (Martinez-Garcia et al, 2010).

Given the number of studies in the late Pleistocene which document La-Nina-like conditions in the tropics and specifically the EEP (Beaufort et al, 2001; Pedersen, 1983; Perks et al, 2002), this portion of the 100-kyr world (ca.800-600 ka) clearly requires further research to fully explain.

5.9 The EEP as a key player in the development of the MPT

There are a number of findings both from ODP site 849 and surrounding EEP sites which suggest that the EEP played a vital role in the development of the MPT. SSTs are particularly cool during MIS 30, dropping to 22.6°C. This particularly cool glacial is evident in Lawrence et al's (2006) EEP SST record (figure 5.11) and Medina-Elizalde and Lea's (2005) tropical Pacific SST record (having the coolest SSTs in the early-mid Pleistocene). McClymont et al (2013) note that their global review of SST records identifies MIS 31 as being an unusually warm interglacial; potentially caused by the increase in amplitude of eccentricity and precessional forcing (as visible in figures 5.10 and 5.11). That EEP SSTs cooled significantly following this, suggests the beginning of a high-amplitude glacial-interglacial cycle prior to the ice sheet expansion at ca. 900 ka (typical of post-MPT 100 ka cycles). Also, semi-precessional SST cycles found between ca.1000-960 ka at ODP site 849 are

arguably able to propagate longer-term 100-kyr cycles (LeTreut and Ghil, 1983). In addition, the lead of SST and productivity over $\delta^{18}O_{benthic}$ suggests that the direct radiative effect of ice sheets cannot have controlled any EEP surface ocean changes. These findings go against the hypothesis that the MPT was purely a state initiated by high-latitude, ice-sheet feedbacks.

Chapter 6: Conclusions and Future Work

6.1 Conclusions

Through the detailed reconstruction and interpretation of surface ocean proxies at ODP site 849 and surrounding sites, this thesis has aimed to assess the response of the tropical Pacific to the MPT. The following 3 objectives of this thesis have been met, as justified by the successful presentation of data spanning 600-1150 ka in figure 4.2:

1. Reconstruct a sub-orbital scale resolution record of sea surface temperatures across the MPT (1.15 to 0.6 Ma) using alkenone biomarkers
2. Reconstruct a sub-orbital scale resolution record of primary productivity using chlorin and alkenone biomarkers
3. Reconstruct a sub-orbital scale resolution record of water column structure using stable isotope analyses of two species of surface-dwelling foraminifera

In summary, paleoclimate data from ODP site 849 suggests that the glacial-stage tropical Pacific operates under a La Niña-like state between 1150-870 ka; displaying upwelling, cool SSTs and moderate to high productivity. A strong SST-precession relationship during this time suggests strengthened meridional temperature gradients modify the tropical atmosphere trade wind system enabling this response. MIS 22 culminates in a highly dynamic EEP surface ocean, indicating a threshold has been crossed. A large upwelling event occurs 5 kyr prior to a maintained decoupling of the SST-productivity relationship that characterises the La Niña-like glacial state seen for the preceding 270 kyr. Further research is required to fully explain the processes operating in the tropical Pacific during phase 3. An apparent weakening of atmospheric circulation suggests by means of elimination that the main control over SST and productivity shifts to changing source water properties via an oceanic connection with the high-latitude Southern Ocean.

The absence of long-term cooling in the EEP prior to the onset of the 100-kyr paced ice sheet expansion argues against strengthened Walker circulation as a driver for the MPT. Instead, feedbacks involving a strengthened glacial biological pump in both the high latitudes and the EEP, encouraging the drawdown of carbon and further cooling of global temperatures, is cited as a possible driver for the MPT. This greenhouse gas-related hypothesis would also account for the 6-7 kyr lead of SST and productivity over $\delta^{18}O_{benthic}$ seen here. The presence of semi-precessional cycles, capable of driving larger 100-kyr cycles, and a particularly cool MIS 30, reminiscent of higher amplitude SST cycles during the MPT, suggest that the EEP may have played a key role in the initiation of the 100-kyr cycles of the late Pleistocene.

6.2 Future work

There are a number of areas highlighted in chapter 5 whereby further research would help to explain and reconcile findings at ODP site 849. Firstly, a longer $\delta^{18}O$ and $\delta^{13}C$ record spanning 600-1150 ka would enable the identification of possible upwelling events during phase 3. A higher-resolution, millennial-scale multi-proxy record between 870-880 ka, a highly dynamic period in the EEP surface ocean, would confirm or negate the presence of a severe upwelling event during the

MIS 22 deglaciation. The carbon and oxygen isotope reconstruction of a non-thermocline, sub-surface ocean dweller, such as *G.tumida,* would enable the position of the thermocline to be estimated, providing further information towards the ENSO-like state of the tropical Pacific during all three phases. The reconstruction of aeolian dust flux would allow the presence of a strengthened atmospheric circulation during phases 2a and 2b to be tested; and further evidence for the controls over SST and productivity post-MIS 22.

References

Altabet, M. A; Higginson, M. J and Murray, D. W (2002) The effect of millennial-scale changes in Arabian Sea denitrification on atmospheric CO_2. *Nature*. Vol 415, pg. 159-162

Amador, J.A; Alfaro, E.J; Lizano, O.G; Magana, V.O (2006) Atmospheric forcing of the eastern tropical Pacific: a review. *Progress in Oceanography*. Vol 69, Issue 2–4, pg.101–142

Anderson, D. M and Prell, W. L (1993) A 300 kyr record of upwelling off Oman during the late Quaternary: Evidence of the asian southwest monsoon. *Paleoceanography*. Vol 8, no. 2, pg. 193-208

Archer, D; Winguth, A; Lea, D; Mahowald, N (2000) What caused the glacial/interglacial atmospheric pCO_2 cycles? *Reviews of Geophysics*. Vol 38, Issue 2, pg. 159-189

Ashkenazy, Y and Tziperman, E (2004) Are the 41 kyr glacial oscillations a linear response to Milankovitch forcing? *Quaternary Science Reviews*. Vol 23, pg. 1879–1890

Barber, R.T and Chavez, F.P (1991) Regulation of primary productivity rate in the equatorial Pacific Ocean. *Limnology and Oceanography*. Vol 36, pg. 179–186

Bard, E (2001b) Paleoceanographic implications of the difference in deep-sea sediment mixing between large and fine particles. *Paleoceanography*. Vol 16, pg. 235-239

Bard, E (2001a) Comparison of alkenone estimates with other paleotemperature proxies. *Geochemistry Geophysics Geosystems*. Vol 2, Issue 1

Barry, R and Chorley, R. J (2003) Atmosphere, Weather, and Climate. Routledge

Bassinot, F. C; Labeyrie, L. D; Vincent, E; Quidelleur, X; Shackleton, N. J; Lancelot, Y (1994) The astronomical theory of climate and the age of the Brunhes-Matuyama magnetic reversal. *Earth and Planetary Science Letters.* Vol 126, pg. 91-108

Be, A. W. H (1960) Ecology of recent planktonic Foraminifera. Part 2: bathymetric and season distributions in the Sargasso Sea off Bermuda. *Micropaleontology*. Vol 6, pg. 144-151

Beaufort, L (1994). Climatic importance ofthe modulation of the 100-kyr cycle inferred from 16 my long Miocene records. *Paleoceanography*. Vol 9, pg. 821-834

Beaufort, L and Aubry, M. P (1990) Fluctuations in the composition of Late Miocene calcareous nannofossil assemblages as a response to orbital forcing. *Paleoceanography*. Vol 5, pg. 845-865

Beaufort, L; Garidel-Thoron, T; Mix, A. C and Pisias, N. G (2001) ENSO-like Forcing on Oceanic Primary Production During the Late Pleistocene. *Science*. Vol 293, pg. 2440-2444

Becquey, S and Gersonde, R (2002) Past hydrographic and climate changes in the Subantarctic Zone of the South Atlantic - the Pleistocene record from ODP site 1090. *Palaeogeography, Palaeoclimatology, Palaeoecology*. Vol 182, pg. 221-239

Behl, R. J and Kennett, J. P (1996) Brief interstadial events in the Santa Barbara Basin, NE Pacific, during the past 60 kyr. *Nature*. Vol 379, pg. 243-246

Bemis, B. E; Spero, H. J; Bjima, J; Lea, D. W (1998) Reevaluation of the oxygen isotopic composition of planktonic foraminifera: Experimental results and revised paleotemperature equations. *Paleoceanography*. Vol 13, pg. 150–160

Benway, H. M; Mix, A. C; Haley, B. A; Klinkhammer, G.P (2006) Eastern Pacific warm pool paleosalinity and climate variability: 0-30 kyr. *Paleoceanography*. Vol 21, pg. 1-11

Berger, A and Loutre, M. F (1991) Insolation values for the climate of the last 10 million years. *Quaternary Science Reviews*. Vol 10, pg. 297-317

Berger, A. L (1978) Long-term variations of daily insolation and quaternary climatic change. *Journal of Atmospheric Sciences*. Vol 35, pg. 2362–2367

Berger, A; Li, X. S; Loutre, M. F (1999) Modelling northern hemisphere ice volume over the last 3 Ma. *Quaternary Science Reviews*. Vol 18, pg. 1-11

Berger, A; Loutre, M. F; Tricot, C (1993) Insolation and the earth's orbital periods. *Journal of Geophysical Research*. Vol 98, pg. 10341-10362

Berger, W. H; Bickert, T; Schmidt, H; Wefer, G (1993a) Quaternary oxygen isotope record of pelagic foraminifers: Site 806, On tong Java Plateau. In Proceedings of the Ocean Drilling Program, Scientific Results, Vol 130. (W. H. Berger; L. W. Kroenke; L. A. Mayer Shipboard Scientific Party, Eds.), pg. 381-395

Berger, W. H and Jansen, E (1994) Mid-Pleistocene climate Pleistocene climate shift: the Nansen connection. *Geophysical Monograph*. Vol 84, pg. 295-311.

Bickert, T; Curry, W. B; Wefer, G (1997) Late Pliocene to Holocene (2.6-0 Ma) western equatorial Atlantic deep-water circulation: inferences from benthic stable isotopes. In Proceedings of the Ocean Drilling Program, Scientific Results. (N. J. Shackleton, W. B. Curry, C. Richter, and T. J. Bralower, Eds.), pg. 239-254

Bloemendal, J; Liu, X. M; Rolph, T. C (1995) Correlation of the magnetic susceptibility stratigraphy of Chinese loess and the marine oxygen isotope record: chronological and palaeoclimatic implications. *Earth and Planetary Science Letters*. Vol 131, pg. 371-380

Blunier, T; Chapellaz, J; Schwander, J; Dällenbach, A; stauffer, B; Stocker, T. F; Raynaud, D; Jouzel, J; Clausen, H. B; Hammer, C. U; Johnsen, S. J (1998) Asynchrony of Antarctic and Greenland climate change during the last glacial period. *Nature*. Vol 394, pg. 739-743

Boersma, A (1980) Foraminifera. In: Introduction to Marine Micropaleontology (B. Haq and A. Boersma, Eds.), pg. 19–78. Elsevier/North Holland, New York

Bolton, C. T; Wilson, P. A; Bailey, I; Friedrich, O; Beer, C. J; Becker, J; Baranwal, S; Schiebel (2010) Millennial?scale climate variability in the subpolar North Atlantic Ocean during the late Pliocene. *Paleoceanography*. Vol 25

Bond, G; Showers, W; Cheseby, M; Lotti, R; Amalsi, P; deMenocal, P; Priore, P; Cullen, H; Hajdas, I; Bonani, G (1997) A pervasive millennial-scale cycle in North Atlantic Holocene and glacial climates. *Science*. Vol 278, pg. 1257-1266

Bond, G; Broecker, W; Johnsen, S; McManus, J; Labeyrie, L; Jouzel, J; Bonani, G (1993) Correlations between climate records from North Atlantic sediments and Greenland ice. *Nature*. Vol 365, pg. 143-147

Brassell, S. C; Eglinton, G; Marlowe, I. T; Pflaumann, U; Sarnthein, M (1986) Molecular stratigraphy: A new tool for climatic assessment. *Nature*. Vol 320, pg. 129–133

Broccoli, A. J (2000) Tropical Cooling at the Last Glacial Maximum: An Atmosphere–Mixed Layer Ocean Model Simulation. *Journal of Climate*. Vol 13, pg. 951-976

Broecker, W. S and Peng, T. H (1982) Tracers in the Sea: Palisades, NY (Eldigio Press)

Broecker, W. S (1994) Massive iceberg discharges as triggers for global climate change. *Nature*. Vol 372, Issue 6505, pg. 421-424

Broecker, W. S (1982) Ocean chemistry during glacial time. *Geochimica et Cosmochimica Acta*. Vol 7, Issue 2, pg. 1689-1705

Broecker, W. S and Denton, G. H (1989) The role of ocean-atmosphere reorganizations in glacial cycles. *Geochimica et Cosmochimica Acta*. Vol 53, pg. 2465-2501

Broecker, W. S (1991) The Great Ocean Conveyor. *Oceanography*. Vol 4, pg. 79-89

Broecker, W. S and Denton, G. H (1990) The role of ocean-atmosphere reorganizations in glacial cycles. *Quaternary Science Reviews*. Vol 9, pg. 305-341

Budziak, D; Schneider, R. R; Rostek, F; Müller, P. J; Bard, E; Wefer, G (2000) Late Quaternary insolation forcing on total organic carbon and C37 alkenone variations in the Arabian Sea. *Paleoceanography*. Vol 15, pg. 307–321

Budziak, D; Schneider, R. R; Rostek, F; Müller, P. J; Bard, E; Wefer, G (2000) Late Quaternary insolation forcing on total organic carbon and alkenone variations in the Arabian Sea. *Paleoceanography*. Vol 15, pg. 307-321

Bush, A. B. G and Philander, S. G. H (1998) The Role of Ocean-Atmosphere Interactions in Tropical Cooling During the Last Glacial Maximum. *Science*. Vol 279, pg. 1341-1344

Callot, H. J (1991) Geochemistry of chlorophylls, in Scheer, H, ed, Chlorophylls: Boca Raton, CRC Press, pg. 339–364

Calvert, S.E and Pedersen, T.F (1992) Organic matter accumulation, remineralization and burial in an anoxic coastal sediment. In: Whelan, J.K., Farrington, J.W (Eds.), Organic Matter: Productivity, Accumulation and Preservation in Recent and Ancient Sediments. Columbia University Press, New York, pg. 231–263

Cane, M. A (1998) Climate Change: A Role for the Tropical Pacific. *Science*. Vol 282, pg. 59-61

Cane, M. A (2005) The evolution of El Niño, past and future. *Earth and Planetary Science Letters*. Vol 230, pg. 227-240

Cannariato, K. G and Ravelo, A. C (1997) Pliocene-Pleistocene evolution of eastern tropical surface water circulation and thermocline depth. *Paleoceanography*. Vol 12, no. 6, pg. 805-820

Chaisson, W. P and Ravelo, A. C (2000) Pliocene development of the east-west hydrographic gradient in the equatorial Pacific. *Paleoceanography*. Vol 15, no. 5, pg. 497-505

Chaisson, W (1995) Planktonic foraminiferal assemblages and paleoceanographic change in the trans-tropical Pacific Ocean: A comparison of West (Leg 130) and East (Leg 138), latest Miocene to Pleistocene. In: Pisias, N.G; Mayer, L.A; Janecek, T.R; Palmer-Julson, A; van Andel, T.H (Eds.), 1995 Proceedings of the Ocean Drilling Program, Scientific Results, Vol. 138

Charles, CD; Wright, J.D; Fairbanks, R.G (1993) Thermodynamic influences on the marine carbon isotope record. *Paleoceanography*. Vol 8, pg. 691-697

Chavez, F. P; Buck, K. R; Barber, R. T (1990) Phytoplankton taxa in relation to primary productivity in the upper Equatorial Pacific Ocean. *Journal of Physical Oceanography*. Vol 37, pg. 1733-1752

Chavez, F. P; Buck, K. R; Coale, K. H; Martin, J. H; Di Tullio, G. R; Welschmeyer, N. A; Jacobson, A. C; and Barber, R. T (1991) Growth rates, grazing, sinking, and iron limitation of equatorial Pacific phytoplankton. *Limnology and Oceanography*. Vol 36, pg. 1816-1833

Chavez, F. P (1989) Size distribution of phytoplankton in the central and eastern tropical Pacific. *Global Biogeochememical Cycles*. Vol 3, pg. 27–35

Chavez, F. P; Buck, K. R; Service, S. K; Newton, J; Barber, R.T (1996a) Phytoplankton variability in the central and eastern tropical Pacific. *Deep-Sea Research II*. Vol 43, pg. 835–870

Chen, J; Farrell, J. W; Murray, D. W; Prell, W. L (1995) Timescale and paleoceanographic implications of a 3.6 m.y. oxygen isotope record from the northeast Indian Ocean (Ocean Drilling Program Site 758). *Paleoceanography*. Vol 10, Issue 1, pg. 21-47

Cheshire, H; Thurow, J; Nederbragt, A. J (2005) Late Quaternary climate change record from two long sediment cores from Guaymas Basin, Gulf of California. *Journal of Quaternary Science*. Vol 20, pg. 457–469

Clark, P. U and Pollard, D (1998) Origin ofthe middle Pleistocene transition by ice sheet erosion of regolith. *Paleoceanography*. Vol 13, pg. 1-9

Clark, P. U; Archer, D; Pollard, D; Blum, J. D; Rial, J. A; Brovkin, V; Mix, A. C; Pisias, N. G; Roy, M (2006) The middle Pleistocene transition: characteristics, mechanisms, and implications for long-term changes in atmospheric pCO_2. *Quaternary Science Reviews*. Vol 25, pg. 3150–3184

Clemens, S. C; Murray, D. W; Prell, W. L (1996) Nonstationary Phase of the PlioPleistocene Asian Monsoon. *Science*. Vol 274, pg. 943-948

Clemens, S; Prell, W. L; Murray, D; Shimmield, G; Weedon, G (1991) Forcing mechanisms of the Indian Ocean monsoon. *Nature*. Vol 353, pg. 720-725

Clement, A. C; Hall, A; Broccoli, A. J (2004) The importance of precessional signals in the tropical climate. *Climate Dynamics*. Vol 22, pg. 327-341

Clement, A. C; Seager, R; Cane, M. A (1999) Orbital controls on the El Niño/Southern Oscillation and the tropical climate. *Paleoceanography*. Vol 14, pg. 441-456

Clement, A. C; Seager, R; Cane, M. A (2000) Suppression of El Niño during the mid-Holocene by changes in the Earth's orbit. *Paleoceanography*. Vol 15, pg. 731-737

Conkright, M. E; Locarnini, R. A; Garcia, H. E; O'Brien, T. D; Boyer, T. P; Stephens, C; Antonov, J. I (2002) World Ocean Atlas 2001: Objective Analyses, Data Statistics, and Figures, CD-ROM Documentation, MD, pg. 17. National Oceanographic Data Center, Silver Spring, MD

Conte, M. H; Eglinton, G; Madureira, L. A. S (1992) Long-chain alkenones and alkyl alkenoates as palaeotemperature indicators: their production, flux and early sedimentary diagenesis in the Eastern North Atlantic. *Organic Geochemistry*. Vol 19, pg. 287-298

Conte, M. H; Thompson, A; Eglinton, G; and Green, J. C (1995) Lipid biomarker diversity in the coccolithophorid Emiliania huxleyi (Prymnesiophyceae) and the related species Gephyrocapsa oceanica. *Journal of Phycology*. Vol 31, pg. 272-282

Conte, M. H; Thompson, A; Lesley, D; Harris, R. P (1998) Genetic and physiological influences on the alkenone/alkenoate versus growth temperature relationship in Emiliania huxleyi and Geophyrocapsa oceanica. *Geochimica et Cosmochimica Acta*. Vol 62, pg. 51-68

Conte, M. H; Sicre, M-A; Rühlemann, C; Weber, J. C; Schulte, S; Schulz-Bull, D; Blanz, T (2006) Global temperature calibration of the alkenone unsaturation index (U37K0) in surface waters and comparison with surface sediments. *Geochemistry Geophysics Geosystems*. Vol 7, issue 2, pg. 1-22

Conte, M.H; Volkman, J.K; Eglinton, G (1994) Lipid biomarkers of the Haptophyta. In: Green, J. C; Leadbeater, B. S. C (Eds.) The Haptophyte Algae. Systematics Association Special Volume No. 51. Clarendon Press, Oxford, pg. 351–377

Crowley, T. J; Kim, K.-Y; Mengel, J. G; Short, D. A (1992) Modelling 100,000-Year Climate Fluctuations in Pre-Pleistocene Time Series. *Science*. Vol 255, pg. 705-707

Curry, W. B and Oppo, D. W (2005) Glacial water mass geometry and the distribution of $\delta^{13}C$ of CO_2 in the western Atlantic Ocean. *Paleoceanography*. Vol 20, pg. 1-12

D'Hondt, S; King, J; Gibson, C (1996) Oscillatory marine response to the Cretaceous-Tertiary impact. *Geology*. Vol 24, no. 7, pg. 611-614

Dansgaard, W; Johnsen, S. J; Clausen, H. B; Dahl-Jensen, D; Gundestrup, N. S; Hammer, C. U; Hvidberg, C. S; Steffensen, J. P; Sveinbjörnsdottir, A. E; Jouzel, J; Bond, G (1993) Evidence for general instability of past climate from a 250-kyr ice-core record. *Nature*. Vol 364, pg. 218–220

Dansgaard, W; Johnsen, S. J; Clausen, H. B; Dahl-Jensen, D; Gundestrup, N; Hammer, C. U; Oeschger, H (1984) North Atlantic Climatic Oscillations Revealed by Deep Greenland Ice Cores. In: Climate Processes and Climate Sensitivity (eds J. E. Hansen and T. Takahashi), American Geophysical Union, Washington, DC, Vol 5, pg. 288-298

de Menocal, P. B (1995) Plio-Pleistocene African climate. *Science*. Vol 270, pg. 53-59

DeBlonde, G and Peltier, W. R (1991) A One-Dimensional Model of Continental Ice Volume Fluctuations through the Pleistocene: Implications for the Origin of the Mid-Pleistocene Climate Transition. *Journal of Climate*. Vol 4, pg. 318-344

Dekens, P. S; Ravelo, A. C; McCarthy, M. D (2007) Warm upwelling regions in the Pliocene warm period. *Paleoceanography*. Vol 22

Delcroix, T; Eldin, G; Hénin, C (1987) Upper ocean water masses and transports in the western tropical Pacific (165°E). *Journal of Physical Oceanography*. Vol 17, pg. 2248-2262

Denton, G. H; Anderson, R. F; Toggweiler, J. R; Edwards, R. L; Schaefer, J. M and Putnam, A. E (2010) The last glacial termination. *Science*. Vol 328, pg. 1652-1656

Deser, C and Wallace, J. M (1990) Large-Scale Atmospheric Circulation Features of Warm and Cold Episodes in the Tropical Pacific. *Journal of Climate*. Vol 3, pg. 1254-1281

Diekmann, B and Kuhn, G (2002) Sedimentary record of the mid-Pleistocene climate transition in the southeastern South Atlantic (ODP site 1090). *Palaeogeography*, *Palaeoclimatology*, *Palaeoecology*. Vol 182, pg. 241-258

Douglas, R.G and Savin, S.M (1978) Oxygen isotopic evidence for the depth stratification of Tertiary and Cretaceous planktic Foraminifera. *Marine Micropaleontology*. Vol 3, pg. 175-196

Dowsett, H (2007) Faunal re-evaluation of Mid-Pliocene conditions in the western equatorial Pacific. *Micropaleontology*. Vol 53, no. 6, pg. 447-456

Dunbar, R. B (1983) Stable isotope record of upwelling and climate from Santa Barbara Basin, California, in Coastal Upwelling: Its Sedimentary Record, Part B, edited by E. Suess and J. Thiede. pg. 217-246, Plenum, New York

Duplessy, J. C; Shackleton, N. J; Matthews, R. K; Prell, W; Ruddiman. W. F; Caralp, M; Hendy, C. H (1984) 13C Record of benthic foraminifera in the last interglacial ocean: Implications for the carbon cycle and the global deep water circulation. *Quaternary Research*. Vol. 21, pg. 225-243

Duplessy, J. C; Labeyrie, L; Arnold, M; Paterne, M; Duprat, J; van Weering, T. C. E (1992) Changes in surface salinity of the North Atlantic Ocean during the last deglaciation. *Nature*. Vol 358, pg. 485-487

Eckardt, C. B; Keely, B. J; Waring, J. R; Chicarelli, M. I; Maxwell, J. R (1991) Preservation of chlorophyll-derived pigments in sedimentary organic matter. *Royal Society of London Philosophical Transactions*, series B. Vol 333, pg. 339–348

Eglinton, T. I; Conte, M. H; Eglinton, G; Hayes, J. M (2001) Proceedings of a workshop on alkenone-based paleoceanographic indicators. *Geochemistry Geophysics Geosystems*. Vol 2, Issue 1

Elderfield, H; Ferretti, P; Greaves, M; Crowhurst, S; McCave, I. N; Hodell, D; Piotrowski, A. M (2012) Evolution of Ocean Temperature and Ice Volume Through the Mid-Pleistocene Climate Transition. *Science*. Vol 337, pg. 704-709

Emeis, K. C; Doose, H; Mix, A. C; Schulz-Bull, D (1995) Alkenone sea-surface temperatures and carbon burial at Site 846 (Eastern equatorial Pacific Ocean): the last 1.3 m.y. In: Proceedings of the Ocean Drilling Program, Scientific Results. (N. G. Pisias, L. A. Mayer, A. Palmer-Julson, and T. H. van Andel, Eds.), pg. 605-613

EPICA community members (2004) Eight glacial cycles from an Antarctic ice core. *Nature*. Vol 429, pg. 623-628

Epstein, S; Buchsbaum, S.R; Lowenstam, H.A; Urey, H.C (1953) Revised carbonate-water isotopic temperature scale. *Geological Society of America Bulletin*. Vol 64, pg. 1315-1326

Epstein, B. L; D'Hondt, S; Hargraves, P.E (2001) The possible metabolic role of C37 alkenones in Emiliania huxleyi. Organic Geochemistry. Vol. 32, Issue 6, pg. 867-875

Epstein, B. L; D'Hondt, S; Quinn, J. G; Zhang, J; Hargraves, P. E (1998) An effect of dissolved nutrient concentrations on alkenone-based temperature estimates. *Paleoceanography*. Vol 13, no. 2, pg. 122-126

Erez, J and Luz, B (1983) Experimental paleotemperature equation for planktonic foraminifera. *Geochimica et Cosmochimica Acta*. Vol 47, pg. 1025–1031

Fairbanks, R. G and Wiebe, P. H (1980) Foraminifera and Chlorophyll Maximum: Vertical Distribution, Seasonal Succession, and Paleoceanographic Significance. *Science*. Vol.209, no. 4464, pg. 1524-1526

Fairbanks, R. G; Sverdlove, M; Free, R; Wiebe, P. H; Bé, A. W. H (1982) Vertical distribution and isotopic fractionation of living planktonic foraminifera from the Panama Basin. *Nature*. Vol 298, pg. 841-844

Falkowski, P; Scholes, R. J; Boyle, E; Canadell, J; Canfield, D; Elser, J; Gruber, N; Hibbard, K; Hogberg, 0; Linder, S; Mackenzie, F. T; Moore Ill, B; Pedersen, T; Rosenthal, Y; Seitzinger, S; Smetacek, V; Steffen, W (2000) The Global Carbon Cycle: A Test of Our Knowledge of Earth as a System. *Science*. Vol 290, pg. 291-296

Farrell, J. W; Murray, D. W; McKenna, V. S; Ravelo, A. C (1995) Upper ocean temperature and nutrient contrasts inferred from Pleistocene planktonic foramininfera $\delta^{18}O$ and $\delta^{13}C$ in the eastern equatorial Pacific. In: Proceedings of the Ocean Drilling Program, Scientific Results, Vol 138. (N. G. Pisias, L. A. Mayer, T. R. Janecek, A. Palmer-Julson, and T. H. van Andel, Eds.), pg. 289-319

Fiedler, P. C and Talley, L. D (2006) Hydrography of the eastern tropical Pacific: A review. *Progress in Oceanography*. Vol 69, pg. 143-180

Fiedler, P. C (2002) Environmental change in the eastern tropical Pacific Ocean: Review of ENSO and decadal variability. *Marine Ecology Progress Series*. Vol 244, pg. 265–283

Finney, B. P; Lyle, M. W; Heath, G. R (1988) Sedimentation at MANOP Site H (eastern equatorial Pacific) over the past 400,000 years: climatically induced redox variations and their effects on transition metal cycling. *Paleoceanography*. Vol 3, pg. 169-189

Flückiger, J; Dallenbach, A; Blunier, T; Stauffer, B; Stacker, T. F; Raynaud, D; Bamola, J. M (1999) Variation in atmospheric N20 concentration during abrupt climatic changes. *Science*. Vol 285, pg. 227-230

Furlong, E. T and Carpenter, R (1988) Pigment preservation and remineralization in oxic coastal marine sediments. *Geochimica et Cosmochimica Acta*. Vol 52, issue 1, pg. 87-99

Gagan, M. K; Ayliffe, L. K; Beck, J. W; Cole, J. E; Druffel, E. R. M; Dunbar, R. B; Schrag, D. P (2000) New views of tropical paleoclimates from corals. *Quaternary Science Reviews*. Vol 19, pg. 45-64

Ganeshram, R. S and Pedersen, T. F (1998) Glacial-interglacial variability in upwelling and bioproductivity off NW Mexico: Implications for Quaternary paleoclimate. *Paleoceanography*. Vol 13, pg. 634–645

Garidel-Thoron, T; Rosenthal, Y; Bassinot, F; Beaufort, L (2005) Stable sea surface temperatures in the western Pacific warm pool over the past 1.75 million years. *Nature*. Vol 433, pg. 294-298

Gasperi, J. T and Kennett, J. P (1992) Isotopic evidence for depth stratification and paleoecology of Miocene planktonic foraminifera: western equatorial Pacific DSDP Site 289. In: Tsuchi, R, Ingle Jr. Jr, J.C. (Eds.), Pacific Neogene Environment, Evolution and Events. Univ. Tokyo Press, Tokyo, pg. 235–254

Gasperi, J. T and Kennett, J. P (1993) Vertical thermocline structure evolution of Miocene surface waters: Western equatorial Pacific DSDP Site 289. *Marine Micropaleontology*. Vol 22, Issue 2, pg. 235-254

Gebhardt, H; Sarnthein, M; Grootes, P. M; Kiefer, T; Kuehn, H; Schmeider, F; Röhl, U (2008) Paleonutrient and productivity records from the subarctic North Pacific for Pleistocene glacial terminations I to V. *Paleoceanography*. Vol 23, Issue 4, pg. 1-21

Gersonde, R; Crosta, X; Abelmann, A; Armand, L (2008) Sea-surface temperature and sea ice distribution of the Southern Ocean at the EPILOG Last Glacial Maximum—a circum-Antarctic view based on siliceous microfossil records. *Quaternary Science Reviews*. Vol 24, pg. 869-896

Gong, C and Hollander, D. J (1999) Evidence for differential degradation of alkenones under contrasting bottom water oxygen conditions: implication for paleotemperature reconstruction. *Geochimica et Cosmochimica Acta*. Vol 63, Issues 3-4, pg. 405-411

Guilderson, T. P; Fairbanks, R. G; Rubenstone, J. L (1994) Tropical Temperature Variations Since 20,000 Years Ago: Modulating Interhemispheric Climate Change. *Science*. Vol 263, pg. 663-665

Guilizzoni, P; G. Bonomi; G. Galanti; D. Ruggiu (1983) Relationship between sedimentary pigments and primary production: evidence from core analyses of twelve Italian lakes. *Hydrobiologia*. Vol 103, pg. 103-106

Hagelberg, T. K; G. Bond; P. deMenocal (1994) Milankovitch band forcing of sub- Milankovitch climate variability during the Pleistocene. *Paleoceanography*. Vol 9, pg. 545–558

Hagelberg, T; Pisias, N; Elgar, S (1991) Linear and nonlinear coupling between orbital forcing and the marine record during the late Neogene. *Paleoceanography*. Vol 6, pg. 729-746

Hain, M. P; Sigman, D. M; Haug, G. H (2010) Carbon dioxide effects of Antarctic stratification, North Atlantic Intermediate Water formation, and subantarctic nutrient drawdown during the last ice age: diagnosis and synthesis in a geochemical box model. *Global Biogeochemical Cycles*. Vol 24

Harmon, C (1957) Isotopic standards for carbon and oxygen & correction factors for mass spectrometric analysis. *Geochimica et Cosmochimica Acta*. Vol 12, pg. 133-149

Harris, P. G; Zhao, M; Rosell-Melé, A; Tiedemann, R; Sarnthein, M; Maxwell, J. R (1996) Chlorin accumulation rate as a proxy for Quaternary marine primary productivity. *Nature*. Vol 383, pg. 63-65

Hay, W. W (1977) Calcareous Nannofossils. In: Ramsay, A. T. S. (Ed.) Oceanic Micropaleontology. Academic Press. London, pg. 1055-1200

Hays, J. D; Imbrie, J; Shackleton, N. J (1976) Variations in the earth's orbit: pacemaker of the ice ages. *Science*. Vol 194, pg. 1121–1132

Hedges, J. I and Keil, R. G (1995) Sedimentary organic matter preservation: an assessment and speculative synthesis. *Marine Chemistry*. Vol 49, pg. 81–115

Heinrich, H (1988) Origin and consequences of cyclic ice rafting in the Northeast Atlantic Ocean during the past 130,000 years. *Quaternary Research*. Vol 29, Issue 2, pg. 142–152

Held, I. M and Soden, B. J (2006) Robust Responses of the Hydrological Cycle to Global Warming. *Journal of Climate*. Vol 19, pg. 5686-5699

Hendy, E. J; Gagan, M. K; Alibert, C. A; McCulloch, M. T; Lough, J. M; Isdale, P. J (2002) Abrupt Decrease in Tropical Pacific Sea Surface Salinity at End of Little Ice Age. *Science*. Vol 295, pg. 1511-1514

Hendy, I. L and Kennett, J. P (2000) Dansgaard-Oeschger cycles and the California Current System: Planktonic foraminiferal response to rapid climate change in Santa Barbara Basin, Ocean Drilling Program hole 893A. *Paleoceanography*. Vol 15, Issue 1, pg. 30-42

Henrichs, S. M and Reeburgh, W. S (1987) Anaerobic mineralization of marine sediment organic matter: rates and the role of anaerobic processes in the oceanic carbon economy. *Geomicrobiology Journal*. Vol 5, Issue 3-4, pg. 191-237

Herbert, T. D; Peterson, L. C; Lawrence, K. T; Liu, Z (2010) Tropical ocean temperatures over the past 3.5 million years. *Science*. Vol 328, pg. 1530-1534

Herbert, T. D; Schuffert, J. D; Andreasen, D; Heusser, L; Lyle, M; Mix, A; Ravelo, A. C; Stott, L. D and Herguera, J. C (2001) Collapse of the California Current during glacial maxima linked to climate change on land. *Science*. Vol 293, pg. 71–76

Herbert, T. D; Schuffert, J. D; Thomas, D; Lange, C; Weinheimer, A; Peleo-Alampay, A; Herguera, J. C (1998) Depth and seasonality of alkenone production along the California margin inferred from a core top transect. *Paleoceanography*. Vol 13, no. 3, pg. 263-271

Hernandez-Almeida, I; Sierro, F. J; Cacho, I; Flores, J. A (2012) Impact of suborbital climate changes in the North Atlantic on ice sheet dynamics at the Mid-Pleistocene Transition. *Paleoceanography*. Vol 27, pg. 1-14

Higginson, M. J and Altabet, M. A (2004) Initial test of the silicic acid leakage hypothesis using sedimentary biomarkers. *Geophysical Research Letters*. Vol 31, Issue 18

Higginson, M.J; Altabet, M.A; Murray, D.W; Murray, R.W; Herbert, T.D (2004) Geochemical evidence for abrupt changes in relative strength of the Arabian monsoons during a stadial/interstadial climate transition. *Geochimica et Cosmochimica Acta*. Vol 68, pg. 3807–3826

Higginson, M.J (2000) Chlorin pigment stratigraphy as a new and rapid paleoceanographic proxy in the Quaternary. Ph.D. thesis, University of Bristol, Bristol

Higginson, M. J; Altabet, M. A; Wincze, L; Herbert, T. D; Murray, D. W (2004) A solar (irradiance) trigger for millennial-scale abrupt changes in the southwest monsoon? *Paleoceanography.* Vol 19, Issue 3, pg. 1-18

Higginson, M. J; Maxwell, J. R; Altabet, M. A (2003) Nitrogen isotope and chlorin paleoproductivity records from the Northern South China Sea: remote vs. local forcing of millennial- and orbital-scale variability. *Marine Geology*. Vol 201, Issue 1-3, pg. 223-250

Hodell, D. A; Venz, K. A; Charles, C. D; Ninneman, U. S (2003) Pleistocene vertical carbon isotope and carbonate gradients in the South Atlantic sector of the Southern Ocean. *Geochemistry, Geophysics, Geosystems*. Vol 4, Issue 1

Hoefs, M. J. L; Versteegh, G. J. M; Rijpstra, W. I. C; de Leeuw, J. W; SinninghеDamste, J. S (1998) Postdepositional oxic degradation of alkenones: implications for the measurement of palaeo sea surface temperatures. *Paleoceanography*. Vol 13, pg. 42-49

Hönisch, B and Hall, J (2007) Paleoceanography, physical and chemical ocean proxies: Carbon Cycle Proxies. *Encyclopedia of Quaternary Science*. pg. 1699-1710

Hönisch, B; Hemming, N. G; Archer, D; Siddall, M; McManus, J. F (2009) Atmospheric Carbon Dioxide Concentration Across the Mid-Pleistocene Transition. *Science*. Vol 324, pg. 1551-1554

Hoogakker, B. A. A; Rohling, E. J; Palmer, M. R; Tyrrell, T; Rothwell, R. G (2006) Underlying causes for long-term global ocean $\delta^{13}C$ fluctuations over the last 1.20 Myr. *Earth and Planetary Science Letters*. Vol 248, pg. 15-29

Hovan, S (1995) Late Cenozoic atmospheric circulation intensity and climatic history recorded by eolian deposition in the eastern equatorial Pacific Ocean, Leg 138. In: Proceedings of the Ocean Drilling Program, Scientific Results, Vol.138. (N. G. Pisias, L. A. Mayer, T. R. Janecek, A. Palmer-Julson, and T. H. van Andel, Eds.) pg. 615-625

Howard, W. R and Prell, W. L (1992) Late Quaternary surface circulation of the Southern Indian Ocean and its relationship to orbital variables. *Paleoceanography*. Vol 7, pg. 79–117

Huybers, P and Wunsch, C (2005) Obliquity pacing of the late Pleistocene glacial terminations. *Nature*. Vol 434, pg. 491-494

Ikehara, M; Kawamura, K; Ohkouchi, N; Murayama, M; Nakamura, T; Taira, A (2000) Variations of terrestrial input and marine productivity in the Southern Ocean (48°S) during the last two deglaciations. *Paleoceanography*. Vol 15, pg. 170–180

Imbrie, J; Boyle, E. A; Clemens, S. C; Duffy, A; Howard, W. R; Kukla, G; Kutzbach, J; Martinson, D. G; McIntyre, A; Mix, A. C; Molfino, B; Morley, J. J; Peterson, L. C; Pisias, N. G; Prell, W. L; Raymo, M. E; Shackleton, N. J; Toggweiler, J. R (1992) On the structure and origin of major glaciation cycles. 1: Linear responses to Milankovich forcing. *Paleoceanography*. Vol 7, no. 6, pg. 701–738

Imbrie, J; Berger, A; Boyle, E. A; Clemens, S. C; Duffy, A; Howard, W. R; Kukla, G; Kutzbach, J; Martinson, D. G; Mcintyre, A; Mix, A. C; Molfino, B; Morley, J. J; Peterson, L. C; Pisias, N. G; Prell, Raymo, M. E; Shackleton, N. J; Toggweiler, J. R (1993) On the structure and origin of major glaciation cycles 2: The 100,000 year cycle. *Paleoceanography*. Vol 8, no.6, pg. 699-735

Ishiwatari, R; Negishi, K; Yoshikawa, H; Yamamoto, S (2009) Glacial–interglacial productivity and environmental changes in Lake Biwa, Japan: A sediment core study of organic carbon, chlorins and biomarkers. *Organic Chemistry*. Vol 40, pg. 520-530

Ivanochko, T. S; Ganeshram, R. S; Brummer, G. A; Ganssen, G; Jung, S. J. A; Moreton, S. G; Kroon, D (2005) Variations in tropical convection as an amplifier of global climate change at the millennial scale. *Earth and Planetary Science Letters*. Vol 235, Issue 1-2, pg. 302-314

Janecek, T. R and Rea, D. K (1985) Quaternary fluctuations in the Northern Hemisphere tradewinds and westerlies. *Quaternary Research*. Vol 24, pg. 150-163

Janecek, T.R (1985) Eolian sedimentation in the Northwest Pacific Ocean: a preliminary examination of the data from Deep Sea Drilling Project Sites 576 and 578. In: Heath, G. R; Burckle, L. H; et al., Init. Repts. DSDP, 86: Washington (U.S. Govt. Printing Office), pg. 589-603

Jansen, E; Fronval, T; Rack, F; Channell, J. E. T (2000) Pliocene–Pleistocene ice rafting history and cyclicity in the Nordic Seas during the last 3.5 Myr. *Paleoceanography*. Vol 15, pg. 709–721

Jasper, J. P and Hayes, J. M (1990) A carbon isotope record of C02 levels during the late Quaternary. *Nature*. Vol 347, pg. 462-464

Jeffrey, S. W; Mantoura, R. F. C; Bjornland, T (1997) Data for the identification of 47 key phytoplankton pigments. In: Phytoplankton pigments in oceanography: guidelines to modern methods. (S. W. Wright, Ed.), pg. 149-559

Jian, Z; Wang, P; Chen, M. P; Li, B; Zhao, Q; Buhring, C; Laj, C; Lin, H. L; Pflaumann, U; Bian, Y; Wang, R; Cheng, X (2000) Foraminiferal responses to major Pleistocene paleoceanographic changes in the southern South China Sea. *Paleoceanography*. Vol 15, pg. 229-243

Jin, H and Jian, Z (2013) Millennial-scale climate variability during the mid-Pleistocene transition period in the northern South China Sea. *Quaternary Science Reviews*. Vol 70, pg. 15-27

Jordan, R. W; Zhao, M; Eglington, G; Weaver, P. P. E (1996) Coccolith and alkenone stratigraphy and palaeoceanography at an upwelling site off NW Africa (ODP 658C) during the last 130,000 years. In: Moguilevsky, A. L and Whatley, R.C (Eds.) Microfossils and Oceanic Environment. University of Wales Press, Aberystwyth, pg. 111–130

Jouzel, J; Masson-Delmotte, V; Cattani, O; Dreyfus, G; Falourd, S; Hoffmann, G; Minster, B; Nouet, J; Barnola, J. M; Chappellaz, J; Fischer, H; Gallet, J. C; Johnsen, S; Leuenberger, M; Loulergue, L; Luethi, D; Oerter, H; Parrenin, F; Raisbeck, G; Raynaud, D; Schilt, A; Schwander, J; Selmo, E; Souchez, R; Spahni, R; Stauffer, B; Steffensen, J. P; Stenni, B; Stocker, T. F; Tison, J. L; Werner, M; Wolff, E. W (2007) Orbital and millennial Antarctic climate variability over the past 800,000 years. *Science*. Vol. 317, pg. 793–796

Keely, B. J; Harris, P. G; Popp, B. N; Hayes, J. M; Meischner, D; Maxwell, J (1994) Porphyrin and chlorin distributions in a Late Pliocene lacustrine sediment. *Geochimica et Cosmochimica Acta*. Vol 58, pg. 3691-3701

Keigwin, L. D (1978) Pliocene closing of the Isthmus of Panama, based on biostratigraphic evidence from nearby Pacific Ocean and Caribbean Sea cores. *Geology*. Vol 6, pg. 630-634

Keigwin, L. D (1979) Late Cenozoic stable isotope stratigraphy and paleoceanography of DSDP sites from the east equatorial and central north Pacific Ocean. *Earth and Planetary Science Letters*. Vol 45, Issue 2, pg. 361-382

Keigwin, L. D and Boyle, E. A (1989) Late Quaternary paleochemistry of high-latitude surface waters. *Paleogeography, Paleoclimatology, Paleoecology*. Vol 73, pg. 85-106

Kienast, M, S; Kienast, S; Calvert, S. E; Eglinton, T. I; Mollenhauer, G; François, R and Mix, A. C (2006) Eastern Pacific cooling and Atlantic overturning circulation during the last deglaciation. *Nature*. Vol 443, pg. 846–849

Kienast, M; MacIntyre, G; Dubois, N; Higginson, S; Normandeau, C; chazen, C; Herbert, T. D (2012) Alkenone unsaturation in surface sediments from the eastern equatorial Pacific: Implications for SST reconstructions. *Paleoceanography*. Vol 27, pg. 1-11

Kornilova, O; and Rosell-Melé, A (2003) Application of microwave-assisted extraction to the analysis of biomarker climate proxies in marine sediments. *Organic Geochemistry*. Vol 34, pg. 1517-1523

Koutavas, A and Sachs, J. P (2008) Northern timing of deglaciation in the eastern equatorial Pacific from alkenone paleothermometry. *Paleoceanography*. Vol 23, pg. 1-10

Koutavas, A; Lynch-Stieglitz, J; Marchitto Jr, T. M and Sachs, J. P (2002) El Niño-like pattern in ice age tropical Pacific sea surface temperature. *Science*. Vol 297, pg. 226–230

Kukla, G and Gavin, J (1992) Insolation regime of the warm to cold transitions. NATO Advanced Research Institute. In: Start of a Glacier (Kukla, G and Went, E, Eds.) pg. 307-339

Labeyrie, L; Labracherie,M; Gorfti, N; Pichon, J. J; Vautravers, M; Arnold, M; Duplessy, J. C; Paterne, M; Michel, E; Duprat, J; Caralp, M; Turon, J. L (1996) Hydrographic changes in the Southern Ocean (southeast Indian sector) over the last 230 kyr. *Paleoceanography*. Vol 11, pg. 57–76

Landry, M. R and Kirchman, D. L (2002) Microbial community structure and variability in the tropical Pacific. *Deep Sea Research Part II: Topical Studies in Oceanography.* Vol 49 Issues 13-14 pg.2669-2693

Lawrence, K. T; Liu, Z; Herbert, T. D (2006) Evolution of the Eastern Tropical Pacific Through Plio-Pleistocene Glaciation. *Science*. Vol 312, pg. 79-83

Le, J; Mix, A. C; Shackleton, N. J (1995) Late Quaternary Paleoceanography in the eastern equatorial Pacific ocean from planktonic foraminifers: a high-resolution record from site 846. In: Proceedings of the Ocean Drilling Program, Scientific Results, Vol 138. (N. G. Pisias, L. A. Mayer, T. R. Janecek, A. Palmer-Julson, and T. H. van Andel, Eds.), pg. 675-693

Lea, D. W (2002) The Glacial Tropical Pacific- Not Just a West Side Story. *Science*. Vol. 297, pg. 202-203

Lea, D. W (2004) The 100 000-Yr Cycle in Tropical SST, Greenhouse Forcing, and Climate Sensitivity. *Journal of Climate*. Vol 17, pg. 2170-2179

Lea, D. W; Pak, D. K and Spero, H. J (2000) Climate Impact of Late Quaternary Equatorial Pacific Sea Surface Temperature Variations. *Science*. Vol 289, pg. 1719-1724

Lear, C. H; Elderfield, H; Wilson, P. A (2000) Cenozoic Deep-Sea Temperatures and Global Ice Volumes from Mg/Ca in Benthic Foraminiferal Calcite. *Science*. Vol 287, pg. 269-272

Leduc, G; Vidal, L; Tachikawa, K and Bard, E (2009) ITCZ rather than ENSO signature for abrupt climate changes across the tropical Pacific? *Quaternary Research*. Vol 72, pg. 123–131

Leduc, G; Vidal, L; Tachikawa, K; Rostek, F; Sonzogni, C; Beaufort, L and Bard, E (2007) Moisture transport across Central America as a positive feedback on abrupt climatic changes. *Nature*. Vol 445, pg. 908–911

LeTreut, H and Ghil, M (1983) Orbital forcing, climatic interactions, and glaciation cycles. *Journal of Geophysical Research*. Vol 88, pg. 5167–5190

Li, Q; Wang, P; Zhao, Q; Tian, J; Cheng, X; Jian, Z; Zhong, G; Chen, M (2008) Paleoceanography of the mid-Pleistocene South China Sea. *Quaternary Science Reviews*. Vol 27, pg. 1217-1233

Lindzen, R. S and Pan, W (1994) A note on orbital control of equator-pole heat fluxes. *Climate Dynamics*. Vol 10, pg. 49-57

Lisiecki, L. E and Raymo, M. E (2005) A Pliocene-Pleistocene stack of 57 globally distributed benthic $\delta^{18}O$ records. *Paleoceanography*. Vol 20

Liu, Z and Herbert, T. D (2004) High-latitude influence on the eastern equatorial Pacific climate in the early Pleistocene epoch. *Nature*. Vol 421, pg. 720-724

Loubere, P and Austin, W (2007) Benthic Foraminifera. *Encyclopedia of Quaternary Science*. pg. 1618-1627

Louda, J. W; Li, J; Liu, L; Winfree, M. N; Baker, E. W (1998) Chlorophyll-a degradation during cellular senescence and death. *Organic Chemistry*. Vol 29, Issues 5-7 pg. 1233-1251

Lowe, J. J and Walker, M. J. C (1994) Reconstructing Quaternary Environments. Longman, Second Edition

Lüthi, D; Le Floch, M; Bereiter, B; Blunier, T; Barnola, J; Siegenthaler, U; Raynaud, D; Jouzel, J; Fischer, H; Kawamura, K; Stocker, T. F (2008) High-resolution carbon dioxide concentration record 650,000–800,000 years before present. *Nature*. Vol. 453, pg.379-382

Lyle, M. W; Prahl, F. G; Sparrow, M. A (1992) Upwelling and productivity changes inferred from a temperature record in the central equatorial Pacific. *Nature*. Vol.355, pg. 812-815

Lynch-Stieglitz, J; Stocker, T. F; Broecker, W. S; Fairbanks, R. G (1995) The influence of air-sea exchange on the isotopic composition of oceanic carbon: Observations and modeling. *Global Biogeochemical Cycles*. Vol.9, no. 4, pg. 653-665

Marchitto, T. M; Lehman, S. J; Ortiz, J. D; Flückiger, J; van Geen, A (2007) Marine Radiocarbon Evidence for the Mechanism of Deglacial Atmospheric CO_2 Rise. *Science*. Vol. 316 pg. 1456-1459

Marlowe, I. T; Brassell, S. C; Eglinton, G; and Green, J. C (1990) Long-chain alkenones and alkyl alkenoates and the fossil coccolith record of marine sediments. *Chemical Geology*. Vol 88, pg. 349-375

Marlowe, I. T; Green, J. C; Neal, A. C; Brassell, S. C; Eglinton, G; Course, P. A (1984) Long-chain (n-C37–C39) alkenones in the Prymnesiophyceae. Distribution of alkenones and other lipids and their taxonomic significance. *British Phycology Journal*. Vol 19, pg. 203–216

Martin, J. H and Fitzwater, S. E (1988) Iron-deficiency limits phytoplankton growth in the northeast Pacific subarctic. *Nature*. Vol 331, pg. 341–343

Martin, J. H (1990) Glacial-interglacial C02 change: The iron hypothesis. *Paleoceanography*. Vol 5, pg. 1-13

Martin, J. H; Gordon, R. M; Fitzwater, S. E (1991) The case for iron. *Limnology and Oceanography*. Vol 36, pg. 1793-1802

Martinez-Garcia, A; Rosell-Melé, A; Geibert, W; Gersonde, R; Masqué, P; Gaspari, V; Barbante, C (2009) Links between iron supply, marine productivity, sea surface temperature, and CO_2 over the last 1.1 Ma. *Paleoceanography*. Vol 24

Martinez-Garcia, A; Rosell-Melé, A; Jaccard, S. L; Geibert, W; Sigman, D. M; Haug, G. H (2011) Southern Ocean dust-climate coupling over the past four million years. *Nature*. Vol 476, Issue 7360, pg. 312-315

Martinez-Garcia, A; Rosell-Melé, A; McClymont, E. L; Gersonde, R; Haug, G. H (2010) Subpolar Link to the Emergence of the Modern Equatorial Pacific Cold Tongue. *Science*. Vol. 328 pg. 1550-1553

Mashiotta, T. A; Lea, D. W; Spero, H. J (1999) Glacial–interglacial changes in Subantarctic sea surface temperature and $\delta^{18}O$-water using foraminiferal Mg. *Earth and Planetary Science Letters*. Vol 170, pg. 417–432

Maslin, M; Shackleton, N. J; Pflaumann, U (1995) Surface water temperature, salinity and density changes in the NE Atlantic during the last 45 000 years: Heinrich events, deep water formation and climatic rebounds. *Paleoceanography*. Vol 10, 527-544

Mayer, L. A (1994) Surface area control of organic carbon accumulation in continental shelf sediments. *Geochimica et Cosmochimica Acta*. Vol 58, pg. 1271-1284

Mayer, L. A; Pisias, N. G; Janecek, T. R; and Shipboard Scientific Party (1992) Site 849. In: Proceedings of the Ocean Drilling Program, Initial Reports, Vol 138 (L.A. Mayer; N. G. Pisias; T. R. Janecek; and Shipboard Scientific Party, Eds.) pg. 735-767

McClymont, E. L (2004) Surface ocean circulation and organic carbon export across the mid-Pleistocene climate transition, Durham theses, Durham University

McClymont, E. L; Ganeshram, R. S; Pichevin, L. E; Talbot, H. M; van Dongen, B. E; Thunell, R. C; Haywood, A. M; Singarayer, J. S; Valdes, P. J (2012) Sea-surface temperature records of Termination 1 in the Gulf of California: Challenges for seasonal and interannual analogues of tropical Pacific climate change. *Paleoceanography*. Vol 27, pg. 1-15

McClymont, E. L; Sosidian, S. M; Rosell-Melé, A; Rosenthal, Y (2013) Pleistocene sea-surface temperature evolution: Early cooling, delayed glacial intensification, and implications for the mid-Pleistocene climate transition. *Earth-Science Reviews*. Vol 123 pg. 173-193

McClymont, E. L and Rosell-Melé, A (2005) Links between the onset of modern Walker Circulation and the mid-Pleistocene climate transition. *Geology*. Vol 33, pg. 389–392

McCrea, J (1950) On the isotopic chemistry of carbonates and palaeo-temperature scale. *Journal of Chemical Physics*. Vol 18, pg. 849-57

McGowan, S (2007) Paleoliminology: Pigment Studies. *Encylopedia of Quaternary Science*. Pg. 2062-2074

McIntyre, A and B. Molfino (1996) Forcing of Atlantic equatorial and subpolar millennial cycles by precession. *Science*. Vol 274, pg. 1867–1870

McManus, J. F; Francois, R; Gherardi, J. M; Keigwin, L. D; Brown-Leger, S (2004) Collapse and rapid resumption of Atlantic meridional circulation linked to deglacial climate changes. *Nature*. Vol 428, pg. 834-837

McManus, J. F; Oppo, D. W and Cullen, J. L (1999) A 0.5-Million-Year Record of Millennial-Scale Climate Variability in the North Atlantic. *Science*. Vol 283, pg. 971-975

Medina-Elizalde, M and Lea, D. W (2005) The Mid-Pleistocene Transition in the Tropical Pacific. *Science*. Vol 310, pg. 1009-1012

Menzel, D; van Bergen, P. F; Schouten, S; Sinninghe Damsté, J. S (2003) Reconstruction of changes in export productivity during Pliocene sapropel deposition: a biomarker approach. *Palaeogeography, Palaeoclimatology, Palaeoecology*. Vol 190, pg. 273-287

Milankovitch, M (1930) Mathematische Klimalehre und astronomische Theorie der Klimaschwankungen. In: Handbuch der Klimatologie, Vol 1 (W. Koppen, and R. Geiger, Eds.) pg. 1-176. Gebriider Borntrager, Berlin

Milankovitch, M (1941) Canon of Insolation and the Ice-Age Problem (in German). Special Publications of the Royal Serbian Academy, Vol. 132, Israel Program for Scientific Translations, pg. 484

Miller, P. J; Kirst, G; Ruhland, G; von Storch, L; Rosell-Melé, A (1998) Calibration of the alkenone pal eo temperature index U^{K}_{37}' based on core-tops from the eastern South Atlantic and the global ocean (60°N-60°S). *Geochimica Et Cosmochimica Acta*. Vol 62, pg. 757-1772

Mills, M. M; Ridame, C; Davey, M; La Roche, J; Geider, R. J (2004) Iron and phosphorus co-limit nitrogen fixation in the eastern tropical North Atlantic. *Nature*. Vol 429, pg. 292–294

Mitchell, T. P and Wallace, J. M (1992) The annual cycle in equatorial convection and surface temperature. *Journal of Climate*. Vol 5, pg. 1140–1156

Mix, A. C; Pisias, N. G; Rugh, W; Wilson, J; Morey, A; Hagelberg, T. K (1995) Benthic foraminifer stable isotope record from Site 849 (0-5 Ma): local and global climate changes. In: Proceedings of the Ocean Drilling Program, Scientific Results, Vol 138. (N. G. Pisias; L. A. Mayer; T. R. Janecek; A. Palmer-Julson; T. H. van Andel, Eds.) pg. 371-389

Molfino, B and McIntyre, A (1990) Precessional forcing of nutricline dynamics in the Equatorial Atlantic. *Science*. Vol 249, pg. 766–769

Mudelsee, M and Schulz, M (1997) The Mid-Pleistocene climate transition: onset of 100ka cycle lags ice volume build-up by 280ka. *Earth and Planetary Science Letters*. Vol 151, pg. 117-123

Mulitza, S; Dürkoop, A; Hale, W; Wefer, G; Niebler, H. S (1997) Planktonic foraminifera as recorders of past surface-water stratification. *Geology*. Vol 25, pg. 335-338

Muller, P. J and Suess, E (1979) Productivity, sedimentation rate, and sedimentary organic matter in the oceans—I. Organic carbon preservation. *Deep Sea Research Part A. Oceanographic Research Papers*. Vol 26, Issue 12, pg. 1347-1362

Murray, R. W; Knowlton, C; Leinen, M; Mix, A. C; Polsky (2000) Export production and carbonate dissolution in the central equatorial Pacific Ocean over the past 1 Myr. *Paleoceanography*. Vol 15, no. 6, pg. 570-592

Ninnemann, U. S and Charles, C. D (2002) Changes in the mode of Southern Ocean circulation over the last glacial cycle revealed by foraminiferal stable isotopic variability. *Earth and Planetary Science Letters*.Vol 201, pg. 383-396

Okada, H and Honjo, S (1973) The distribution of oceanic coccolithophorids in the Pacific. *Deep-Sea Research*. Vol 26, pg. 355-374

Okada, H and Mclntyre, A (1977) Modern coccolithophores of the Pacific and North Atlantic Oceans. *Micropaleontology*. Vol 23, pg. 1-55

Ono, A; Takahashi, K; Katsuki, K; Okazaki (2005) The Dansgaard-Oeschger cycles discovered in the up stream source region of the North Pacific Intermediate Water formation. *Geophysical Research Letters*. Vol 32

Oppo, D. W; McManus, J. F; Cullen, J. L (1998) Abrupt Climate Events 500,000 to 340,000 Years Ago: Evidence from Subpolar North Atlantic Sediments. *Science*. Vol 279, pg. 1335-1338

Orr, W. L; Emery, K. O; Grady, J. R (1958) Preservation of chlorophyll derivatives in sediments off Southern California. *American Association of Petroleum Geologists Bulletin*. Vol 42, pg. 925–959

Paillard, D (2001) Glacial Cycles: Toward a New Paradigm. *Reviews of Geophysics*. Vol 39, Issue 3, pg. 325-346

Park, J and Maasch, K. A (1993) Plio-Pleistocene Time Evolution of the 100-kyr Cycle in Marine Paleoclimate Records. *Journal of Geophysical Research*. Vol 98, no. 81, pg. 447-461

Patience, A. J and Kroon, D (1991) Oxygen-isotope chronostratigraphy. In: Quaternary Dating Methods- A User's Guide. (P. L. Smart and P. D. Prances, Eds.) pg. 199-228. Technical Guide 4, Quaternary Research Association, Cambridge

Pearson, P (2012) Oxygen Isotopes in Foraminifera: Overview and Historical Review Reconstructing Earth's Deep-Time Climate—The State of the Art in 2012, Paleontological Society Short Course, November 3, 2012. The Paleontological Society Papers, Vol 18, Linda C. Ivany and Brian T. Huber (eds.), pg. 1–38

Pedersen, T. F; Pickering, M; Vogel J. S; Southon, J. N; Nelson, D. E (1988) The response of benthic foraminifera to productivity cycles in the eastern equatorial Pacific: faunal and geochemical constraints on glacial bottom water oxygen levels. *Paleoceanography*. Vol 3, pg. 157-168

Pedersen, T. F; Nielsen, B; Pickering, M (1991) Timing of late Quaternary productivity pulses in the Panama Basin and implications for atmospheric CO_2. *Paleoceanography*. Vol 6, pg. 657-678

Pedersen, T. F (1983) Increased productivity in the eastern equatorial Pacific during the last glacial maximum (19,000 to 14,000 yr B.P.). *Geology*. Vol 11, pg. 16-19

Pedersen, T. F and Calvert, S. E (1990) Anoxia vs. productivity: what controls the formation of organic-rich sediments and sedimentary rocks? *American Association of Petroleum Geologists Bulletin*. Vol 74, pg. 454–466

Pelejero, C and J. O. Grimalt (1997) The correlation between the UK? 37 index and sea surface temperatures in the warm boundary: The South China Sea, *Geochimica et Cosmochimica Acta*. Vol 61, Issue 22, pg. 4789–4797

Pena, L. D; Cacho, I; Ferretti, P and Hall, M. A (2008) El Niño–Southern Oscillation–like variability during glacial terminations and interlatitudinal teleconnections. *Paleoceanography*. Vol 23, pg. 1-8

Pennington, J. T; Mahoney, K. L; Kuwahara, V. S; Kolber, D. D; Calienes, R; Chavez, F. P (2006) Primary production in the eastern tropical Pacific: A review. *Progress in Oceanography*. Vol. 69, pg. 285-317

Perks, H; Charles, C. D; Keeling, R. F (2002) Precessionally forced productivity variations across the equatorial Pacific. *Paleoceanography*. Vol 17, pg. 63–69

Peterson, L. C; Haug, G. H; Hughen, K. A and Röhl, U (2000) Rapid changes in the hydrologic cycle of the tropical Atlantic during the last glacial. *Science*. Vol 290, pg. 1947–1951

Petit, J. R; Jouzel, J; Raynaud, D; Barkov, N. L; Barnola, J. M; Basile, L; Bender, M; Chappellax, J; Davis, M; Delaygue, G; Delmotte, M; Kotlyakov, V. M; Legrand, M; Lipenkov, V. Y; Lorius, C; Pepin, L; Ritz, C; Saltzman, E; Stievenard, M (1999) Climate and atmospheric history of the past 420,000 years from the Vostok ice core, Antarctica. *Nature*. Vol 399, pg. 429-436

Philander, S. G and Fedorov, A. V (2003) Role of tropics in changing the response to Milankovitch forcing some three million years ago. *Paleoceanography*. Vol 18, no.2

Pichevin, L. E; Reynolds, B. C; Ganeshram, R. S; Cacho, I; Pena, L; Keefe, K; Ellam, R. M (2009) Enhanced carbon pump inferred from relaxation of nutrient limitation in the glacial ocean. *Nature*. Vol 459, pg. 1114-1118

Pichon, J. J; Labeyrie, L. D; Bareille, G; Labracherie, M; Duprat, J; Jouzel, J (1992) Surface water temperature changes in the high latitudes of the southern hemisphere over the last glacial–interglacial cycle. *Paleoceanography*. Vol 7, pg. 289–318

Pickard, G. L and Emery, W. J (1990) Descriptive physical oceanography: an introduction. Butterworth-Heinemann

Pisias, N. G and Mix, A. C (1997) Spatial and temporal oceanographic variability of the eastern equatorial Pacific during the late Pleistocene: Evidence from Radiolaria microfossils. *Paleoceanography*. Vol 12, no. 3, pg. 381-393

Pisias, N. G; Mayer, L. A; Mix, A. C (1995b) Paleoceanography of the eastern equatorial Pacific during the Neogene: synthesis of Leg 138 drilling results. In: Proceedings of the Ocean Drilling Program, Scientific Results, Vol 138. (N. G. Pisias, L. A. Mayer, T. R. Janecek, A. Palmer-Julson, and T. H. van Andel, Eds.), pg. 5-21

Pisias, N. G and Moore, T. C (1981) The Evolution of Pleistocene Climate: A time series approach. *Earth and Planetary Science Letters*. Vol. 52, pg. 450-458

Prahl, F. G and Wakeham, S. G (1987) Calibration ofunsaturation patterns in long-chain ketone compositions for palaeotemperature assessment. *Nature*. Vol 320, pg. 367-369

Prahl, F. G; Cowie, G. L; de Lange, G; Sparrow, M. A (2003) Selective organic matter preservation in bum-down turbidites on the Madeira Abyssal Plain. *Paleoceanography*. Vol 18, pg. 1052

Prahl, F. G; Delange, G. J; Lyle, M; Sparrow, M. A (1989) Post-Depositional Stability of Long-Chain Alkenones under Contrasting Redox Conditions. *Nature*. Vol 341, pg. 434-437

Prahl, F. G; Muehlhausen, L. A; Zahnle, D. I (1988) Further evaluation oflong-chain alkenones as indicators of paleoceanographic conditions. *Geochimica et Cosmochimica Acta.* Vol 52, pg. 2303-2310

Prahl, F; Popp, B. N; Karl, D. M; Sparrow, M. A (2005) Ecology and biogeochemistry of alkenone production at Station ALOHA. *Deep-Sea Research I*. Vol 52, pg. 699–719

Prahl, F.G; Dymond, J; Sparrow, M.A (2000) Annual biomarker record for export production in the central Arabian Sea. *Deep-Sea Research II*. Vol 47, pg. 1581–1604

Prahl, F. G; Mix, A. C; Sparrow, M. A (2006a) Alkenone paleothermometry: lessons from marine sediment records off western South America. *Geochimica et Cosmochimica Acta*. Vol 70, pg. 101–117

Prahl, F. G; Pisias, N; Sparrow, M. A; Sabin, A (1995) Assessment of sea-surface temperature at 42° N in the California Current over the last 30,000 years. *Paleoceanography*. Vol 10, pg. 763-773

Prahl, F. G; Rontani, J. F; Volkman, J. K; Sparrow, M. A; Royer, I. M (2006b) Unusual C35 and C36 alkenones in a paleoceanographic benchmark strain of Emiliania huxleyi. *Geochimica et Cosmochimica Ac*ta. Vol 70, pg. 2856–2867

Prell, W. L (1982) Oxygen and carbon isotope stratigraphy for the Quaternary of hole 502B: evidence for two modes of isotopic variability. *Initial Reports DSDP*. Vol 68, pg. 455–464

Rahmstorf, S (1995) Bifurcations of the Atlantic thermohaline circulation in response to changes in the hydrological cycle. *Nature*. Vol 378, pg. 145-149

Rahmstorf, S (2002) Ocean circulation and climate during the past 120,000 years. *Nature*. Vol 419, pg. 207-214

Ravelo, A. C and Fairbanks, R. G (1992) Oxygen isotopic composition of multiple species of planktonic foraminifera: recorders of the modern photic zone temperature gradient. *Paleoceanography.* Vol 7, pg. 815-831

Ravelo, A. C and Fairbanks, R. G (1995) Carbon isotopic fractionation in multiple species of planktonic-foraminifera from core-tops in the tropical Atlantic. *Journal of Foraminiferal Research*. Vol 25, pg. 53–74

Ravelo, A. C and Shackleton, N. J (1995) Evidence for surface-water circulation changes at site 851 in the eastern tropical Pacific Ocean. In: Proceedings of the Ocean Drilling Program, Scientific Results, Vol 138. (N. G. Pisias, L. A. Mayer, T. R. Janecek, A. Palmer-Julson, and T. H. van Andel, Eds.), pg. 503-514

Ravelo, A. C (1991) Reconstructing the tropical Atlantic seasonal thermocline using planktonic foraminifera [Ph.D. thesis]. Columbia University. NY

Ravelo, A. C and Hillaire-Marcel, C (2007) The use of oxygen and carbon isotopes of foraminifera in paleoceanography. *Developments in Marine Geology*. Vol 1, Chapter 18, pg. 735-764

Ravelo, A. C; Andreasen, D. H; Lyle, M; Lyle, A. O; Wara, M. W (2004) Regional climate shifts caused by gradual global cooling in the Pliocene epoch. *Nature*. Vol 429, pg. 263-267

Raymo, M. E; Ganley, K; Carter, S; Oppo, D. W; McManus, J (1998) Millennial-scale climate instability during the early Pleistocene epoch. *Nature*. Vol 392, pg. 699-702

Raymo, M. E (1994) The Himalayas, organic carbon burial, and climate in the Miocene. *Paleoceanography*. Vol 9, pg. 399-404

Raymo, M. E (1997) The timing of major climate terminations. *Paleoceanography.* Vol 12, pg. 577–585

Raymo, M. E and Niscancioglu, K (2003) The 41 kyr world: Milankovitch's other unsolved mystery. *Paleoceanography*. Vol 18, no. 1

Raymo, M. E; Oppo, D. W; Curry, W (1997) The mid-Pleistocene climate transition: A deep sea carbon isotope perspective. *Paleoceanography*. Vol 12, pg. 546-559

Raymo, M. E; Rind, D; Ruddiman, W. F (1990a) Climatic effects of reduced Arctic sea ice limits in the GISS 11 general circulation model. *Paleoceanography*. Vol 5, pg. 367- 382

Raymo, M. E; Ruddiman, W. F; Shackleton, N. J; Oppo, D. W (1990b) Evolution of Atlantic-Pacific $\delta^{13}C$ gradients over the last 2.5 m.y. *Earth and Planetary Science Letters*. Vol 97, pg. 353-368

Raymo, M. E; Hodell, D; Jansen, E (1992) Response of deep ocean circulation to initiation of northern hemisphere glaciation (3–2 MA). *Paleoceanography*. Vol 7, Issue 5, pg. 645-672

Reichart, G. J; Lourens, L. J; Zachariasse, W. J (1998) Temporal variability in the northern Arabian Sea Oxygen Minimum Zone (OMZ) during the last 225,000 years. *Paleoceanography*. Vol 13, no. 6, pg. 607-621

Reynolds-Sautter, L and Thunell, R. C (1991) Seasonal variability in the $\delta^{18}O$ and $\delta^{13}C$ of planktonic foramininfera from an upwelling environment: sediment trap results from the San Pedro basin, southern California bight. *Paleoceanography*. Vol 6, no. 3, pg. 307-334

Rohling, E. J (2007) Peleoceanography, physical and chemical proxies: Oxygen Isotopic Composition of Seawater. *Encyclopedia of Quaternary Science*. Pg. 1748-1756

Rontani, J. F; Volkman, J. K; Prahl, F. G; Wakeham, S. G (2013) Biotic and abiotic degradation of alkenones and implications for U^{K}_{37}' paleoproxy applications: A review. *Organic Geochemistry*. Vol 59, pg. 95-113

Ropelewski, C. F and Halpert, M. S (1987) Global and regional scale precipitation patterns associated with the El Niño/Southern Oscillation. *Monthly Weather Review*. Vol 114, pg. 2352-2362

Ropelewski, C. F and Halpert, M. S (1989) Precipitation patterns associated with the high index phase of the Southern Oscillation. *Journal of Climate*. Vol 2, pg. 268-284

Rosell-Melé, A and McClymont, E. L (2007) Chapter Eleven: Biomarkers as Paleoceanographic Proxies. *Developments in Marine Geology*. Vol 1, pg. 441-490

Rosell-Melé, A and Prahl, F. G (2013) Seasonality of UK'37 temperature estimates as inferred from sediment trap data. *Quaternary Science Reviews*. Vol 72, pg. 128-136

Rosell-Melé, A (1998) Interhemispheric appraisal ofthe value ofalkenone indices as temperature and salinity proxies in high-latitude locations. *Paleoceanography*. Vol 13, pg. 694-703

Rosell-Melé, A and Kos, N (1997) Paleoclimatic significance of the stratigraphic occurrence of photosynthetic biomarker pigments in the Nordic Seas. *Geology*. Vol 25, pg. 49-52

Rosell-Melé, A; Bard, E; Emeis, K. C; Grieger, B; Hewitt, C; Muller, P. J; Schneider, R. R (2004) Sea surface temperature anomalies in the oceans at the LGM estimated from the alkenone- U^{K}_{37}' index: comparison with GCMs. *Geophysical Research Letters*. Vol 31

Rosell-Melé, A; Eglinton, G; Pflaumann, U; Sarnthein, M (1995b) Atlantic core-top calibration of the U^{K}_{37} index as a sea-surface palaeotemperature indicator. *Geochimica et Cosmochimica Acta*. Vol 59, pg. 3099-3107

Rosell-Melé, A; Maslin, M. A; Maxwell, J. R; Schaeffer, P (1997) Biomarker evidence for Heinrich events. *Geochimica et Cosmochimica Acta*. Vol 61, pg. 1671-1678

Rostek, F; Bard, E; Beaufort, L; Sonzogni, C; Ganssen, G (1997) Sea surface temperature and productivity records for the past 240 kyr in the Arabian Sea. *Deep Sea Research II*. Vol 44, pg. 1461–1480

Ruddiman, W. F and McIntyre, A (1981) The Mode and Mechanism of the Last Deglaciation: Oceanic Evidence. *Quaternary Research*. Vol 16, Issue 2, pg. 125-134

Ruddiman, W. F (2003) Orbital insolation, ice volume, and greenhouse gases. *Quaternary Science Reviews*. Vol 22, pg. 1597-1629

Ruddiman, W. F; Mclntyre, A; Raymo, M. E (1986) Paleoenvironmental Results from North Atlantic Sites 607 and 609. In: Initial Reports, DSDP 94 (W. F. Ruddiman; R. B. Kidd; E. Thomas,; et al, Eds.) pg. 855-878. U.S. Govt. Printing Office, Washington

Ruddiman, W. F; Raymo, M. E; Mclntyre, A (1986) Matuyama 41,000-year cycles: North Atlantic Ocean and northern hemisphere ice sheets. *Earth and Planetary Science Letters*. Vol 80, pg. 117-129

Ruddiman, W; Raymo, M; Martinson, D; Clement, B; Backman, J (1989) Pleistocene evolution: Northern Hemisphere ice sheets and North Atlantic Ocean. *Paleoceanography*. Vol 4, pg. 353–412

Rutherford, S and D'Hondt, S (2000) Early onset and tropical forcing of 100,000-year Pleistocene glacial cycles. *Nature*. Vol 408, pg. 72-75

Sarmiento, J. L and Toggweiler, J. R (1984) A new model for the role of the oceans in determining atmospheric pCO_2. *Nature*. Vol 308, pg. 621-624

Sarnthein, M; Winn, K; Duplessy, J-C; Fontugne, M. R (1998) Global variations of surface ocean productivity in low and mid latitudes: influence on CO_2 reservoirs of the deep ocean and atmosphere during the last 21,000 years. *Paleoceanography*. Vol 3, no. 3, pg. 361-399

Schefuβ, E (2003) Paleo-environmental effects of the Mid-Pleistocene Transition in the tropical Atlantic and equatorial Africa. Universiteit Utrecht.

Schefuβ, E; Ratmeyer, V; Stuut, J, B. W; Jansen, J. H. F; Sinninghe Damasté, J. S (2003) Carbon isotope analyses of n-alkanes in dust from the lower atmosphere over the central eastern Atlantic. *Geochimica et Cosmochica Acta*. Vol 67, no. 10, pg. 1757-1767

Schefuβ, E; Schouten, S; Jansen, J. H; Sinninghe Damasté, J. S (2003) African vegetation controlled by tropical sea surface temperatures in the mid-Pleistocene period. *Nature*. Vol 422, pg. 418-421

Schefuβ, E; Sinninghe-Damsté, J. S; Jansen, J. H. F (2004) Forcing of tropical Atlantic sea surface temperatures during the mid-Pleistocene transition. *Paleoceanography*. Vol 19, Issue 4, pg. 1-12

Schefuβ, E; Versteegh, G. J. M; Jansen, J. H. F; Sinninghe-Damsté, J. S (2004) Lipid biomarkers as major source and preservation indicators in SE Atlantic surface sediments. *Deep Sea Research Part I: Oceanographic Research Papers*. Vol 51, Issue 9, pg. 1199-1228

Schmittner, A and Clement, A. C (2002) Sensitivity of the thermohaline circulation to tropical and high latitude freshwater forcing during the last glacial-interglacial cycle. *Paleoceanography*. Vol 17, Issue 2

Schmittner, A; Appenzeller, C; Stocker, T.F (2000) Enhanced Atlantic freshwater export during El Niño. *Geophysical Research Letters*. Vol 27, pg. 1163-1166

Schneider, B; Leduc, G; Park, W (2010) Disentangling seasonal signals in Holocene climate trends by satellite-model-proxy integration. *Paleoceanography*. Vol 25, pg.1-13

Schneider, R. R; Müller, P; Ruhland, G (1995) Late Quaternary surface circulation in the east equatorial South Atlantic: Evidence form alkenone sea surface temperatures. *Paleoceanography*. Vol 10, pg. 197–219

Schubert, C. J; Villanueva, J; Calvert, S. E; Cowie, G. L; von Rad, U; Schulz, H; Berner, U; Erlenleuser, H (1998) Stable phytoplankton community structure in the Arabian Sea over the past 200,000 years. *Nature*. Vol 394, pg. 563-566

Schulte, S; Rostek, F; Bard, E; Rullkötter, J; Marchal, O (1999) Variations of oxygen-minimum and primary productivity recorded in sediments of the Arabian Sea. Earth and *Planetary Science Letters*. Vol 173, Issue 3, pg. 205

Schulz, M and Stattegger, K (1997) SPECTRUM: spectral analysis of unevenly spaced paleoclimatic time series. *Computers and Geosciences.* Vol 23, no. 9, pg. 929-945

Shackelton, N. J; Hall, M. A; Line, J; Shuxi, C (1983) Carbon isotope data in core V19-30 confirm reduced carbon dioxide concentration in the ice age atmosphere. *Nature*. Vol 306, Issue 5911, pg. 319-322

Shackleton, N. J and Opdyke, N. D (1973) Oxygen isotope and palaeomagnetic stratigraphy of equatorial Pacific core V28-238: Oxygen isotope temperatures and ice volumes on a 105 and 10 year scale. *Quaternary Research*. Vol 3, pg. 39–55

Shackleton, N. J and Opdyke, N. D (1976) Oxygen isotope and paleomagnetic stratigraphy of Pacific core V28-239. Late Pliocene to Latest Pleistocene. *Geological Society of America Memoir*. Vol 145, pg. 449-464

Shackleton, N. J; Berger, A; Peltier, W. R (1990) An alternative astronomical calibration of the lower Pleistocene timescale based on ODP Site 677. *Transactions of the Royal Society of Edinburgh, Earth Sciences*. Vol 81, pg. 251-261

Shackleton, N. J; Hall, M. A; and Vincent, E (2000) Phase relationships between millennial-scale events 64,000 to 24,000 years ago. *Paleoceanography*. Vol 15, pg. 565-569

Shackleton, N. J and Shipboard Scientific Party (1992) Sedimentation rates: toward a GRAPE density stratigraphy for Leg 138 carbonate sections. In: Proceedings of the Ocean Drilling Program, Initial Repts, Vol 138 (part 1) (N. G. Pisias, L. A. Mayer, T. R. Janecek, A. Palmer-Julson, and T. H. van Andel, Eds.), pg. 87-91

Shaffer, G (1993) Effects of the marine biota on global carbon cycling. In: The Global Carbon Cycle. (M. Heimann, Ed) pg. 431-456. NATO ASI Series 1: Global Environmental Change. Springer-Verlag.

Shankle, A. M; Goericke, R; Franks, P. J. S; Levin, L. A (2002) Chlorin distribution and degradation in sediments within and below the Arabian Sea oxygen minimum zone. *Deep-Sea Research I*. Vol 49, pg. 953-969

Short, D. A; Mengel, J. G; Crowley, T. J; Hyde, W. T; North, G. R (1991) Filtering of Milankovitch cycles by Earth's geography. *Quaternary Research*. Vol 35, Issue 2, pg. 157–173

Siegenthaler, U; Stocker, T. F; Monnin, E; Lüthi, D; Schwander, J; Stauffer, B; Raynaud, D; Barnola, J-M; Fischer, H; Masson-Delamotte, V; Jouzel, J (2005) Stable Carbon Cycle–Climate Relationship During Late Pleistocene. *Science*. Vol 310, pg. 1313-1317

Sigman, D. M and Boyle, E. A (2000) Glacial/interglacial variations in atmospheric carbon dioxide. *Nature*. Vol 407, pg. 859-869

Sikes, E. L and Volkman, J. K (1993) Calibration of alkenone unsaturation ratios (Uk'37) for paleotemperature estimation in cold polar waters. *Geochimica et Cosmochimica Acta*. Vol 57, Issue 8; pg. 1883-1889

Sikes, E. L and Sicre, M. A (2002) Relationship of the tetra-unsaturated C37 alkenone to salinity and temperature: Implications for paleoproxy applications. *Geochemistry Geophysics Geosystems*. Vol 3

Sorokin, Y. I; Sukhanova, I. N; Konovalova, G. V; Pavelyeva, E. B (1977) Primary production and the phytoplankton of the equatorial region in the eastern Pacific Ocean. *Polish Archives of Hydrobiology*. Vol 24, pg. 145–162

Sosdian, S and Rosenthal, Y (2009) Deep-Sea Temperature and Ice Volume Changes Across the Pliocene-Pleistocene Climate Transitions. *Science*. Vol 325, pg. 306-310

Spero, H. J and Deniro, M. J (1987) The influence of symbiont photosynthesis on the $\delta^{18}O$ and $\delta^{13}C$ values of planktonic foraminiferal shell calcite. *Symbiosis*. Vol 4, pg. 213–228

Spero, H. J and Lea, D. W (2002) The cause of carbon isotope minimum events on glacial terminations. *Science*. Vol 296, pg. 522–525

Spero, H. J (1998) Life history and stable isotope geochemistry of planktonic foraminifera. In: Isotope Paleobiology and Paleoecology (R. D. Norris and R. M. Corfield, Eds.), pg. 7– 36. Paleontological Society, Pittsburg, PA

Start, G. G and W. L. Prell (1984) Evidence for two Pleistocene climatic modes: Data from DSDP site 502. In: New Perspectives in Climate Modelling, (A. Berger and C. Nicolis, Eds) pg. 3-22, Elsevier Sci, New York

Stauffer, B; Blunier, T; Dallenbach, A; Indermilhle, A; Schwander, J; Stacker, T. F; Tschumi, J; Chappellaz, J; Raynaud, D; Hammer, C. U; Clausen, H. B (1998) Atmospheric C02 concentration and millenial-scale climate change during the last glacial period. *Nature*. Vol 392, pg. 59-62

Stein, R; Rullkotter, J; Welte, D (1986) Accumulation of organic-carbon rich sediments in the late Jurassic and Cretaceous Atlantic ocean-a synthesis. *Chemical Geology*. Vol 56, pg. 1–32

Stephens, B. B and Keeling, R. F (2000) The influence of Antarctic sea ice on glacialinterglacial C02 variations. *Nature*. Vol 404, pg. 171-174

Stocker, T. F and Wright, D. G (1991) Rapid transitions of the ocean's deep circulation induced by changes in surface water fluxes. *Nature*. Vol 351, pg. 729-732

Stott, L; Poulsen, C; Lund, S and Thunell, R (2002) Super ENSO and global climate oscillations at millennial time scales. *Science*. Vol 297, pg. 222–226

Summerhayes, C. P; Kroon, D; Rosell-Melé, A; Jordan, R. W; Schrader, H. J; Hearn, R; Villanueva, J; Grimalt, J. O; Eglinton, G (1995) Variability in the Benguela Current upwelling system over the past 70,000 years. *Progress in Oceanography*. Vol 35, pg. 207-251

Sun, X; Luo, Y; Huang, F; Tian, J; Wang, P (2003) Deep-sea pollen from the South China Sea: Pleistocene indicators of East Asian monsoon. Marine Geology. Vol 201, pg. 97-118

Swain, E. B (1985) Measurement and interpretation of sedimentary pigments. *Freshwater Biology*. Vol 15, pg. 53–75

Teller, J. T; Leverington, D. W; Mann, J. D (2002) Freshwater outbursts to the oceans from glacial Lake Agassiz and their role in climate change during the last deglaciation. *Quaternary Science Reviews*. Vol 21, pg. 879-887

Thierstein, H. R; Geitzenauer, K. R; Molfino, B; Shackleton, N. J (1977) Global synchroneity of late Quaternary coccolith datum levels Validation by oxygen isotopes. *Geology*. Vol 5, no.7 pg. 400-404

Tian, J; Wang, P; Cheng, X; and Li, Q (2002) Astronomically tuned Plio-Pleistocene benthic 8180 record from the South China Sea and Atlantic-Pacific comparison. *Earth and Planetary Science Letters*. Vol 203, pg. 1015-1029

Toggweiler, J. R; Russell, J. L; Carson, S. R (2006) Midlatitude westerlies, atmospheric CO_2, and climate change during the ice ages. *Paleoceanography*. Vol 21, Issue 2

Toggweiler, J. R (1999) Variation of atmospheric CO_2 by ventilation of the ocean's deepest water. *Paleoceanography*. Vol 14, no. 5, pg. 571-588

Toggweiler, J. R; Dixon, K; Broecker, W (1991) The Peru upwelling and the ventilation of the South Pacific thermocline. *Journal of Geophysical Research*. Vol 96, pg. 20467-20497

Trenberth, K. E; Branstator, G. W; Karoly, D; Kumar, A; Lau, N. C; Ropelewski, C (1998) Progress during TOGA in understanding and modelling global teleconnections associated with tropical sea surface temperatures. *Journal of Geophysical Research*. Vol 103, pg. 14291-14324

Tudhope, A. W; Chilcott, C. P; McCulloch, M. T; Cook, E. R; Chappell, J; Ellam, R. M; Lea, D. W; Lough, J. M; Shimmield, G. B (2001) Variability in the El Niño-Southern Oscillation through a Glacial-Interglacial Cycle. *Science*. Vol 291, pg. 1511-1517

Visser, K; Thunell, R; Stott, L (2003) Magnitude and timing of temperature change in the Indo-Pacific warm pool during deglaciation. *Nature*. Vol 421, pg. 152-155

Volkman, J. K; Barrett, S. M; Blackburn, S. I; Sikes, E. L (1995) Alkenones in Gephyrocapsa oceanica: Implications for studies of paleoclimate. *Geochimica et Cosmochimica Acta*. Vol 59, pg. 513-520

Volkman, J. K; Eglinton, G; Corner, E. D. S; Sargent, J. R (1980) Novel unsaturated straight-chain C37-C39 methyl and ethyl ketones in marine sediments and coccolithophore Emiliana huxleyi. In: Advances in Organic Geochemistry 1979 (A. G. Douglas, and J. R. Maxwell, Eds.) pg. 219-227. Pergamon, Oxford

Wakeham, S. G; Peterson, M. L; Hedges, J. I; Lee, C (2002) Lipid biomarker fluxes in the Arabian Sea, with a comparison to the equatorial Pacific Ocean. *Deep Sea Research Part II: Topical Studies in Oceanography*. Vol 49, Issue 12, pg. 2265-2301

Wang, B; Clemens, S. C; Lui, P (2003) Contrasting the Indian and East Asian monsoons: implications on geologic timescales. *Marine Geology*. Vol 201, pg. 5-21

Wang, R and Abelmann, A (2002) Radiolarian responses to paleoceanographic events of the South China Sea during the Pleistocene. *Marine Micropaleontology*. Vol 46, pg. 25-44

Wang, R; Li, J; Li, B (2004) Data report: Late Miocene-Quaternary biogenic opal accumulation at ODP Site 1143, southern South China Sea. In: Prell, W. L; Wang, P; Blum, P; Rea, D. K; Clemens, S. C (Eds.) Proceeding of ODP, scientific results: Vol. 184

Wang, Y.J; Cheng, H; Edwards, R.L; An, Z.S; Wu, J.Y; Shen, C.C and Dorale, J.A (2001) A high resolution absolute-dated late Pleistocene monsoon record from Hulu Cave, China. *Science*. Vol 294, pg. 2345–234

Watson, A. J; Bakker, D. C. E; Ridgwell, A. J; Boyd, P. W; Law, C. S (2010) Effect of iron supply on Southern Ocean CO_2 uptake and implications for glacial atmospheric CO_2. *Nature*. Vol 407, pg. 730–733

Wefer, G; Dunbar, R. B; E. Suess (1984) Stable isotopes of foraminifers off Peru recording high fertility and changes in upwelling history. In: Coastal Upwelling: Its Sedimentary Record, Part B (E. Suess and J. Thiede, Eds) pg. 295-308, Plenum, New York

Weirauch, D; Billups, K; Martin, P (2008) Evolution of millennial-scale climate variability during the mid-Pleistocene. *Paleoceanography*. Vol 23

Weldeab, S; Lea, D. W; Schneider, R. R; Anderson, N (2007) 155,000 Years of West African Monsoon and Ocean Thermal Evolution. *Science*. Vol 316, pg. 1303-1307

Wells, M. L; Vallis, G. K; Silver, E. A (1999) Tectonic processes in Papua New Guinea and past productivity in the eastern equatorial Pacific Ocean. *Nature*. Vol 398, pg. 601–604

Wilson, R. C. L; Drury, S. A; Chapman, J. L (2000) The Great Ice Age: Climate Change and Life. Routledge, London

Winckler, G; Anderson, R. F; Schlosser, P (2005) Equatorial Pacific productivity and dust flux during the mid-Pleistocene climate transition. *Paleoceanography*. Vol 20

Winograd, I. J; Coplen, T. B; Landwehr, J. M; Riggs, A. C; Ludwig, K. R; Szabo, B. J; Kolesar, P. T; Revesz, K. M (1992) Continuous 500,000-Year Climate Record from Vein Calcite in Devils Hole, Nevada. *Science*. Vol 258, pg. 255

Wyrtki, K (1981) An estimate of equatorial upwelling in the Pacific. *Journal of Physical Oceanography*. Vol 11, pg. 1205-1214

Xiao, J and Z. An (1999) Three large shifts in East Asian monsoon circulation indicated by loess-paleosol sequences in China and late Cenozoic deposits in Japan. *Palaeogeography, Palaeoclimatology, Palaeoecology*. Vol 154, pg. 179–189

Xu, J; Wang, P; Huang, B; Li, Q; Jian, Z (2005) Response of planktonic foraminifera to glacial cycles: Mid-Pleistocene change in the southern South China Sea. *Marine Micropaleontology*. Vol 54, pg. 89–105

Yamamoto, M; Shiraiwa, Y; Inouye, I (2000) Physiological responses of lipids in Emiliania huxleyi and Gephyrocapsa oceanica (Haptophyceae) to growth status and their implications for alkenone paleothermometry. *Organic Geochemistry*. Vol 31, pg. 799-811

Zahn, R; Winn, K; Sarnthein, M (1986) Benthic foraminiferal ^{13}C and accumulation rates of organic carbon: Uvigerina peregrina group and Cibicidoides wuellerstorfi. *Paleoceanography*. Vol 1, pg. 27–42

Zhao, M; Eglinton, G; Haslett, S. K; Jordan, R. W; Sarnthein, M; and Zhang, Z (2000) Marine and terrestrial biomarker records for the last 35,000 years at ODP site 658C offNW Africa. *Organic Geochemistry*. Vol 31, pg. 919-930

Zhao, M; Mercer, J. L; Eglinton, G; Higginson, M. J; Huang, C. Y (2006) Comparative molecular biomarker assessment of phytoplankton paleoproductivity for the last 160 kyr off Cap Blanc, NW Africa. *Organic Geochemistry*. Vol 37, pg. 72-97

Zheng, F; Li, Q; Li, B; Chen, M; Tu, X; Tian, J; Jian, Z (2005) A millennial scale planktonic foraminifer record of the mid-Pleistocene climate transition from the northern South China Sea. *Palaeogeography, Palaeoclimatology, Palaeoecology*. Vol 223, pg. 349– 363

Zhonghui, L and Herbert, T.W (2004) High-latitude influence on the eastern equatorial pacific climate in the early Pleistocene epoch. *Nature*. Vol 427, pg. 720–723

Appendix

Data Source key: (1=McClymont, 2004; 2=this thesis)

Data Source	ODP 849	Depth	LR04 Age	Bulk MAR	P410	AR P410	P665	AR P665	S/I	K37	MAR K37	U^{K}_{37}'	SST
	ODP Sample Label	(Rmcd)	(ka)	(g/cm²/kyr)	(AU/g)	(AU/cm²/kyr)	(AU/g)	(AU/cm²/kyr)		(ng/g)	(µg/cm2/kyr)		(ºC)
2	849C-2H-4W, 14-15cm	18.14	598.97	1.573	67.57	106.32	7.69	12.10	8.78	133.99	210.81		
1	849C-2H-4W, 21-22cm	18.21	601.73	1.845	7.47	14.81	0.50	0.98	15.08	100.01	198.32	0.887	25.544
2	849C-2H-4W, 29-30cm	18.29	604.98	1.518	18.64	28.30	1.25	1.90	14.87	3.39	5.15		
1	849C-2H-4W, 36-37cm	18.36	607.83	1.595	8.70	16.06	0.40	0.74	21.83	159.31	293.98	0.905	26.087
2	849C-2H-4W, 42-43cm	18.43	610.79	1.476	22.62	33.39	2.12	3.13	10.68	10.12	14.95		
1	849C-2H-4W, 48-49cm	18.48	612.92	1.446	4.40	7.01	0.35	0.55	12.70	28.91	46.11	0.874	25.150
2	849C-2H-4W, 54-55cm	18.55	615.91	1.475	13.71	20.22	1.16	1.71	11.83	16.18	23.86		
1	849C-2H-4W, 60-61cm	18.6	618.04	1.286	7.66	11.08	0.26	0.38	29.37	36.49	52.76	0.867	24.941
2	849C-2H-4W, 65-66cm	18.65	620.18	1.475	11.42	16.85	0.93	1.37	12.26	9.72	14.33		
1	849C-2H-4W, 70-71cm	18.7	622.32	1.244	5.05	6.49	0.70	0.90	7.20	46.37	59.62	0.863	24.822
2	849C-2H-4W, 75-76cm	18.75	624.45	1.475	27.87	41.11	2.74	4.04	10.17	113.53	167.44	0.875	25.177
1	849C-2H-4W, 80-81cm	18.8	626.59	1.249	13.39	16.66	2.04	2.54	6.57	0.00	0.00	0.000	
2	849C-2H-4W, 85-86cm	18.85	628.72	1.475	17.30	25.52	1.78	2.62	9.74	24.60	36.29		
1	849C-2H-4W, 90-91cm	18.9	630.86	3.528	2.83	3.53	0.27	0.34	10.53	104.96	131.06	0.850	24.423
2	849C-2H-4W, 95-96cm	18.95	632.99	1.476	21.20	31.29	1.59	2.34	13.37	47.51	70.11	0.842	24.182
1	849D-2H-2W, 4-5cm	19.04	636.84	0.619	0.00	0.00	0.00	0.00	0.00	130.33	459.80	0.845	24.267
2	849C-2H-4W, 106-107cm	19.06	637.69	1.475	11.30	16.67	1.09	1.60	10.39	15.72	23.19		
1	849D-2H-2W, 12-13cm	19.11	639.83	1.592	5.31	7.31	0.65	0.89	8.18	66.56	41.23	0.844	24.228
2	849D-2H-2W, 19-20cm	19.18	642.81	1.475	7.75	11.43	0.73	1.08	10.56				
1	849D-2H-2W, 23-25cm	19.24	645.38	1.732	1.96	3.12	0.27	0.43	7.22	90.63	144.27	0.838	24.049
2	849D-2H-2W, 35-36cm	19.37	650.93	1.475	25.70	37.91	2.27	3.36	11.30	39.29	57.94	0.839	24.083

1	849D-2H-2W, 36-37cm	19.39	651.79	1.863	2.92	5.06	0.27	0.46	10.90	59.79	103.58	0.842	24.174
2	849D-2H-2W, 44-45cm	19.46	654.78	1.476	9.27	13.68	0.76	1.12	12.26	14.07	20.76		
1	849D-2H-2W, 52-53cm	19.53	657.77	1.913	7.02	13.07	0.38	0.72	18.26	72.44	134.93	0.859	24.701
2	849D-2H-2W, 61-62cm	19.61	661.18	1.525	23.16	35.31	2.81	4.28	8.24	99.65	151.99	0.842	24.169
1	849D-2H-2W, 68-69cm	19.69	664.53	1.957	11.98	22.91	1.45	2.78	8.25	181.71	347.56	0.818	23.467
2	849D-2H-2W, 77-78cm	19.76	667.37	1.586	26.26	41.66	2.90	4.61	9.04	169.36	268.65	0.834	23.934
1	849D-2H-2W, 85-86cm	19.84	670.63	2.021	4.25	8.32	0.80	1.56	5.32	108.64	212.56	0.834	23.930
2	849D-2H-2W, 93-94cm	19.92	673.73	1.942	30.22	58.68	2.25	4.37	13.44	40.23	78.14	0.916	26.427
1	849D-2H-2W, 100-101cm	19.99	676.13	2.140	7.84	15.85	1.79	3.62	4.38	81.87	165.47	0.858	24.668
2	849D-2H-2W, 108-109cm	20.09	679.24	2.023	29.85	60.38	2.61	5.28	11.44	41.73	84.41	0.835	
1	849D-2H-2W, 116-117cm	20.17	681.73	2.238	5.28	11.30	0.60	1.28	8.82	236.62	506.31	0.870	25.025
2	849D-2H-2W, 124-125cm	20.26	684.54	2.023	38.70	78.30	3.08	6.23	12.56				
1	849D-2H-2W, 135-136cm	20.37	687.96	2.217	22.81	51.06	3.14	7.02	7.27	307.84	688.96	0.901	25.959
2	849D-2H-2W, 142-143cm	20.44	690.14	2.023	50.82	102.81	6.60	13.36	7.70	194.06	392.60	0.871	25.075
1	849D-2H-3W, 3-4cm	20.54	693.26	2.073	8.30	18.41	0.80	1.78	10.33	272.30	603.79	0.873	25.108
2	849D-2H-3W, 14-15cm	20.61	695.44	2.023	31.92	64.57	2.35	4.76	13.57	26.35	53.30		
1	849D-2H-3W, 23-24cm	20.67	697.31	1.885	9.58	19.87	1.66	3.44	5.77	91.05	188.78	0.882	25.389
2	849D-2H-3W, 34-35cm	20.77	700.42	1.843	10.90	20.10	0.80	1.47	13.67				
1	849D-2H-3W, 43-44cm	20.82	702.04	1.615	15.13	28.51	2.61	0.00	5.80	269.68	508.24	0.897	25.854
2	849D-2H-3W, 53-54cm	20.89	704.52	1.577	64.50	101.71	7.72	12.17	8.36	284.24	448.19		
1	849D-2H-3W, 61-62cm	20.95	706.86	-0.012	14.69	23.72	1.68	2.72	8.73	104.77	169.22	0.885	25.476
2	849D-2H-3W, 68-69cm	21.03	710.12	1.549	14.10	21.83	1.40	2.17	10.04	31.17	48.29		
2	849D-2H-3W, 73-74cm	21.08	712.15	0.008					0.00				
2	849D-2H-3W, 82-83cm	21.13	714.18	1.549					0.00				
1	849D-2H-3W, 87-88cm	21.17	715.81	1.213	23.12	31.54	3.43	4.67	6.75	220.55	300.85	0.845	24.274
2	849D-2H-3W, 94-95cm	21.23	718.25	1.548	42.85	66.35	5.25	8.12	8.17	190.08	294.33	0.903	26.017
1	849D-2H-3W, 99-100cm	21.27	719.88	1.163	33.58	40.73	4.14	5.02	8.12	555.84	674.17	0.829	23.781

2	849D-2H-3W, 105-106cm	21.32	721.91	1.416	11.50	16.28	1.22	1.73	9.40	12.05	17.07		
1	849D-2H-3W, 111-112cm	21.36	723.53	1.119	11.53	13.40	1.22	1.42	9.46	250.18	290.87	0.851	24.468
2	849D-2H-3W, 116-117cm	21.41	725.92	1.992	43.24	86.11	4.03	8.03	10.73	59.44	118.38	0.888	
1	849D-2H-3W, 119-120cm	21.45	726.98	1.077	15.81	17.68	1.43	1.60	11.06	116.73	130.59	0.836	24.002
2	849D-2H-3W, 125-126cm	21.5	728.76	1.771	31.24	55.32	2.67	4.73	11.69	27.52	48.73		
1	849D-2H-3W, 130-131cm	21.54	730.19	1.056	10.06	10.83	0.98	1.06	10.26	74.24	79.95	0.917	26.466
2	849D-2H-3W, 135-136cm	21.58	731.61	1.743	30.59	53.32	2.21	3.86	13.82	8.68	15.12		
1	849D-2H-3W, 140-141cm	21.63	733.41	1.029	11.90	12.57	0.44	0.47	26.77	132.48	139.88	0.896	25.830
2	849D-2H-3W, 145-146cm	21.67	734.86	1.475	23.44	34.57	2.46	3.63	9.53	60.53	89.29	0.891	25.669
1	849D-2H-4W, 0-1cm	21.69	735.72	1.031	10.45	10.74	0.92	0.94	11.38	47.07	48.42	0.000	
2	849D-2H-4W, 5-6cm	21.75	738.28	1.475	35.69	52.65	3.15	4.65	11.32	51.67	76.22	0.767	21.915
1	849D-2H-4W, 9-11cm	21.78	739.56	1.051	7.17	7.39	0.48	0.49	15.07	325.49	335.45	0.856	24.610
2	849D-2H-4W, 14-15cm	21.83	741.70	1.352	55.12	74.55	4.60	6.22	11.99	181.30	245.18	0.801	22.939
1	849D-2H-4W, 19-20cm	21.87	743.54	1.084	7.26	7.63	1.07	1.12	6.81	95.69	100.60	0.869	24.998
2	849D-2H-4W, 24-25cm	21.91	745.42	1.240	44.41	55.07	4.79	5.95	9.26	163.07	202.21	0.854	
1	849D-2H-4W, 28-29cm	21.95	747.40	1.168	28.63	31.02	4.70	5.09	6.09	321.05	347.90	0.799	22.885
2	849D-2H-4W, 33-36cm	22	750.00	1.164	17.54	20.41	1.79	2.08	9.80	49.56	57.69	0.886	25.513
1	849D-2H-4W, 38-39cm	22.05	752.65	1.352	9.62	11.23	0.79	0.92	12.24	71.28	83.25	0.871	25.074
2	849D-2H-4W, 43-44cm	22.1	755.41	1.081	33.67	36.41	3.21	3.47	10.48	69.01	74.64	0.899	25.911
1	849D-2H-4W, 48-49cm	22.15	758.25	1.555	5.75	7.78	0.45	0.61	12.68	463.74	627.06	0.835	23.974
2	849D-2H-4W, 53-54cm	22.22	762.40	1.100	11.92	13.11	1.13	1.25	10.52				
1	849D-2H-4W, 60-61cm	22.28	765.89	1.946	3.29	5.12	0.32	0.49	10.36	58.86	91.54	0.884	25.453
2	849D-2H-4W, 66-67cm	22.36	770.42	1.382	14.04	19.41	1.24	1.71	11.35	7.29	10.07		
1	849D-2H-4W, 73-74cm	22.43	773.78	2.356	2.58	5.01	0.15	0.29	17.27	54.71	106.44	0.898	25.886
2	849D-2H-4W, 82-83cm	22.53	778.16	1.705	12.64	21.55	1.39	2.37	9.10				
1	849D-2H-4W, 91-92cm	22.62	781.62	2.364	1.93	4.55	0.09	0.21	21.89	37.03	87.25	0.898	25.887
2	849D-2H-4W, 102-103cm	22.72	785.18	1.633	7.25	11.84	0.67	1.09	10.25	3.84	6.27		

1	849D-2H-4W, 110-111cm	22.81	788.60	1.543	4.53	10.70	0.29	0.70	15.38	0.00	0.00	0.000	0.000
2	849D-2H-4W, 116-117cm	22.85	790.20	1.447	22.51	32.57	1.56	2.26	14.40	9.89	14.31		
1	849D-2H-4W, 125-126cm	22.93	793.61	1.383	8.18	12.62	1.07	1.66	7.63	91.02	178.42	0.831	23.848
2	849D-2H-4W, 131-132cm	22.98	795.86	1.332	6.08	8.10	0.53	0.71	11.39	27.53	36.68		
1	849D-2H-4W, 136-138cm	23.03	798.13	1.077	2.12	2.94	0.12	0.16	18.27	107.40	148.54	0.861	24.753
2	849D-2H-4W, 141-142cm	23.07	800.12	1.224	14.99	18.34	1.35	1.65	11.12	22.82	27.93		
1	849D-2H-4W, 146-147cm	23.12	802.59	1.054	4.66	5.02	0.48	0.52	9.74	148.18	159.58	0.835	23.977
2	849D-2H-5W, 0-1cm	23.17	805.26	1.180	16.43	19.39	1.32	1.56	12.45	31.32	36.96		
1	849D-2H-5W, 5-6cm	23.21	807.40	0.985	7.07	7.45	0.52	0.54	13.71	139.31	146.77	0.864	24.835
2	849D-2H-5W, 8-9cm	23.25	809.53	1.180	29.30	34.57	2.71	3.20	10.80	69.66	82.18	0.858	24.652
1	849D-2H-5W, 10-11cm	23.26	810.07	0.992	6.92	6.81	0.82	0.81	8.43	114.27	112.56	0.869	24.985
2	849D-2H-5W, 14-15cm	23.32	813.27	1.258	28.73	36.14	3.01	3.78	9.56	92.73	116.65	0.885	25.485
1	849D-2H-5W, 18-19cm	23.36	815.33	1.096	6.58	6.53	0.60	0.59	11.00	165.95	164.66	0.859	24.697
2	849D-2H-5W, 21-22cm	23.42	818.28	1.312	13.06	17.14	1.32	1.73	9.33	15.17	19.91		
1	849D-2H-5W, 25-26cm	23.46	820.25	1.252	4.35	4.77	0.39	0.42	11.24	52.03	57.05	0.909	26.201
2	849D-2H-5W, 28-29cm	23.49	821.64	1.403	14.51	20.36	1.85	2.59	7.86	65.73	92.23	0.860	24.740
1	849D-2H-5W, 34-35cm	23.59	826.13	1.668	3.10	3.89	0.21	0.26	14.79	96.06	120.28	0.905	26.094
2	849D-2H-5W, 35-36cm	23.6	826.58	1.460	21.28	31.05	2.03	2.96	10.50				
1	849D-2H-5W, 41-42cm	23.66	829.18	2.116	5.92	9.87	0.52	0.86	11.44	115.70	192.96	0.898	25.889
2	849D-2H-5W, 46-47cm	23.75	833.05	1.790	26.82	48.01	2.28	4.07	11.78				
1	849D-2H-5W, 52-53cm	23.84	836.49	2.811	5.77	12.20	0.25	0.52	23.43	214.22	453.34	0.861	24.767
2	849D-2H-5W, 62-63cm	23.95	840.09	2.237	36.43	81.51	2.59	5.79	13.26	6.03	13.50		
1	849D-2H-5W, 73-74cm	24.07	843.60	2.880	4.09	11.49	0.40	1.13	10.20	136.02	382.37	0.849	24.401
2	849D-2H-5W, 85-86cm	24.2	847.13	2.342	64.43	150.93	4.60	10.79	13.99	23.20	54.34		
1	849D-2H-5W, 95-96cm	24.29	849.54	-0.008	2.53	7.28	0.51	1.47	4.96	62.67	180.51	0.899	25.907
2	849D-2H-5W, 100-101cm	24.35	851.17	2.308	6.86	15.84	0.61	1.42	11.18	79.06	182.46		
2	849D-2H-5W, 106-107cm	24.4	852.53	2.087	37.39	78.04	3.72	7.75	10.06	40.60	84.73		

1	849D-2H-5W, 113-114cm	24.47	854.53	-0.010	2.86	6.43	0.18	0.40	16.17	45.02	101.30	0.905	26.103
2	849D-2H-5W, 120-121cm	24.54	856.76	1.828	11.23	20.53	0.80	1.45	14.11	12.33	22.54		
2	849D-2H-5W, 124-125cm	24.6	858.83	1.457	30.08	43.83	2.98	4.35	9.49	83.16	121.17	0.956	27.622
1	849D-2H-5W, 126-127cm	24.61	859.17	1.432	11.22	20.64	0.88	1.63	12.69	138.41	254.60	0.908	26.180
2	849D-2H-5W, 132-133cm	24.68	862.28	1.242	11.59	14.39	1.62	2.02	7.13				
1	849D-2H-5W, 136-137cm	24.72	864.06	1.400	25.85	37.02	2.68	3.84	9.65	125.07	179.07	0.842	24.168
2	849D-2H-5W, 141-142cm	24.79	867.87	1.130					0.00	157.08	177.55		
1	849D-2H-5W, 146-147cm	24.84	870.58	-0.005	26.87	37.62	4.45	6.23	6.04	296.18	414.65	0.799	22.867
2	849D-2H-5W, 147-148cm	24.86	871.77	1.062	36.62	38.88	4.98	5.29	7.36	353.48	375.30	0.866	24.915
2	849D-2H-6W, 2-3cm	24.91	874.73	1.062	62.51	66.37	7.16	7.60	8.73	94.87	100.73	0.891	25.667, 21.796, 24.032
2	849D-2H-6W-3-5cm	24.93	875.92	1.062	34.17	36.30	2.86	3.04	11.95	145.28	154.30	0.844	24.235
1	849D-2H-6W, 5-6cm	24.94	876.51	1.340	15.53	20.82	1.42	1.90	10.97	173.58	232.67	0.832	23.891
2	849D-2H-6W, 10-11cm	24.99	879.48	1.062	11.07	11.76	1.13	1.20	9.20	14.88	15.81		
2	849D-2H-6W, 13-14cm	25.04	882.44	1.077	7.68	8.27	1.01	1.09	7.13	56.23	60.55		
1	849D-2H-6W, 16-17cm	25.06	883.63	1.500	7.60	10.76	0.56	0.79	13.67	128.54	181.98	0.813	23.308
2	849D-2H-6W, 22-23cm	25.13	887.71	1.364	41.04	55.97	4.40	6.00	9.32				
1	849D-2H-6W, 27-28cm	25.17	889.72	1.745	10.69	16.04	1.27	1.90	8.42	129.66	194.49	0.790	22.598
2	849D-2H-6W, 34-35cm	25.25	893.25	1.688	18.90	31.90	2.05	3.47	8.66	19.39	32.73		
1	849D-2H-6W, 41-42cm	25.31	895.56	-0.006	22.59	39.42	4.33	7.56	5.21	280.46	489.35	0.788	22.548
2	849D-2H-6W, 43-44cm	25.35	896.99	1.858	31.57	58.66	4.17	7.75	7.57	163.31	303.46	0.891	25.678
2	849D-2H-6W, 48-49cm	25.4	898.68	2.008	47.89	96.15	5.42	10.88	8.84	228.61	459.01	0.865	24.868
2	849D-2H-6W, 62-63cm	25.54	903.07	2.023	26.27	53.14	3.83	7.75	6.86	264.76	535.59	0.857	24.636
2	849B-3H-4W, 79-80cm	25.57	904.01	2.023	48.20	97.50	3.43	6.95	14.04				
2	849B-3H-4W, 84-85cm	25.6	904.94	2.023	13.17	26.63	0.94	1.89	14.07				
1	849B-3H-4W, 89-91cm	25.64	906.19	-0.006	2.99	6.08	0.26	0.52	11.69	58.28	118.73	0.861	24.752
2	849B-3H-4W, 94-95cm	25.69	907.75	2.023	16.77	33.92	1.67	3.38	10.04	93.61	189.36	0.838	24.064

2	849B-3H-4W, 99-100cm	25.73	908.99	2.023	28.74	58.13	1.93	3.91	14.87	41.35	83.65		
2	849B-3H-4W, 103-104cm	25.8	911.17	2.023	14.80	29.93	1.38	2.78	10.76	53.60	108.43	0.849	24.404
2	849B-3H-4W, 107-108cm								0.00				
2	849B-3H-4W, 109-111cm	25.87	913.35	2.023	8.78	17.77	0.93	1.89	8.84	35.79	72.41		
2	849B-3H-4W, 117-118cm	25.92	914.91	2.023	50.84	102.84	5.48	11.08	9.28	27.40	55.44		
2	849B-3H-4W, 121-123cm	25.98	916.78	2.023	19.30	39.05	1.85	3.75	10.41	124.82	252.52	0.895	25.774
1	849B-3H-4W, 126-127cm	26.01	917.71	-0.006	68.85	158.95	5.98	13.81	11.51	351.12	810.61	0.834	23.945
2	849B-3H-4W, 131-132cm	26.07	919.58	2.023	31.63	64.00	4.72	9.55	6.30	191.79	388.02	0.885	25.471
2	849B-3H-4W, 135-136cm	26.1	920.51	2.023	34.91	70.62	3.59	7.27	9.14				
2	849B-3H-4W, 143-145cm	26.2	923.63	1.916	23.76	45.51	2.87	5.50	7.78	105.07	201.29		
2	849B-3H-5W, 1-2cm	26.27	925.93	1.876	83.47	156.58	6.49	12.17	12.11				
2	849B-3H-5W, 4-6cm	26.31	927.27	1.672	36.22	60.58	3.83	6.41	9.45	427.65	715.23	0.848	24.359
1	849B-3H-5W, 9-10cm	26.34	928.38	-0.005	31.33	64.86	3.53	7.32	8.87	286.20	592.46	0.828	23.765
2	849B-3H-5W, 12-13cm	26.38	929.91	1.643	62.67	102.96	9.93	16.32	5.94	118.83	195.21		
2	849B-3H-5W, 15-16cm	26.41	931.06	1.643	48.20	79.18	6.08	9.99	7.46	16.71	27.46		
2	849B-3H-5W, 19-20cm	26.45	932.59	1.643	20.80	34.18	2.27	3.73	9.15	65.94	108.33	0.810	23.217
2	849B-3H-5W, 23-24cm	26.49	934.13	1.604					8.31	43.81	70.25		
2	849B-3H-5W, 29-30cm	26.54	936.09	1.548	47.97	74.28	4.59	7.11	10.44	48.05	74.40		
2	849B-3H-5W, 38-39cm	26.64	940.16	1.549	17.58	27.23	2.47	3.83	6.69	91.35	141.49		
2	849B-3H-5W, 41-42cm	26.66	940.97	1.549	26.24	40.64	2.69	4.16	9.76	34.04	52.71		
2	849C-3H-1W, 29-30cm	26.7	942.60	1.549	10.53	16.31	1.14	1.76	8.71	99.37	153.93		
2	849C-3H-1W, 33-34cm	26.74	944.23	1.549	11.87	18.38	1.34	2.07	8.36	149.48	231.56	0.922	26.608
2	849C-3H-1W, 37-38cm	26.77	945.45	1.549	30.50	47.25	3.29	5.10	9.26	42.25	65.46		
1	849B-3H-5W, 57-58cm	26.82	947.48	-0.004	9.58	14.62	0.24	0.37	39.65	108.69	165.91	0.898	25.893
2	849B-3H-5W, 59-60cm	26.85	948.70	1.599	6.13	9.80	0.72	1.16	7.96	76.06	121.63		
2	849C-3H-1W, 47-48cm	26.88	949.88	1.706	15.14	25.83	1.34	2.29	11.28				
1	849C-3H-1W, 53-54cm	26.93	951.82	1.369	3.05	4.04	0.30	0.40	10.07	35.39	46.94	0.899	25.922

2	849C-3H-1W, 58-59cm	26.98	953.58	2.184	20.19	44.10	1.64	3.58	12.30				
1	849C-3H-1W, 63-64cm	27.03	955.06	1.492	1.93	2.65	0.23	0.32	8.31	35.51	48.60	0.872	
2	849C-3H-1W, 69-70cm	27.1	957.04	2.313	31.52	72.91	2.70	6.24	11.69				
1	849C-3H-1W, 75-76cm	27.15	958.40	1.570	9.77	14.59	1.23	1.83	7.97	40.38	60.27	0.918	26.475
2	849C-3H-1W, 81-82cm	27.22	960.31	2.390	46.25	110.53	3.40	8.13	13.59	26.51	63.36		
1	849C-3H-1W, 88-89cm	27.28	961.91	-0.005	24.49	38.44	4.51	7.08	5.43	309.72	486.27	0.892	25.694
2	849C-3H-1W, 92-93cm	27.33	963.21	2.436	20.18	49.17	2.89	7.05	6.57	187.15	455.94	0.963	27.837
2	849C-3H-1W, 95-96cm	27.36	963.98	2.294	45.58	104.56	6.46	14.82	7.05	283.44	650.29	0.876	25.217
1	849C-3H-1W, 103-104cm	27.43	965.88	2.244	13.35	25.74	2.30	4.44	5.80	157.17	303.00	0.852	24.470
2	849C-3H-1W, 108-109cm	27.49	967.55	2.212	44.16	97.70	4.84	10.70	9.13	228.91	506.41	0.883	25.420
2	849C-3H-1W, 112-113cm	27.53	968.69	2.196	42.37	93.07	5.30	11.65	7.99	38.92	85.48		
2	849C-3H-1W, 117-118cm	27.58	970.13	2.163	34.24	74.08	4.17	9.02	8.21	134.22	290.35	0.845	24.268
1	849C-3H-1W, 121-122cm	27.61	970.99	-0.007	15.00	33.83	2.33	5.26	6.44	268.14	604.75	0.865	24.874
2	849C-3H-1W, 127-128cm	27.68	973.04	2.124	31.37	66.64	4.33	9.19	7.25	543.44	1154.22	0.923	26.630
2	849C-3H-1W, 131-132cm	27.72	974.22	2.124	28.45	60.42	4.03	8.55	7.07	206.04	437.62	0.889	25.596
2	849C-3H-1W, 134-135cm	27.75	975.11	2.037	25.57	52.07	3.88	7.89	6.60	389.19	792.66	0.923	26.623
1	849C-3H-1W, 140-141cm	27.8	976.65	-0.006	11.04	26.81	1.23	2.99	8.96	116.64	283.20	0.863	24.821
2	849C-3H-1W, 144-145cm	27.85	978.21	1.647	15.44	25.43	2.09	3.44	7.40	112.83	185.85	0.950	27.441
2	849C-3H-1W, 149-150cm	27.9	980.12	1.573					0.00				
2	849C-3H-2W, 3-4cm	27.94	981.72	1.555	47.43	73.74	6.89	10.70	6.89	356.33	553.92	0.891	25.661
1	849C-3H-2W, 7-8cm	27.97	982.93	-0.005	29.23	61.97	4.99	10.57	5.86	448.03	949.79	0.838	24.067
2	849C-3H-2W, 10-12cm	28.02	984.96	1.548	44.52	68.94	5.82	9.01	7.65	223.67	346.31	0.867	24.952
2	849C-3H-2W, 16-17cm	28.04	985.78	1.548	31.72	49.12	2.62	4.06	12.11				
2	849C-3H-2W, 17-18cm	28.08	987.40	1.548	23.56	36.48	2.85	4.41	8.28	120.15	186.05	0.860	24.734
1	849C-3H-2W, 20-21cm	28.1	988.22	-0.004	7.58	12.35	1.06	1.73	7.12	114.16	185.95	0.841	24.151
2	849C-3H-2W, 23-24cm	28.13	989.44	1.549	26.44	40.95	3.75	5.80	6.64	136.47	211.34	0.944	27.282
2	849C-3H-2W, 27-28cm	28.16	990.66	1.549	30.93	47.91	2.75	4.26	11.25	28.76	44.55		

1	849C-3H-2W, 31-32cm	28.2	992.29	1.260	3.66	5.12	0.38	0.53	9.73	132.50	185.50	0.863	24.833
2	849C-3H-2W, 36-37cm	28.27	995.13	1.549	29.36	45.48	2.17	3.37	13.50				
1	849C-3H-2W, 40-41cm	28.3	996.35	-0.004	2.88	3.63	0.25	0.32	11.31	41.49	52.28	0.892	25.711
2	849C-3H-2W, 43-44cm	28.35	998.39	1.549	12.41	19.23	1.06	1.64	11.72	48.37	74.92	0.865	24.871
2	849C-3H-2W, 45-46cm	28.36	998.79	1.549	30.34	47.01	2.02	3.13	15.02	32.60	50.50	0.909	26.204
1	849C-3H-2W, 50-52cm	28.41	1000.83	1.216	6.49	7.77	1.00	1.20	6.49	70.36	84.24	0.881	25.369
2	849C-3H-2W, 54-55cm	28.46	1002.86	1.549	29.37	45.50	2.75	4.26	10.69	52.87	81.91		
1	849C-3H-2W, 59-60cm	28.5	1004.49	1.277	5.20	6.32	0.52	0.63	10.04	68.04	82.75	0.866	24.914
2	849C-3H-2W, 65-66cm	28.55	1006.52	1.549	27.34	42.35	2.59	4.01	10.56	45.63	70.69	0.901	25.981
1	849C-3H-2W, 70-71cm	28.6	1008.55	1.430	4.08	5.21	0.41	0.53	9.89	128.81	164.47	0.868	24.972
2	849C-3H-2W, 76-77cm	28.66	1010.99	1.549	36.92	57.19	3.24	5.02	11.40	65.42	101.33	0.892	25.704
1	849C-3H-2W, 85-86cm	28.74	1014.25	1.565	3.58	5.12	0.32	0.45	11.32	96.50	138.03	0.875	25.192
2	849C-3H-2W, 89-90cm	28.78	1015.87	1.549	25.52	39.53	2.28	3.53	11.21	12.39	19.19		
1	849C-3H-2W, 95-96cm	28.84	1018.31	1.665	7.30	11.42	0.55	0.86	13.33	108.93	170.50	0.844	24.241
2	849C-3H-2W, 100-101cm	28.91	1021.16	1.548	33.63	52.07	2.73	4.23	12.30	15.23	23.58		
1	849C-3H-2W, 107-108cm	28.97	1023.60	1.588	5.03	8.38	0.65	1.08	7.73	90.22	150.24	0.886	25.515
2	849C-3H-2W, 113-114cm	29.04	1026.45	1.548	36.56	56.61	2.53	3.92	14.45	22.01	34.08		
1	849C-3H-2W, 120-121cm	29.1	1028.89	1.499	4.75	7.54	0.58	0.92	8.19	81.82	129.94	0.906	26.124
2	849C-3H-2W, 126-127cm	29.16	1031.33	1.549	34.64	53.66	2.44	3.79	14.17	27.64	42.81		
1	849C-3H-2W, 133-134cm	29.22	1033.77	1.385	5.38	8.07	0.48	0.72	11.15	92.20	138.21	0.886	25.519
2	849C-3H-2W, 138-139cm	29.28	1036.21	1.549	19.41	30.07	2.62	4.06	7.41	119.21	184.65	0.869	25.012
1	849C-3H-2W, 146-147cm	29.36	1039.47	1.405	12.10	16.77	1.77	2.45	6.85	310.94	430.76	0.866	24.895
2	849C-3H-2W, 148-149cm	29.39	1040.69	1.549					0.00				
1	849C-3H-3W, 3-4cm	29.43	1042.32	1.406	5.55	7.80	1.00	1.40	5.58	164.07	230.45	0.875	25.187
2	849D-3H-3W, 2-3cm	29.5	1045.16	1.549	49.88	77.26	6.67	10.33	7.48	451.40	699.19	0.870	25.017
1	849D-3H-3W, 7-9cm	29.54	1046.79	1.576	13.17	18.52	2.38	3.34	5.54	65.94	92.68	0.890	25.642
2	849D-3H-3W, 10-11cm	29.62	1050.04	1.549	37.72	58.42	4.38	6.78	8.61	52.92	81.96		

1	849D-3H-3W, 15-16cm	29.67	1052.08	1.718	23.60	37.19	2.36	3.72	10.00	283.20	446.18	0.853	24.517
2	849D-3H-3W, 21-22cm	29.75	1055.33	1.549	60.04	92.99	5.91	9.15	10.16	50.72	78.57		
1	849D-3H-3W, 29-30cm	29.82	1058.18	2.078	11.49	19.74	0.90	1.54	12.78	298.97	513.52	0.860	24.716
2	849D-3H-3W, 37-38cm	29.9	1061.43	1.548	37.61	58.24	2.43	3.77	15.46	44.50	68.91	0.791	22.645
1	849D-3H-3W, 45-46cm	29.98	1064.69	-0.010	6.80	14.14	0.82	1.70	8.30	95.34	198.15	0.878	25.270
2	849D-3H-3W, 52-53cm	30.07	1068.35	1.548	39.88	61.75	3.68	5.70	10.84				
2	849D-3H-3W, 60-61cm	30.15	1071.60	1.549	39.32	60.89	2.35	3.65	16.70				
2	849D-3H-3W, 67-68cm	30.23	1074.86	1.549	53.18	82.37	4.14	6.42	12.84	55.46	85.91		
1	849D-3H-3W, 75-76cm	30.3	1077.71	-0.008	13.94	28.33	1.97	4.00	7.08	79.25	161.06	0.918	26.472
2	849D-3H-3W, 83-84cm	30.38	1080.96	1.549	31.31	48.51	3.96	6.14	7.90	66.69	103.31		
2	849D-3H-3W, 90-91cm	30.44	1083.40	1.549					0.00				
2	849D-3H-3W, 98-99cm	30.5	1085.84	1.549	15.95	24.71	2.16	3.35	7.37				
1	849D-3H-3W, 106-107cm	30.55	1087.87	1.346	25.33	40.49	3.80	6.08	6.66	215.69	344.88	0.871	25.069
2	849D-3H-3W, 111-112cm	30.61	1090.31	1.549	12.59	19.50	1.32	2.04	9.54				
1	849D-3H-3W, 117-118cm	30.66	1092.35	1.260	8.06	10.85	0.43	0.58	18.58	163.94	220.61	0.892	25.710
2	849D-3H-3W, 121-122cm	30.72	1094.79	1.549	22.39	34.68	2.30	3.56	9.74	28.89	44.75		
1	849D-3H-3W, 125-126cm	30.76	1096.41	1.345	2.99	3.77	0.49	0.62	6.05	229.55	289.23	0.866	24.900
2	849D-3H-3W, 129-130cm	30.81	1098.45	1.549	33.18	51.39	2.10	3.25	15.83				
1	849D-3H-3W, 133-135cm	30.87	1100.89	1.420	5.80	7.80	0.77	1.04	7.52	170.69	229.51	0.872	25.080
2	849D-3H-3W, 137-138cm	30.92	1102.92	1.549	50.25	77.81	4.93	7.63	10.20				
1	849D-3H-3W, 142-143cm	30.99	1105.77	1.620	5.27	7.48	0.55	0.79	9.52	41.19	58.48	0.894	25.758
2	849D-3H-3W, 147-148cm	31.04	1107.80	1.548	24.92	38.59	2.11	3.27	11.80				
1	849D-3H-4W, 2-3cm	31.1	1110.25	1.742	4.16	6.73	0.34	0.55	12.22	51.40	83.27	0.884	25.462
2	849D-3H-4W, 9-10cm	31.18	1113.50	1.549	25.89	40.10	2.26	3.50	11.46	29.21	45.24		
1	849D-3H-4W, 16-17cm	31.24	1115.94	2.039	6.50	11.33	0.48	0.83	13.64	35.81	62.38	0.918	26.485
2	849D-3H-4W, 25-26cm	31.33	1119.60	1.549	28.05	43.45	2.12	3.28	13.23	19.38	30.02		
1	849D-3H-4W, 32-33cm	31.42	1123.26	1.953	11.77	23.98	1.69	3.45	6.96	47.11	96.03	0.887	25.534

2	849D-3H-4W, 39-40cm	31.49	1126.11	1.549	16.87	26.13	1.44	2.23	11.72				
1	849D-3H-4W, 46-47cm	31.56	1128.96	1.671	14.54	28.38	1.80	3.51	8.09	269.93	527.04	0.863	24.804
2	849D-3H-4W, 52-53cm	31.63	1131.80	1.549	33.70	52.19	4.72	7.30	7.15				
1	849D-3H-4W, 58-59cm	31.69	1134.24	1.485	11.48	19.19	1.32	2.21	8.70	200.12	334.49	0.872	25.088
2	849D-3H-4W, 65-66cm	31.76	1137.09	1.549	17.03	26.38	1.97	3.05	8.66	17.96	27.82		
1	849D-3H-4W, 70-71cm	31.81	1139.12	1.310	6.05	8.99	0.31	0.45	19.78	68.18	101.25	0.904	26.070
2	849D-3H-4W, 74-75cm	31.86	1141.16	1.549	23.70	36.71	2.19	3.39	10.83	39.22	60.74		
1	849D-3H-4W, 79-80cm	31.91	1143.19	-0.006	15.48	20.28	0.97	1.27	15.92	197.15	258.27	0.875	25.187
2	849D-3H-4W, 83-84cm	31.97	1145.63	1.549	38.23	59.21	4.48	6.93	8.54	66.25	102.60	0.866	24.919
2	849D-3H-4W, 88-89cm	32.01	1147.26	1.548					0.00				
2	849D-3H-4W, 90-91cm	32.07	1149.70	1.548	55.48	85.91	4.14	6.41	13.40	25.22	39.05		

Stable Isotope data

Data Source	**ODP 849**	**Depth**	**LR04 Age**	**Bulk MAR**	**G. Ruber**	**G. Ruber**	**G. Sacculifer**	**G. Sacculifer**	**N. Dutertrei**	**N. Dutertrei**
	ODP Sample Label	**(Rmcd)**	**(ka)**	**(g/cm²/kyr)**	**$\delta^{18}O$**	**$\delta^{13}C$**	**$\delta^{18}O$**	**$\delta^{13}C$**	**$\delta^{18}O$**	**$\delta^{13}C$**
2	849D-2H-4W, 14-15cm	21.83	741.70	1.352	-0.23	+0.80			+0.69	+1.28
2	849D-2H-4W, 43-44cm	22.1	755.41	1.081	-0.70	+1.16			+0.36	+1.32
2	849D-2H-4W, 102-103cm	22.72	785.18	1.633	-0.47	+1.03			+0.15	+1.14
2	849D-2H-4W, 116-117cm	22.85	790.20	1.447					+1.21	+1.00
2	849D-2H-5W, 0-1cm	23.17	805.26	1.180					+0.53	+1.68
2	849D-2H-5W, 8-9cm	23.25	809.53	1.180	-0.46	+1.51			+0.86	+1.69
2	849D-2H-5W, 21-22cm	23.42	818.28	1.312	-0.74	+1.26			+0.53	+1.10
2	849D-2H-5W, 28-29cm	23.49	821.64	1.403					+0.41	+1.38
2	849D-2H-5W, 35-36cm	23.6	826.58	1.460					+0.67	+1.28
2	849D-2H-5W, 46-47cm	23.75	833.05	1.790					+0.67	+1.26
2	849D-2H-5W, 62-63cm	23.95	840.09	2.237	-0.45	+1.05			+0.30	+1.30

2	849D-2H-5W, 85-86cm	24.2	847.13	2.342					+0.87	+0.82
2	849D-2H-5W, 120-121cm	24.54	856.76	1.828			-0.05	+1.11	+0.28	+0.96
2	849D-2H-5W, 124-125cm	24.6	858.83	1.457	-0.64	+0.93			+0.30	+1.05
2	849D-2H-5W, 132-133cm	24.68	862.28	1.242	-0.62	+0.84			+1.03	+1.12
2	849D-2H-5W, 141-142cm	24.79	867.87	1.130	-0.19	+0.93			+1.04	+1.11
2	849D-2H-5W, 147-148cm	24.86	871.77	1.062	+0.14	+0.56			+1.34	+0.91
2	849D-2H-6W, 2-3cm	24.91	874.73	1.062	+0.42	+1.31			+0.46	+1.35
2	849D-2H-6W-3-5cm	24.93	875.92	1.062	+0.18	+0.71			+0.78	+1.37
2	849D-2H-6W, 10-11cm	24.99	879.48	1.062	+1.69/-0.07	+1.37/+0.79			+0.69	+1.17
2	849D-2H-6W, 13-14cm	25.04	882.44	1.077	+0.09	+0.97			+0.98	+1.23
2	849D-2H-6W, 22-23cm	25.13	887.71	1.364	-0.03	+1.04			+0.89	+1.32
2	849D-2H-6W, 34-35cm	25.25	893.25	1.688	+0.47	+0.59			+1.07	+1.10
2	849D-2H-6W, 43-44cm	25.35	896.99	1.858	-0.64	+0.58			+0.76	+1.20
2	849D-2H-6W, 48-49cm	25.4	898.68	2.008	+0.04	+0.76			+1.27	+1.13
2	849D-2H-6W, 62-63cm	25.54	903.07	2.023	+0.05	+0.57			+0.91	+1.10
2	849B-3H-4W, 79-80cm	25.57	904.01	2.023					+0.50	+1.42
2	849B-3H-4W, 84-85cm	25.6	904.94	2.023	-0.38	+0.96			+0.59	+1.15
2	849B-3H-4W, 94-95cm	25.69	907.75	2.023	-0.11	+0.73			+0.84	+1.11
2	849B-3H-4W, 103-104cm	25.8	911.17	2.023	-0.93	+1.13			+0.55	+1.14
2	849B-3H-4W, 109-111cm	25.87	913.35	2.023	-0.36	+0.93			+0.62	+0.89
2	849B-3H-4W, 117-118cm	25.92	914.91	2.023	-0.32	+1.06			+0.47	+0.96
2	849B-3H-4W, 121-123cm	25.98	916.78	2.023	-0.46	+1.06			+1.04	+0.70
2	849B-3H-4W, 131-132cm	26.07	919.58	2.023	+0.10	+0.75			+0.86	+0.78
2	849B-3H-4W, 135-136cm	26.1	920.51	2.023	-0.12	+0.56	+0.31	+1.27	+0.82	+1.03
2	849B-3H-4W, 143-145cm	26.2	923.63	1.916	-0.18	+0.42			+0.68	+1.07
2	849B-3H-5W, 1-2cm	26.27	925.93	1.876	+0.06	+0.56			+0.79	+1.02
2	849B-3H-5W, 4-6cm	26.31	927.27	1.672	-0.31	+0.68			+0.78	+1.20

2	849B-3H-5W, 12-13cm	26.38	929.91	1.643	-0.38	+0.75			+0.07	+1.09
2	849B-3H-5W, 15-16cm	26.41	931.06	1.643	-0.56	+1.02			+0.74	+0.95
2	849B-3H-5W, 19-20cm	26.45	932.59	1.643	-0.88	+0.98			+0.37	+1.04
2	849B-3H-5W, 23-24cm	26.49	934.13	1.604					+0.90	+0.80
2	849B-3H-5W, 29-30cm	26.54	936.09	1.548	-0.25	+1.13			+0.56	+1.25
2	849B-3H-5W, 38-39cm	26.64	940.16	1.549			-0.71	+0.82	+0.14	+0.93
2	849C-3H-1W, 29-30cm	26.7	942.60	1.549	-0.21	+0.46			+0.80	+0.75
2	849C-3H-1W, 33-34cm	26.74	944.23	1.549	-0.45	+1.36	+0.23	+1.13	+0.73	+1.38
2	849C-3H-1W, 37-38cm	26.77	945.45	1.549	-0.75	+1.30			+0.54	+1.06
2	849B-3H-5W, 59-60cm	26.85	948.70	1.599					+0.59	+1.14
2	849C-3H-1W, 58-59cm	26.98	953.58	2.184					+0.76	+0.91
2	849C-3H-1W, 69-70cm	27.1	957.04	2.313	+0.17	+1.19			+0.19	+0.78
2	849C-3H-1W, 81-82cm	27.22	960.31	2.390	-0.44	+0.25			+0.77	+0.58
2	849C-3H-1W, 92-93cm	27.33	963.21	2.436	-0.63	+0.49			+1.24	+0.76
2	849C-3H-1W, 95-96cm	27.36	963.98	2.294	-0.45	+0.43			+0.66	+0.90
2	849C-3H-1W, 108-109cm	27.49	967.55	2.212	-0.67	+1.25			+0.66	+1.19
2	849C-3H-1W, 117-118cm	27.58	970.13	2.163	-0.63	+1.83			+0.42	+1.16
2	849C-3H-1W, 134-135cm	27.75	975.11	2.037	-0.57	+1.60			+0.73	+1.69
2	849C-3H-1W, 144-145cm	27.85	978.21	1.647	-0.78	+1.77			+0.64	+1.09
2	849C-3H-2W, 23-24cm	28.13	989.44	1.549	-0.49	+1.49				
2	849C-3H-2W, 65-66cm	28.55	1006.52	1.549	-0.62	+1.25			+0.23	+1.68